

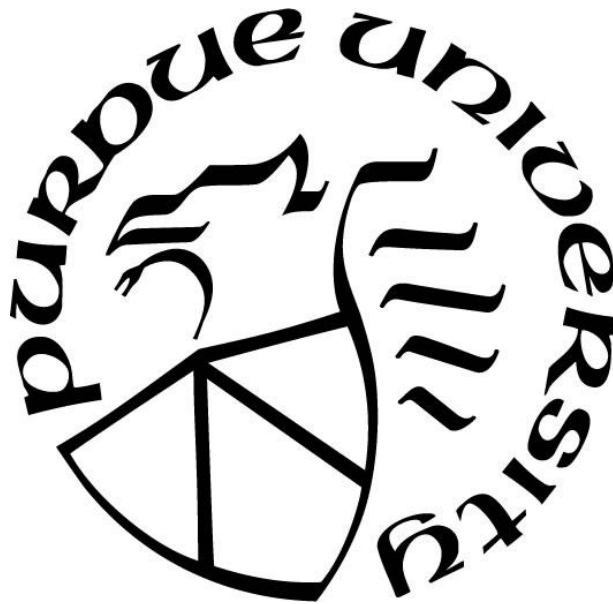
**TRPV4 IMPLICATIONS IN INFLAMMATION AND HYDROCEPHALIC
NEUROLOGICAL DISEASE**

by
Stefanie J. Simpson

A Thesis

*Submitted to the Faculty of Purdue University
In Partial Fulfillment of the Requirements for the degree of*

Master of Science



Department of Biological Sciences

Indianapolis, Indiana

May 2019

**THE PURDUE UNIVERSITY GRADUATE SCHOOL
STATEMENT OF COMMITTEE APPROVAL**

Dr. Bonnie Blazer-Yost, Chair

Department of Biology

Dr. Teri Belecky-Adams

Department of Biology

Dr. Nicolas Berbari

Department of Biology

Dr. Charles Goodlett

Department of Psychology

Approved by:

Dr. James Marrs

Head of the Graduate Program

To my friends and family who always support what is best for me.

ACKNOWLEDGMENTS

I would like to acknowledge my committee for all their help and support throughout my graduate career. I would also like to thank Daniel Preston, Hillary Smith, Keith Gafunderi, Adrian Oblack, and Shane Bemiller for their help with data collection.

TABLE OF CONTENTS

LIST OF TABLES	7
LIST OF FIGURES	8
LIST OF ABBREVIATIONS.....	10
ABSTRACT.....	11
CHAPTER 1. INTRODUCTION	12
1.1 Hydrocephalus	12
1.2 Hydrocephalus Treatment Options	13
1.3 The Choroid Plexus and CSF Flow	14
1.4 Transient Receptor Potential Vanilloid 4.....	15
1.5 Rat Model of Hydrocephalus	16
1.6 Choroid Plexus Cell Line.....	17
1.7 Ion Channels in the Choroid Plexus.....	18
1.8 Inflammation and Cytokines.....	20
1.9 TRPV4 and Inflammatory Mediators	22
1.10 Translational Potential.....	22
1.11 References	26
CHAPTER 2. HYDROCEPHALUS IN A RAT MODEL WITH A TMEM67 MUTATION ..	33
2.1 Preface.....	33
2.2 Hydrocephalus in a rat model of Meckel Gruber syndrome with a TMEM67 mutation..	34
2.3 Abstract	34
2.4 Introduction.....	35
2.5 Results.....	37
2.6 Discussion	42
2.7 Methods.....	46
2.8 Acknowledgements.....	51
2.9 Author Contributions	52
2.10 References	73
CHAPTER 3. ACTIVATION OF TRPV4 STIMULATES ION FLUX IN PCP-R CELLS.....	77
3.1 Preface.....	77

3.2	Activation of TRPV4 Stimulates Transepithelial Ion Flux in a Porcine CP Cell Line.....	78
3.3	Abstract.....	79
3.4	Introduction.....	79
3.5	Materials and Methods.....	81
3.6	Results.....	83
3.7	Discussion.....	85
3.8	Acknowledgements.....	90
3.9	Grants.....	90
3.10	Disclosures.....	90
3.11	References.....	113
CHAPTER 4. INFLAMMATORY EFFECTS ON TRPV4 IN THE CHOROID PLEXUS ...		117
4.1	Preface.....	117
4.2	Inflammatory mediator effects on TRPV4 function in the choroid plexus.....	117
4.3	Introduction.....	117
4.4	Materials and Methods.....	120
4.5	Results.....	121
4.6	Discussion.....	124
4.7	References.....	152
CHAPTER 5. ADDITIONAL DATA.....		158
5.1	TRPV4 in the Choroid Plexus.....	158
5.2	Characterizing the PCP-R cell line.....	159
5.3	SPAK and Associated Channels in the Choroid Plexus.....	160
5.4	Microglia in Wpk rat brain.....	162
5.5	Discussion.....	163
5.6	References.....	181
CHAPTER 6. SUMMARY.....		182
6.1	References.....	185

LIST OF TABLES

Table 3.1 Primer pairs used for the RT-PCR with corresponding product sizes (bp).	91
Table 4.1 Primer sequences used for RT-PCR with corresponding product sizes (bp).....	129
Table 5.1 Primer sequences used for RT-PCR with corresponding product sizes (bp).....	165

LIST OF FIGURES

Figure 1.1 Head measurements post-TRPV4 antagonist treatment in rats at P15.....	25
Figure 2.1 Characterization of the TMEM67 genotype in the Wpk rat.....	54
Figure 2.2 Correlation of phenotypic and genotypic characteristics in the Wpk rat.	56
Figure 2.3 MRI of the three genotypes of juvenile Wpk rat model with TMEM67 mutations....	59
Figure 2.4 Midline malformation and ciliary phenotype at birth in the TMEM67 ^{+/-} rats.....	61
Figure 2.5 Hemorrhage at birth and neonatal ventriculomegaly.	63
Figure 2.6 Communicating hydrocephalus.	65
Figure 2.7 MRI of WT and TMEM67 ^{+/-} Wpk rats at 8 months of age.....	67
Figure 2.8 Immunofluorescence of membrane proteins in the Wpk CP.....	69
Figure 2.9 Ventricular Evans blue leakage and CSF ionic composition from TMEM67 rats.....	71
Figure 3.1 Development of transepithelial resistance of the PCP-R cell line.....	92
Figure 3.2 Effect of TRPV4 agonist and antagonists in the PCP-R cells.	94
Figure 3.3 Dose response for TRPV4 agonist GSK1016790A in PCP-R cells.....	96
Figure 3.4 Dose response for TRPV4 antagonist RN1734 pre-treatment in PCP-R cells.....	98
Figure 3.5 Reversibility of a TRPV4 agonist response by a TRPV4 antagonist.	100
Figure 3.6 Immunohistological staining of claudin 1 in the PCP-R cell line.	101
Figure 3.7 RT-PCR of selected ion channels in the PCP-R cell line.....	103
Figure 3.8 Effect of BK channel inhibitor on TRPV4-mediated responses.	104
Figure 3.9 Effect of SK channel inhibitor on TRPV4-mediated responses.....	106
Figure 3.10 Effect of high/low doses of IK channel inhibitor on TRPV4-mediated responses.	108
Figure 3.11 Sidedness of IK channel inhibitor on TRPV4-mediated responses.....	110
Figure 3.12 Diagram of selected transporters in the choroid plexus epithelia.....	112
Figure 4.1 RT-PCR in PCP-R cells.....	131
Figure 4.2 Pre-treatment of PCP-R cells with IL-1 β 24-hrs pre-TRPV4 agonist addition.....	133
Figure 4.3 Pre-treatment of PCP-R cells with TNF- α 24-hrs pre-TRPV4 agonist addition.	135
Figure 4.4 Pre-treatment of PCP-R cells with IL-10 24 hrs pre-TRPV4 agonist addition.	137
Figure 4.5 Pre-treatment of PCP-R cells with IL-4 24 hrs pre-TRPV4 agonist addition.....	139
Figure 4.6 Pre-treatment of PCP-R cells with TGF- β 1 24 hrs pre-TRPV4 agonist addition.....	141
Figure 4.7 Pre-treatment of PCP-R cells with IL-6 24 hrs pre-TRPV4 agonist addition.....	143

Figure 4.8 Pre-treatment of PCP-R cells with PDTC 10 min pre-TRPV4 agonist addition.....	145
Figure 4.9 Pre-treatment of PCP-R cells with PDTC 24 hrs pre-TRPV4 agonist addition.....	147
Figure 4.10 Pre-treatment of PCP-R cells with AA or metabolites pre-TRPV4 agonist.....	149
Figure 4.11 Pre-treatment of PCP-R cells 5,6-EET 10-min pre-TRPV4 agonist addition.....	151
Figure 5.1 Immunofluorescence of TRPV4 in the Wpk rat CP.....	166
Figure 5.2 Immunofluorescence of Claudin-1 and TRPV4 in RN-1734-treated P15 Wpk CP..	167
Figure 5.3 RT-PCR in PCP-R epithelial cells.....	169
Figure 5.4 Immunofluorescence of SPAK in P15 Wpk CP treated with RN-1734.....	170
Figure 5.5 Immunofluorescence of pNKCC1 in TRPV4 agonist (GSK)-treated PCP-R cells...	171
Figure 5.6 PCP-R epithelial cells pretreated with SPAK/OSR1 inhibitor Rafoxanide.	173
Figure 5.7 Microglia in P356 Wpk WT and TMEM67 (+/-) rats.	174
Figure 5.8 Microglia in P460 Wpk WT and TMEM67 (+/-) rats.	176
Figure 5.9 Microglia in P330 Wpk WT and TMEM67 (+/-) rats.....	178
Figure 5.10 Microglia in P15 Wpk WT, TMEM67 (+/-) and TMEM67 (-/-) rats.....	179
Figure 5.11 Microglia in P17 Wpk WT and TMEM67 (-/-). rats.	180

LIST OF ABBREVIATIONS

MKS3: Meckel Gruber Syndrome type 3
TMEM67: Transmembrane Protein 67
Wpk: Wistar Polycystic Kidney
PKD: Polycystic Kidney Disease
JS: Joubert Syndrome
BBS: Bardet Biedl Syndrome
CP: Choroid Plexus
CSF: Cerebrospinal Fluid
PCP-R: Porcine Choroid Plexus-Reims
TRPV4: Transient Receptor Potential Vanilloid 4
NKCC1: $\text{Na}^+/\text{K}^+/2\text{Cl}^-$ co-transporter
SK: Small Conductance K^+ channel
IK: Intermediate Conductance K^+ channel
BK: Big Conductance K^+ channel
TER: Transepithelial Electrical Resistance
SCC: Short Circuit Current
AD: Alzheimer's Disease
PD: Parkinson's Disease
TBI: Traumatic Brain Injury
NPH: Normal Pressure Hydrocephalus
AA: Arachidonic Acid
EET: Epoxyeicosatrienoic Acids
IL: Interleukin
TNF: Tumor Necrosis Factor
TGF: Transforming Growth Factor
TLR: Toll-like Receptor
CYP: Cytochrome P
LOX: Lipoxygenase
COX: Cyclooxygenase

ABSTRACT

Author: Simpson, Stefanie, J. MS

Institution: Purdue University

Degree Received: May 2019

Title: TRPV4 Implications in Inflammation and Hydrocephalic Neurological Disease

Committee Chair: Bonnie Blazer-Yost

Hydrocephalus is a debilitating disease characterized by an increase in cerebrospinal fluid (CSF) in the brain, leading to increases in pressure that can ultimately result in death. Current treatments for hydrocephalus include only invasive brain surgery. Therefore, the need for a pharmaceutical therapy is great. In order to develop a suitable treatment, we first must be able to study the disease and the mechanisms by which it develops. By characterizing appropriate in vivo and in vitro models, we are better able to study this disease. In this thesis, the Wpk rat model and the PCP-R cell line are described as such appropriate models.

In addition to suitable models, we also require a target for drug treatment. Transient Receptor Potential Vanilloid 4 (TRPV4) is a non-selective cation ion channel present in the main CSF-producing organ in the brain, the choroid plexus (CP). Preliminary data suggest this channel plays a role in the development of hydrocephalus. In the following work, some of the mechanisms by which TRPV4 functions in the brain are also described, including through calcium-sensitive potassium channels and inflammation.

From this research, we are able to achieve a better understanding of the function of TRPV4 and how it can affect the development and progression of hydrocephalus.

CHAPTER 1. INTRODUCTION

1.1 Hydrocephalus

Neurodegenerative diseases consist of a wide range of pathologies affecting neurons in the brain. In the majority of cases, these diseases are incurable as they progressively destroy neurons, leading to the debilitation of the patients affected by them. The most common of these diseases alter motor function and mental cognition (1). Some of these diseases include dementias, such as Alzheimer's disease (AD), which is synonymous with a loss of function in memory, thinking and behavior, and Lewy body diseases, such as Parkinson's disease (PD) which can lead to gait ataxias and motion tremors, and traumatic brain injury (TBI), caused by inflammation and hemorrhage due to a severe impact to the skull and/or brain (1, 2). While all these diseases are different in their own right, they each can have similar symptoms, such as problems with mental function and gait abnormalities. Specifically, these diseases share a common effect, which is the enlargement of the ventricles.

Hydrocephalus can be a devastating condition seen in numerous neurological diseases in adults as well as children. Characterized by a buildup of cerebrospinal fluid (CSF) in the ventricular space either due to under-absorption, over-production, or a blockage of CSF flow, hydrocephalus is also known as "water on the brain" and is seen in approximately 85 out of every 100,000 or 6.4 million individuals worldwide across all ages (3). Tumors, infection, head trauma, hemorrhage, genetic defects, inflammation, and neurogenerative disease can all be associated with the development of hydrocephalus (4-14). In these instances, there can be two different types of hydrocephalus: communicating and non-communicating. In communicating hydrocephalus, there is either an under-absorption or an over-production of CSF. While the choroid plexus is considered the main producer of CSF, other cells such as ependymal cells, the cells lining the ventricles, or cells in the subarachnoid space, another area of the brain where CSF flows can also contribute to fluid production. The relative contribution of these, particularly in disease states, is determined by the nature of the pathology. In non-communicating hydrocephalus, there is a blockage in the flow of CSF, usually in the aqueducts connecting the different ventricles. The subsequent increase in hydrostatic pressure from either form can lead to neuronal damage and cell death (14).

The most severe cases of the disorder occur in children with a prevalence of about 1 in every 1000 live births (6). Because infant skulls are not yet ossified, the increase in fluid can cause doming of their skulls, leading to even more complications as the child develops. In adults and elderly patients, hydrocephalus is often seen as the poorly understood form called “normal pressure hydrocephalus” (NPH). This type of hydrocephalus shows increased ventricular size, but often the brain does not have an increase in intracranial pressure. However, the term “normal pressure” can be a misnomer as “intracranial pressure is not always normal in NPH” (15). This condition experiences symptoms similar to those of other neurological disorders including urinary incontinence, gait ataxia, progressive mental impairment and dementia. If caught in the early stages, NPH is considered “potentially reversible” (15). Often, NPH is misdiagnosed for the other neurological disorders with which it shares symptomatic similarities. As noted above, hydrocephalus can also be secondarily caused by other diseases such as TBI, PD, and AD.

1.2 Hydrocephalus Treatment Options

Currently, treatments for the disease include three main surgical methods. In endoscopic third ventriculostomy (ETV) the third ventricle is perforated to allow a bypass for blocked CSF in non-communicating hydrocephalus. Surgical implantation of a shunt into the ventricles allows drainage of excess CSF from the affected areas to alternative cavities of the body for reabsorption. Cauterization of the choroid plexus, the main producer of CSF, sometimes in conjunction with ETV, can slow down the accumulation of fluid (14, 16, 17). However, ETVs can be associated with bleeding, fever, and, in 10-30% of cases, a closure of the third ventricle puncture (18). In neonatal patients, ETVs have extremely low survival rates in infants 3 months or younger. This rate only improves to about 64% by 6 months of age (14). In most cases, failure of an ETV means the necessity of a shunt (19).

Cauterization of the choroid plexus is considered more effective than ETV alone and is most often performed on infants in developing countries where shunt infections are more prevalent and surgical care less available (20). However, this procedure is irreversible as it permanently destroys the majority of cells producing CSF, and the long-term effects are unknown.

Shunt implantation is the most common approved treatment. Still, due to children growing out of their shunts, shunt blockage, and infection, survival of a shunt lies around 70% at one-year post-implantation and drops to as low as 40% ten years post-implantation (19). In the adult population, while lower than in children, there is still a substantial percentage of the patients in need of shunt revisions. Infections can occur in as many as 30% of patients (19). While a select group of elderly NPH patients, when diagnosed early, experienced a reversal of symptoms upon shunt implantation, older patients are particularly susceptible to developing subdural hemorrhage, infection, and other postsurgical complications after shunt placement, with the benefits declining over time (15). These issues with shunt use only lead to more surgeries which can be detrimental for the physical and mental health of the patient and the financial state of the family. Therefore, the need for a long-term, efficient pharmaceutical treatment is critical to give these patients a more healthful, normal life.

1.3 The Choroid Plexus and CSF Flow

As previously stated, it is estimated that about 80% of CSF is produced by the choroid plexus (CP) with the remaining 20% coming from the brain parenchyma and interstitial fluid (21, 22). The CP is present in the third, fourth, and both lateral ventricles and is composed of a high-resistance barrier epithelium covering a network of leaky capillaries which allow ions and water to enter the space between the capillaries and the epithelium (21). However, these ions and water are strictly regulated by the CP epithelial (CPE) cells from entering the ventricular space. Multiple ion channels and co-transporters on either membrane of the polarized epithelial cells control transepithelial ion flux in both directions. As ions move across the epithelium, water follows in order to maintain osmotic concentrations, thus producing CSF (21). Therefore, this regulation allows the CP to control the amount and composition of CSF produced. The CSF is not a simple plasma filtrate. It contains a different ionic composition than plasma. For example, chloride concentrations are increased in the CSF (130 mM) compared to blood (106 mM), but potassium ions are higher in the blood (4.3 mM) than in the CSF (2.9 mM) (21). Currently, the main hypothesis of our lab is that aberrant regulation of these various transporters can result in the overproduction of CSF seen in the communicating form of hydrocephalus.

On a daily basis, the CP of an adult brain can produce over 0.5 liters of CSF at about 0.3 – 0.4 mL per minute. This fluid will circulate “from the lateral to the third ventricle via the foramen of Monro, on into the fourth ventricle via the aqueduct of Sylvius, and then out of the fourth ventricle via the midline foramen of Magendie, and the lateral foramina of Lushka” into the cisterns and subarachnoid space to cushion the brain until it is then absorbed back into the bloodstream at the arachnoid villi (22, 23). As CSF flows throughout the brain, it has been associated with not only bathing the various surfaces of the brain, but also works in tandem with another system to clear out wastes and accumulated proteins within the brain (24). This filtering occurs via the recently described glymphatic system located in the brain. Previously, it was believed that the body’s lymphatic system did not extend into the brain region. However, in 2012, data in rodent brains suggests that there is, in fact, a glymphatic system used by the brain to allow for fluid-clearance through the influx and efflux of the CSF and interstitial fluid (ISF) via water channels throughout the brain called aquaporin 4 (AQP4) (24). Indeed, several neurodegenerative diseases are associated with decreased clearance of protein aggregates from the brain, such as amyloid- β and neurofibrillary tangles in AD patients. Stroke and TBI have also been associated with decreases in glymphatic flow and clearance (24). Up until recently, the mechanism was unknown how the brain is able to clear these proteins from its extracellular space. However, with the discovery of the glymphatic system, we now have a basic, but still incomplete, understanding of how CSF and ISF flow is utilized to distribute and clear metabolites, proteins, and other constituents throughout the brain. Proper CSF flow is necessary for the glymphatic system to function. Therefore, assuming CSF flow is impaired in instances of hydrocephalus, particularly non-communicating hydrocephalus, we can also now infer how the disorder can potentially cause a decrease in glymphatic flow and an increase in waste accumulation in the brain parenchyma and CSF.

1.4 Transient Receptor Potential Vanilloid 4

One ion channel of interest in the control of the production of CSF is a mechano-, osmo-, chemo-, and temperature-sensitive, non-selective cation channel called Transient Receptor Potential Vanilloid 4 (TRPV4) (25-27). This ion channel is ubiquitous throughout the body, but specifically in neurons and the apical plasma membrane of the epithelial cells lining CP (21). TRPV4 is associated with the influx of calcium into the CP epithelium upon activation (21). This increase in

intracellular calcium can stimulate several different cascade pathways in a cell type-specific manner. In particular, the increase in intracellular calcium can be utilized to stimulate calcium-activated ion channels, such as potassium and chloride channels. Once activated, these channels can cause significant ion flux across the CP epithelium and subsequent water movement through AQP channels, thus allowing for the secretion or absorption of CSF into and out of the ventricles (13, 21, 28, 29).

In many regards, TRPV4 is considered a hub protein as it has many different types of stimuli that can subsequently activate several different pathways within the cell. The various stimuli that have been reported to activate TRPV4 include physical stress, such as shear, mechanical forces and pressure or flow alterations, osmotic changes, such as variation in ionic composition, temperature changes, such as that seen in inflammation, and chemical activators, such as cytokines and inflammatory mediators (25-28). Our laboratory is particularly interested in TRPV4 because we have shown that treatment with an antagonist of this channel ameliorates hydrocephalic development in an animal model of the disease.

1.5 Rat Model of Hydrocephalus

In order to study the effects of TRPV4 and various factors on hydrocephalus, our laboratory utilizes an in vivo rodent model called the Wistar polycystic kidney (Wpk) rat. This model is orthologous to the ciliopathy Meckel-Gruber Syndrome type 3 (MKS3), a rare genetic disorder characterized by renal cysts and central nervous system malformations, such as occipital encephaloceles (30-33). The development of MKS3 in humans involves a genetic single point mutation on chromosome 5 encoding the transmembrane protein 67 (TMEM67). An orthologous mutation in Wistar rats results in the Wpk rat with polycystic kidney disease (PKD) and severe, rapidly-progressing, communicating form of hydrocephalus in the homozygous recessive animals. These animals only live for about 3 weeks as their disease phenotypes progress (30, 31, 33). In terms of a reliable model, the homozygous Wpk rat is analogous to the congenital pediatric form of hydrocephalus.

Data suggest that the mutation in TMEM67 is a gene dose-dependent hydrocephalic phenotype as the heterozygous Wpk rats also develop a mild, asymmetrical form of hydrocephalus (33).

However, this hydrocephalus does not become physically evident until about one year of age, about half the lifespan of a normal wild type rat, at which time the afflicted animal begins to show evidence of decline including failure to groom. Because the condition does not appear until later in life, this form of hydrocephalus is considered a slowly-progressing type similar to that seen in adult hydrocephalic patients. It is also of note that the heterozygous animals do not develop the confounding variable of PKD like that seen in the homozygous animals (33).

Preliminary data from our lab suggest that treatment of hydrocephalic rats with a TRPV4 antagonist is able to prevent enlargement of the ventricles (Figure 1.1). Head dimensions were measured in normal and hydrocephalic rats. We found that the hydrocephalic rats treated with the TRPV4 antagonist RN1734 developed head dimensions comparable to those of the wild type both treated and untreated with the same antagonist (Figure 1.1) (34). From this data, we believe that TRPV4 antagonism may be used as a pharmaceutical alternative to invasive surgery. No significant adverse effects have been established so far in relation to TRPV4 inhibition. Several TRPV4 knockout models have been developed with mild abnormalities. The majority of knockout mouse phenotypes are related to osmotic regulation or sensory stimulation. However, none of these knockouts experience severe phenotypes detrimental to the animal (35, 36). In addition, currently, TRPV4 channel blockers have been approved for use in clinical trials by GlaxoSmithKline to assess safety and efficacy in treating problems with pulmonary gas transfer and respiration in human congestive heart failure patients (37). Together, this implies that utilization of TRPV4 antagonists as a treatment option may be a safe alternative with minimal adverse effects in patients.

1.6 Choroid Plexus Cell Line

In addition to the *in vivo* model, our laboratory has also performed extensive research on an *in vitro* model of CP cells. The porcine choroid plexus-Rheims (PCP-R) cell line is derived from primary porcine choroid plexus epithelial cells that were selected through a series of subcultivation steps until the viable continuous line was obtained (38). This cell line is a high resistance, barrier epithelium capable of mimicking the blood-CSF barrier seen *in vivo* (28, 38). The epithelial cells of the CP are interesting in that they are highly polarized, meaning important ion channels can be present on either the apical or basolateral sides. This polarity allows the cells to regulate the

composition and production of the CSF (21, 28). Much of the following research involves elucidating the characteristic localization of these imperative ion channels in the CP epithelium utilizing the PCP-R cell line.

As the cells are grown as a monolayer on supported Transwell filters, we are able to alter the composition of the apical and basolateral media by the addition of various compounds in order to influence changes to the expression of TRPV4 into the epithelial membrane. Mounting the monolayer of cells in Ussing chambers and using electrophysiology is a technique that allows for the measurement of the transepithelial ion flux and cellular permeability of the PCP-R cells in response to experimental compounds. Specifically, an agonist for TRPV4, GSK1016790A, is utilized to stimulate TRPV4 activation in the cells (28). We pretreat the cells with other compounds that either block or activate various channels or genes thought to be involved in the TRPV4 pathway prior to activating TRPV4 itself with its agonist. In this way, we are able to piece together how TRPV4 is involved in the regulation of these channels and how the various pathways can be utilized for future pharmacotherapies.

1.7 Ion Channels in the Choroid Plexus

The CP is home to many different ion channels capable of transporting a plethora of ions to and from the blood and CSF. While not all of these channels are believed to be modulated by TRPV4, many are still important to the production of CSF and maintenance of the epithelial cell.

Many of these ion channels are responsible for the unique polarity seen in CP cells as specific channels are located on either the apical or basolateral side. For example, the Na^+/K^+ ATPase pump responsible for transporting sodium out of the cell and potassium into the cell is normally found on the basolateral membrane in all other tissues of the body. However, in the CP, this pump is found on the apical membrane and is believed to play a major role in establishing the ion gradient responsible for ion movement and CSF production (21).

In addition to the Na^+/K^+ ATPase, another ion channel normally found on the basolateral membrane in other tissues but found on the apical membrane of the CP is the $\text{Na}^+/\text{K}^+/\text{2Cl}^-$ co-

transporter NKCC1 (21). This cotransporter is responsible for moving sodium, potassium, and two chloride ions across the cell membrane. In particular, NKCC1 has been reported to play a major role in the production of CSF (7, 39). In the WNK signaling pathway, the intracellular Ste20-Related Proline/Alanine-Rich Kinase (SPAK) and Odd-skipped-related 1 (OSR1) play an integral role for the regulation of various ion channels, importantly including the activation of NKCCs and the sodium and chloride influx co-transporter (NCC) as well as the the inhibition of the potassium and chloride efflux co-transporters (KCCs) (7, 40). SPAK has also been reported to be activated in response to increases in NF- κ B binding, a transcription factor involved in the regulation of inflammatory pathways; this pathway has been implemented in the hypersecretion of CSF through the binding and phosphorylation of NKCC1 at the apical membrane, potentially linking it to hydrocephalus (7, 40). The multitude of related pathways through which SPAK is involved in ion transportation makes this kinase an important target for current ion transport studies.

In all tissues studied to date, NKCC1 activation results in influx of sodium, potassium, and chloride into the intracellular space. However, recent studies have suggested that when ion gradients have reached favorable intracellular concentrations, NKCC1 can be stimulated to change direction and instead transport its ions out of the cell and into the ventricular space (41). This change in direction has been postulated to be responsible for the outward flow of water necessary for CSF production. Much of the regulation for this change in direction is unknown and highly controversial. However, in order to establish the change in the ion gradient responsible for switching NKCC1's directionality, there must be other channels involved to allow ions to enter and exit the cell. Due to the fact that TRPV4 is known for bringing calcium into the cell, it is feasible that the channels involved include calcium-sensitive channels, such as potassium and chloride channels.

Among the potassium channels, there are three different types of calcium-sensitive channels: the large or big conductance potassium channel (BK; KCa1.1), the intermediate conductance potassium channel (IK; KCa3.1; KCNN4), and the three small conductance potassium channels (SK1, SK2, SK3; KCa2.1, 2.2, 2.3) (42). While there is currently not concrete evidence as to the localization of these channels, some data suggest that the BK channel as well as the KCNN4c isoform of the IK channel exist on the apical membrane (28, 43-46). Therefore, the secretion of

potassium ions from these channels into the ventricular space can result in the subsequent movement of water and thus play a role in the production of CSF.

Among the calcium-sensitive chloride channels reported to interact with TRPV4 is the “transmembrane protein with unknown function 16A” (TMEM16A) (47-49). TMEM16A activation leads to an influx of chloride ions rather than an efflux of ions as seen in the potassium channels (49). Due to this influx of ions, it is unlikely that TMEM16A is directly resulting in the production of CSF as water would then be transported inside the cell. However, it is possible that TMEM16A is a regulator for CSF absorption for this very reason. It is also possible that the influx of chloride and subsequent increase in intracellular chloride could stimulate other ion channels, not dissimilar to how TRPV4 calcium influx has the potential to activate TMEM16A itself. For example, NKCC1, being a chloride co-transporter, could be stimulated to reverse direction of ion flux in response to TMEM16A’s increasing of intracellular chloride. Together, this shows how connected the various ion channels of the CP are and how they can potentially interact in order to regular CSF production and absorption.

1.8 Inflammation and Cytokines

Inflammation in the brain can be caused by a number of chemical and physical means, including neuronal injury from intracranial trauma, tumors, infection, hemorrhage, and aberrant protein accumulation due to insufficient clearance (5, 7, 50-54). The initiation of inflammation can occur when these different types of brain injury trigger the activation of microglia, the innate immune cells of the central nervous system (CNS). Microglia mediate immune responses and are responsible for the release of pro- and anti-inflammatory cytokines as well as the accumulation of inflammatory mediators at the site of injury (50, 51, 55).

Aberrant protein resulting in increases in inflammatory mediators is common in neurodegenerative disease; amyloid- β plaques from irregular processing of amyloid precursor protein (APP) and neurofibrillary tangles, aggregates of the protein tau, are found in AD patients (50). Alpha-synuclein deposits called Lewy bodies are hallmarks of PD and dementia with Lewy bodies (56). In addition to protein accumulations, physical injury to the cranium, as in TBI, results in cellular

stress and subsequent activation of the inflammatory immune response by astrocytes and microglia (51). Such inflammation can be associated with the development of hydrocephalus, with several of the inflammatory mediators shared among the aforementioned diseases upon distress. Among the pro-inflammatory cytokines upregulated in neurodegenerative states, interleukin (IL)-1 β and tumor necrosis factor (TNF)- α are two of the most prominent. Anti-inflammatory cytokines are also found in hydrocephalic-associated diseases, including IL-10 and IL-4. Finally, some cytokines are considered “paradoxical” in that they are implicated in both pro- and anti-inflammatory effects. TGF- β and IL-6 have both been found to cause these conflicting effects (51, 57-62).

Production of cytokines occurs when one of several Toll-like receptors (TLRs) are stimulated at the plasma membrane. TLRs vary between species, but most mammals are known to express a TLR family consisting of 10 different receptors (TLR1-TLR10) (63). Not all of these TLRs are stimulated by the same ligand. For example, TLR3 ligands include double-stranded RNA often present during viral infection (63). TLR4, however, is more often associated with pro-inflammatory ligands such as heat-shock proteins or “danger signals” which can also stimulate macrophages and dendritic cells to begin pro-inflammatory cytokine secretion (63). Upon stimulation, TLRs can activate downstream signaling pathways to initiate cytokine production. Indeed, TLR4-deficient mice were shown to have decreases in inflammatory cytokine production. The same results were seen in mice deficient in TLR1 (63). Cytokines have also been reported to regulate the expression TLRs. For example, one inflammatory cytokine, macrophage migration inhibitory factor (MIF), is believed to increase expression of TLR4 as there was a decrease in the receptor in MIF-deficient mice (63). Several cytokines, including IL-1 β and TNF- α , induce the expression of the gene encoding TLR2 in macrophages (63). Other studies have found specific TLRs upregulated in response to various cytokines. As an example, a leukemia cell line was treated with IL-6 for 6 hours resulting in an increased expression in all TLRs, but specifically a 12-fold increase in TLR7 (64). Therefore, it can be said that TLRs not only induce the production of cytokines, but cytokines can also act as ligands and activators of TLRs.

In the canonical pathway, stimulation of TLRs by inflammatory mediators or cytokines, such as IL-1 β or TNF- α , leads to the activation of the inflammatory signaling pathway NF- κ B through the use of a MyD88-dependent signaling cascade, termed the I κ B kinase (IKK) complex (65).

Phosphorylation of NF- κ B by IKK allows the nuclear factor to be dissociated from its regulator protein, I κ B, and transported into the nucleus, where it can begin transcription of several inflammatory cytokines (65, 66). Hence, NF- κ B is a major contributor towards inflammation in the body.

1.9 TRPV4 and Inflammatory Mediators

Activation of TRPV4 can occur at temperatures above approximately 27°C (27). Inflammation can result in an increase in temperature at the affected areas. Therefore, inflammation has the potential to activate TRPV4 directly and indirectly. Indeed, it has been thoroughly reported that the inflammatory lipid endocannabinoid anandamide (AEA) and its metabolite arachidonic acid (AA) are associated with activation of TRPV4 (27). AA can be further metabolized through one of three pathways. The first utilizes the enzymes cyclooxygenases (COX) 1 and 2 to produce the proinflammatory prostaglandins, prostacyclin, and thromboxane A2 (67, 68). The second uses one of several lipoxygenase (LOX) enzymes to produce pro-inflammatory leukotrienes, lipoxins, and hydroxyeicosatetraenoic acids (HETEs) (69). Finally, cytochrome P(CYP)-450 epoxygenases metabolize AA into epoxyeicosatrienoic acids (EETs) (70). These metabolites of AA are also believed to stimulate TRPV4 activity (27, 71). In particular, EETs have most often been cited as the predominant activator of TRPV4 within the AA pathway (27, 51, 72, 73). However, there is some controversy as to which isoform of the EETs is the most responsible (74). Therefore, inflammation initiated through inflammatory mediators, such as AA and its metabolites, can activate TRPV4 and lead to downstream effects in ion flux and CSF production. While the scope of inflammatory factors capable of activating TRPV4 is unclear, there is potential for those involved with the ion channel to also play a role in neurodegenerative disease and hydrocephalus.

1.10 Translational Potential

Understanding one of the most common brain disorders (how it develops, how it can be contained or reversed, etc.) is vital for the millions of people worldwide affected by hydrocephalus. Therefore, developing and characterizing both in vitro and in vivo models to better this understanding of not only the disease, but also the molecular components, will greatly advance research going forward.

In addition to this, developing a comprehensive mechanism for how ion channels and CSF regulation affect and are affected by hydrocephalus and other neurological disorders can provide a basis for future treatment options. In particular, TRPV4 is implicated in several pathways for ion channel activation and also has the potential to be acted on secondarily by the immune response to injury and disease, making TRPV4 a target of interest in the study of hydrocephalus.

For my dissertation research, I have been involved in several aspects of the studies directed toward understanding CSF production and developing drugs to treat hydrocephalus. Some of this work has been published and will form chapters of this thesis. Each of these publications have a preface explaining how I contributed towards the published work and the findings associated with those data.

In Chapter 2, I will elaborate on the characterization and development of the Wpk rat hydrocephalic model in the published article, “Hydrocephalus in a rat model of Meckel Gruber syndrome with a TMEM67 mutation” (33). Chapter 3 will focus on the characterization of the PCP-R in vitro model. In the article “Activation of TRPV4 Stimulates Transepithelial Ion Flux in a Porcine Choroid Plexus Cell Line,” we elucidate the relationship between TRPV4 and calcium-sensitive potassium channels (28). Chapter 4 encompasses the manuscript in final preparation for submission titled, “Cytokine and inflammatory mediator effects on hydrocephalus and TRPV4 function in the choroid plexus.” This article focuses on how TRPV4 is affected by inflammatory cytokines and mediators associated with hydrocephalus as well as other neurological disorders.

In addition to these manuscripts, Chapter 5 contains additional data I have obtained that have not yet been published but remain pertinent to my dissertation research. These data include further characterization of the in vivo models by showing the expression of TRPV4 and the tight junctional protein, claudin-1, in the rat model. I compared these images from the hydrocephalic rat to its wild type counterpart as well as to the hydrocephalic rat treated with the TRPV4 antagonist.

The in vitro PCP-R model is also further characterized in Chapter 5 through RT-PCR with which the presence of additional ion channels and genes within the CP epithelia are clarified. Data expounding other pathways potentially involving TRPV4 is also included, such as the WNK

signaling pathway and its associated ion channels. Finally, I observed whether microglia activation is present in adult and juvenile Wpk brain sections in order to determine the presence of inflammation in these animals.

These data provide a better understanding for the development of hydrocephalus. They also illuminate the impact of the ion channel TRPV4 in the choroid plexus by its ability to modulate and be modulated by various ion channels and mediators. Together, this research establishes the connection between hydrocephalus and TRPV4, bringing the field one step closer to finding an efficient pharmacotherapy for the disease.

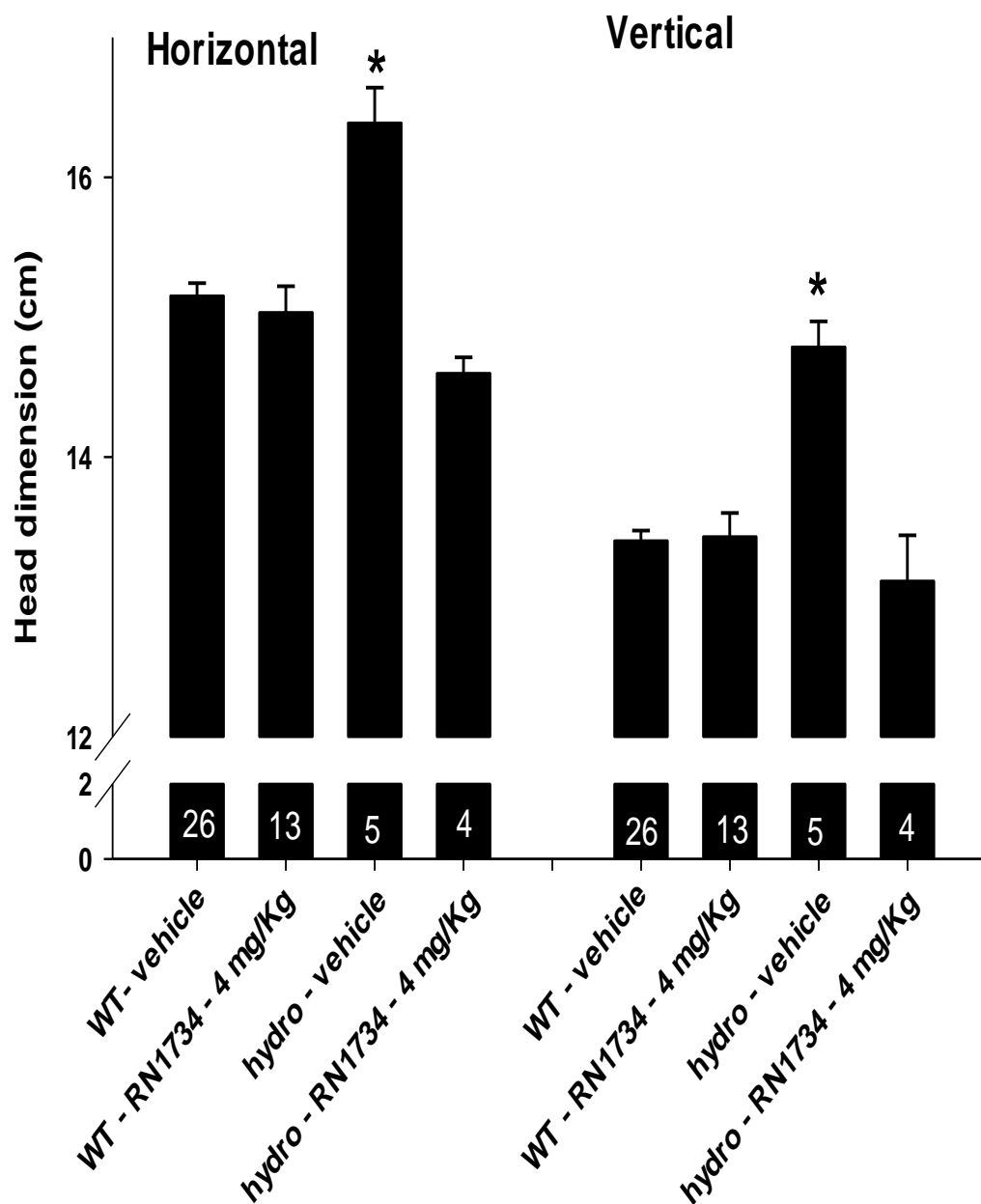


Figure 1.1 Head measurements post-TRPV4 antagonist treatment in rats at P15.

Wild-type (WT) and *TMEM67*(*-/-*) hydrocephalic pups were treated with RN1734, a TRPV4 antagonist, by daily i.p. injections from day 7 to 15. Hydrocephalus caused an increase in both horizontal and vertical head dimensions (* = $p < 0.0001$). This increase was inhibited by drug treatment. The numbers at the base of the columns are the number (n) of animals. Figure is unpublished data from the Blazer-Yost and Gattone laboratories.

1.11 References

1. Kovacs, G. (2016). Molecular pathological classification of neurodegenerative diseases: Turning towards precision medicine. *International Journal Of Molecular Sciences*, 17(2), 189.
2. Zhao, J., Chen, Z., Xi, G., Keep, R., and Hua, Y. (2014). Deferoxamine attenuates acute hydrocephalus after traumatic brain injury in rats. *Translational Stroke Research*, 5(5), 586-594.
3. Isaacs, A., Riva-Cambrin, J., Yavin, D., Hockley, A., Pringsheim, T., and Jette, N. et al. (2018). Age-specific global epidemiology of hydrocephalus: Systematic review, meta-analysis and global birth surveillance. *PLOS ONE*, 13(10), e0204926.
4. Erickson, K., Baron, I. and Fantie, B. (2001). Neuropsychological functioning in early hydrocephalus: Review from a developmental perspective. *Child Neuropsychology*, 7(4), pp.199-229.
5. Vadivelu, S., Rekate, H., Esernio-Jenssen, D., Mittler, M. and Schneider, S. (2016). Hydrocephalus associated with childhood nonaccidental head trauma. *Neurosurgical Focus*, p.E8.
6. Tully, H. and Dobyns, W. (2014). Infantile hydrocephalus: A review of epidemiology, classification and causes. *European Journal of Medical Genetics*, 57(8), pp.359-368.
7. Karimy, J., Zhang, J., Kurland, D., Theriault, B., Duran, D., and Stokum, J. et al. (2017). Inflammation-dependent cerebrospinal fluid hypersecretion by the choroid plexus epithelium in posthemorrhagic hydrocephalus. *Nature Medicine*, 23(8), 997-1003.
8. Krauss, J., Regel, J., Droste, D., Orszagh, M., Borremans, J. and Vach, W. (1997). Movement disorders in adult hydrocephalus. *Movement Disorders*, 12(1), pp.53-60.
9. Golomb, J., Wisoff, J., Miller, D. C., Boksay, I., Kluger, A., Weiner, H., Salton, J., and Graves, W. (2000). Alzheimer's disease comorbidity in normal pressure hydrocephalus: prevalence and shunt response. *Journal of Neurology, Neurosurgery & Psychiatry*, 68(6), pp.778-781.
10. Jankovic, J., Newmark, M. and Peter, P. (1986). Parkinsonism and acquired hydrocephalus. *Movement Disorders*, 1(1), pp.59-64.

11. Kushel', Y., Belova, Y. and Tekoev, A. (2017). Intramedullary spinal cord tumors and hydrocephalus: an analysis of the results of surgical treatment in 541 patients. *Voprosy neurokhirurgii imeni N.N. Burdenko*, 81(4), p.56.
12. Lin, C. and Riva-Cambrin, J. (2015). Management of posterior fossa tumors and hydrocephalus in children: a review. *Child's Nervous System*, 31(10), pp.1781-1789.
13. Lu, K., Huang, T., Tsai, Y. and Yang, Y. (2017). Transient receptor potential vanilloid type 4 channels mediate Na-K-Cl-co-transporter-induced brain edema after traumatic brain injury. *Journal of Neurochemistry*, 140(5), pp.718-727.
14. Groat, J. and Neumiller, J. (2013). Review of the treatment & management of hydrocephalus. *US Pharm*, 38(3), pp.HS8-HS11.
15. Shprecher, D., Schwalb, J., and Kurlan, R. (2008). Normal pressure hydrocephalus: diagnosis and treatment. *Current Neurology and Neuroscience Reports*, 8(5), 371-376.
16. Cinalli, G. (2005). Endoscopic Third Ventriculostomy. In *Pediatric Hydrocephalus* (pp. 361-388). N.p.: Springer Milan.
17. Simon, T. D., Riva-Cambrin, J., Srivastava, R., Bratton, S. L., Dean, J. M., and Kestle, J. R. (2008). Hospital care for children with hydrocephalus in the United States: Utilization, charges, comorbidities, and deaths. *Journal of Neurosurgery: Pediatrics*, 1(2), 131-137.
18. Mahapatra, A., Mehr, S., Singh, D., Tandon, M., Ganjoo, P., and Singh, H. (2011). Ostomy closure and the role of repeat endoscopic third ventriculostomy (re-ETV) in failed ETV procedures. *Neurology India*, 59(6), 867-873.
19. Vinchon, M., Rekate, H., and Kulkarni, A. V. (2012). Pediatric hydrocephalus outcomes: A review. *Fluids and Barriers of the CNS*, 9(1), 18.
20. Warf, B. C. (2005). Comparison of endoscopic third ventriculostomy alone and combined with choroid plexus cauterization in infants younger than 1 year of age: a prospective study in 550 African children. *Journal of Neurosurgery: Pediatrics*, 103(6), 475-481.
21. Damkier, H., Brown, P., and Praetorius, J. (2013). Cerebrospinal fluid secretion by the choroid plexus. *Physiological Reviews*, 93(4), 1847-1892.
22. Brinker, T., Stopa, E., Morrison, J., and Klinge, P. (2014). A new look at cerebrospinal fluid circulation. *Fluids And Barriers Of The CNS*, 11(1), 10.
23. Brodbelt, A., and Stoodley, M. (2007). CSF pathways: a review. *British Journal Of Neurosurgery*, 21(5), 510-520.

24. Rasmussen, M., Mestre, H., and Nedergaard, M. (2018). The glymphatic pathway in neurological disorders. *The Lancet Neurology*, *17*(11), 1016-1024.
25. Liedtke, W., Choe, Y., Martí-Renom, M. A., Bell, A. M., Denis, C. S., Sali, A., Hudspeth, A.J., Friedman, J.M., and Heller, S. (2000). Vanilloid Receptor–Related Osmotically Activated Channel (VR-OAC), a candidate vertebrate osmoreceptor. *Cell*, *103*(3), 525-535.
26. Strotmann, R., Harteneck, C., Nunnenmacher, K., Schultz, G., and Plant, T. D. (2000). OTRPC4, a nonselective cation channel that confers sensitivity to extracellular osmolarity. *Nature Cell Biology*, *2*, 695-702.
27. Nilius, B., Vriens, J., Prenen, J., Droogmans, G., and Voets, T. (2004). TRPV4 calcium entry channel: A paradigm for gating diversity. *AJP: Cell Physiology*, *286*(2), C195-C205.
28. Preston, D., Simpson, S., Halm, D., Hochstetler, A., Schwerk, C., Schroten, H., and Blazer-Yost, B. (2018). Activation of TRPV4 stimulates transepithelial ion flux in a porcine choroid plexus cell line. *American Journal Of Physiology-Cell Physiology*, *315*(3), C357-C366.
29. Toft-Bertelsen, T., Križaj, D. and MacAulay, N. (2017). When size matters: transient receptor potential vanilloid 4 channel as a volume-sensor rather than an osmo-sensor. *The Journal of Physiology*, *595*(11), pp.3287-3302.
30. Smith, U. M., Consugar, M., Tee, L. J., McKee, B. M., Maina, E. N., Whelan, S., and Morgan, N. V. (2006). The transmembrane protein meckelin (MKS3) is mutated in Meckel-Gruber syndrome and the wpk rat. *Nature Genetics*, *38*(2), 191-196.
31. Gattone, V., Tourkow, B., Trambaugh, C., Yu, A., Whelan, S., Phillips, C., Harris, P. and Peterson, R. (2004). Development of multiorgan pathology in the wpk rat model of polycystic kidney disease. *The Anatomical Record*, *277A*(2), pp.384-395.
32. Kheir, A., Imam, A., Omer, I., Hassam, I., Elamin, S., and Awadalla, E. et al. (2012). Meckel-Gruber syndrome: A rare and lethal anomaly. *Sudan Journal Of Paediatrics*, *12*(1), 93-96.
33. Shim, J., Territo, P., Simpson, S., Watson, J., Jiang, L., Riley, A., McCarthy, B., and Blazer-Yost, B. (2019). Hydrocephalus in a rat model of Meckel Gruber syndrome with a TMEM67 mutation. *Scientific Reports*, *9*(1).
34. Simpson, S., Scherer, A., Fulkerson, D., and Blazer-Yost, B. (2017). TRPV4 expression in hydrocephalic rat choroid plexus. Abstract *FASEB J.* 31S: A1007.34.

35. Sands, J. M., Mount, D. B., and Layton, H. E. (2013). Core concepts in the disorders of fluid, electrolytes and acid-base balance (p. 7). N.p.: *Springer Science & Business Media*.
36. Trpv4. (2017). In *Mouse Genome Informatics*. Retrieved April 30, 2017, from <http://www.informatics.jax.org/marker/MGI:1926945>
37. A study to evaluate the effect of the Transient Receptor Potential Vanilloid 4 (TRPV4) channel blocker, GSK2798745, on pulmonary gas transfer and respiration in patients with congestive heart failure. (2017). In *ClinicalTrials.gov*. Retrieved April 30, 2017, from <https://clinicaltrials.gov/ct2/show/study/NCT02497937>
38. Schrotten, M., Hanisch, F., Quednau, N., Stump, C., Riebe, R., and Lenk, M. et al. (2012). A novel porcine in vitro model of the blood-cerebrospinal fluid barrier with strong barrier function. *Plos ONE*, 7(6), e39835.
39. Steffensen, A., Oernbo, E., Stoica, A., Gerkau, N., Barbuskaite, D., and Tritsarlis, K. et al. (2018). Cotransporter-mediated water transport underlying cerebrospinal fluid formation. *Nature Communications*, 9(1).
40. Yan Y, Dalmaso G, Nguyen HTT, Obertone TS, Sitaraman SV, et al. (2009) Ste20-Related Proline/Alanine-Rich Kinase (SPAK) regulated transcriptionally by hyperosmolarity is involved in intestinal barrier function. *PLoS ONE* 4(4): e5049.
41. Delpire, E., and Gagnon, K. (2018). Elusive role of the Na-K-2Cl cotransporter in the choroid plexus. *American Journal Of Physiology-Cell Physiology*.
42. Vergara, C., Latorre, R., Marrion, N., and Adelman, J. (1998). Calcium-activated potassium channels. *Current Opinion In Neurobiology*, 8(3), 321-329.
43. Basalingappa, K., Rajendran, V., and Wonderlin, W. (2011). Characteristics of Kcnn4 channels in the apical membranes of an intestinal epithelial cell line. *American Journal Of Physiology-Gastrointestinal And Liver Physiology*, 301(5), G905-G911.
44. Halm, S., Liao, T., and Halm, D. (2006). Distinct K⁺ conductive pathways are required for Cl⁻ and K⁺ secretion across distal colonic epithelium. *American Journal Of Physiology-Cell Physiology*, 291(4), C636-C648.
45. Singh, S., O'Hara, B., Talukder, J., and Rajendran, V. (2012). Aldosterone induces active K⁺ secretion by enhancing mucosal expression of Kcnn4c and Kcma1 channels in rat distal colon. *American Journal Of Physiology-Cell Physiology*, 302(9), C1353-C1360.

46. Millar, I., Bruce, J., and Brown, P. (2007). Ion channel diversity, channel expression and function in the choroid plexuses. *Cerebrospinal Fluid Research*, 4(1), 8.
47. Huang, F., Wong, X., and Jan, L. (2011). International union of basic and clinical pharmacology. LXXXV: Calcium-activated chloride channels. *Pharmacological Reviews*, 64(1), 1-15.
48. Takayama, Y., Shibasaki, K., Suzuki, Y., Yamanaka, A., and Tominaga, M. (2014). Modulation of water efflux through functional interaction between TRPV4 and TMEM16A/anoctamin 1. *The FASEB Journal*, 28(5), 2238-2248.
49. Wang, H., Zou, L., Ma, K., Yu, J., Wu, H., Wei, M., and Xiao, Q. (2017). Cell-specific mechanisms of TMEM16A Ca²⁺-activated chloride channel in cancer. *Molecular Cancer*, 16(1).
50. Wyss-Coray, T., and Mucke, L. (2002). Inflammation in neurodegenerative disease—a double-edged sword. *Neuron*, 35, 419-432.
51. Corrigan, F., Mander, K. A., Leonard, A. V., and Vink, R. (2016). Neurogenic inflammation after traumatic brain injury and its potentiation of classical inflammation. *Journal of Neuroinflammation*, 13(264).
52. Kant, S., Stopa, E., Johanson, C., Baird, A. and Silverberg, G. (2018). Choroid plexus genes for CSF production and brain homeostasis are altered in Alzheimer's disease. *Fluids and Barriers of the CNS*, 15(1).
53. Ott, B., Jones, R., Daiello, L., de la Monte, S., Stopa, E., Johanson, C., Denby, C. and Grammas, P. (2018). Blood-cerebrospinal fluid barrier gradients in mild cognitive impairment and Alzheimer's disease: Relationship to inflammatory cytokines and chemokines. *Frontiers in Aging Neuroscience*, 10.
54. Block, M. and Hong, J. (2005). Microglia and inflammation-mediated neurodegeneration: Multiple triggers with a common mechanism. *Progress in Neurobiology*, 76(2), pp.77-98.
55. Cao, Q., Karthikeyan, A., Dheen, S., Kaur, C., and Ling, E. (2017). Production of proinflammatory mediators in activated microglia is synergistically regulated by Notch-1, glycogen synthase kinase (GSK-3 β) and NF- κ B/p65 signalling. *PLOS ONE*, 12(10), e0186764.
56. Spillantini, M., Schmidt, M., Lee, V., Trojanowski, J., Jakes, R., and Goedert, M. (1997). α -Synuclein in Lewy bodies. *Nature*, 388(6645), 839-840.

57. Lee, P., Monaco, E., and Friedlander, R. (2013). Blocking TGF- β activity and associated inflammation may halt hydrocephalus. *Neurosurgery*, 73(6), N13-N14.
58. Sosvorova, L., Mohapl, M., Vcelak, J., Hill, M., Vitku, J., and Hampl, R. (2015). The impact of selected cytokines in the follow-up of normal pressure hydrocephalus. *Physiological Research*, 64, S283-S290.
59. Woodcock, T., and Morganti-Kossmann, M. C. (2013). The role of markers of inflammation in traumatic brain injury. *Frontiers in Neurology*, 4(18).
60. Herrero, M., Estrada, C., Maatouk, L., and Vyas, S. (2015). Inflammation in Parkinson's disease: role of glucocorticoids. *Frontiers in Neurology*, 9(32).
61. Azizi, G., Navabi, S. S., Al-Shukaili, A., Seyedzadeh, M. H., Yazdani, R., and Mirshafiey, A. (2015). The role of inflammatory mediators in the pathogenesis of Alzheimer's disease. *Sultan Qaboos University Medical Journal*, 15(3), e305-e316.
62. Scheller, J., Chalaris, A., Schmidt-Arras, D., and Rose-John, S. (2011). The pro- and anti-inflammatory properties of the cytokine interleukin-6. *Biochimica Et Biophysica Acta (BBA) - Molecular Cell Research*, 1813(5), 878-888.
63. Takeda, K., Kaisho, T., and Akira, S. (2003). Toll-like receptors. *Annual Review Of Immunology*, 21(1), 335-376.
64. Zarembek, K., and Godowski, P. (2002). Tissue expression of human toll-like receptors and differential regulation of toll-like receptor mRNAs in leukocytes in response to microbes, their products, and cytokines. *The Journal Of Immunology*, 168(2), 554-561.
65. Lawrence, T. (2009). The nuclear factor NF κ -B pathway in inflammation. *Cold Spring Harbor Perspectives In Biology*, 1(6), a001651-a001651.
66. Matsusaka, T., Fujikawa, K., Nishio, Y., Mukaida, N., Matsushima, K., Kishimoto, T., and Akira, S. (1993). Transcription factors NF-IL6 and NF-kappa B synergistically activate transcription of the inflammatory cytokines, interleukin 6 and interleukin 8. *Proceedings Of The National Academy Of Sciences*, 90(21), 10193-10197.
67. Ricciotti, E., and FitzGerald, G. (2011). Prostaglandins and inflammation. *Arteriosclerosis, Thrombosis, And Vascular Biology*, 31(5), 986-1000.
68. Palumbo, S. (2017). Pathogenesis and progression of multiple sclerosis: the role of arachidonic acid-mediated neuroinflammation. *Multiple Sclerosis: Perspectives in Treatment and Pathogenesis*, pp.111-124.

69. Trachte, G., Lefer, A., Aharony, D., and Smith, J. (1979). Potent constriction of cat coronary arteries by hydroperoxides of arachidonic acid and its blockade by anti-inflammatory agents. *Prostaglandins*, 18(6), 909-914.
70. Shahabi, P., Siest, G., Meyer, U. and Visvikis-Siest, S. (2014). Human cytochrome P450 epoxygenases: Variability in expression and role in inflammation-related disorders. *Pharmacology & Therapeutics*, 144(2), pp.134-161.
71. Node, K., Huo, Y., Ruan, X., Yang, B., Spiecker, M., Ley, K., and Zeldin, D. C. (1999). Anti-inflammatory properties of cytochrome P450 epoxygenase-derived eicosanoids. *Science*, 285(5431), 1276-1279.
72. Watanabe, H., Vriens, J., Prenen, J., Droogmans, G., Voets, T. and Nilius, B. (2003). Anandamide and arachidonic acid use epoxyeicosatrienoic acids to activate TRPV4 channels. *Nature*, 424(6947), pp.434-438.
73. Cao, S., Anishkin, A., Zinkevich, N., Nishijima, Y., Korishettar, A., Wang, Z., Fang, J., Wilcox, D. and Zhang, D. (2018). Transient receptor potential vanilloid 4 (TRPV4) activation by arachidonic acid requires protein kinase A-mediated phosphorylation. *Journal of Biological Chemistry*, 293(14), pp.5307-5322.
74. Filosa, J., Yao, X. and Rath, G. (2013). TRPV4 and the regulation of vascular tone. *Journal of Cardiovascular Pharmacology*, 61(2), pp.113-119.

CHAPTER 2. HYDROCEPHALUS IN A RAT MODEL WITH A TMEM67 MUTATION

2.1 Preface

In this journal article submitted to *Scientific Reports* in April of 2018 and accepted in December of the same year, I was named as co-author for conducting and analyzing experiments included in the article. Specifically, I contributed by performing hematoxylin and eosin (H&E) staining of the Wpk rat kidneys in wild type (WT), heterozygous (TMEM67^{+/-}), and homozygous (TMEM67^{-/-}) juveniles at birth (P0) and at the day of sacrifice (P15) to show the severity of the PKD in the TMEM67^{-/-} animals compared to normal kidneys in the WT and TMEM67^{+/-} animals (Figure 2.2e). I also provided the H&E staining of adult kidneys in WT and TMEM67^{+/-} Wpk rats at P389 and P460 to illustrate that even in the older animals, there is no PKD phenotype in either the WT or TMEM67^{+/-} animals (Figure 2.2f). These data provided important characteristics of the animal model.

Further H&E staining I provided included the WT, TMEM67^{+/-}, and TMEM67^{-/-} P15 and the WT and TMEM67^{+/-} P389 and P460 sections of the aqueduct of Sylvius (Figure 2.6a). These data lead to the conclusion that our rat model has a communicating form of hydrocephalus as no stenosis was observed in the aqueducts.

The last of the data that I conducted included the immunofluorescence confocal images taken of P0 and P15 Wpk choroid plexus in the lateral ventricles of WT and TMEM67^{-/-} animals (Figure 2.8). In this experiment, I stained for aquaporin-1 and claudin-1 in order to determine whether the water channel and junctional protein were mislocalized in the affected animals. From these data, we were able to make the conclusion that the polarity of the CP cells is maintained in the affected animals as compared to the WT animals. Negative controls were also included in this figure to confirm the results.

In addition to the data included in this article, I also contributed by writing the methods for both the “Hematoxylin and Eosin” and “Immunofluorescence” sections. Finally, I assisted with reviewing and editing the manuscript multiple times during the initial writing and revision periods.

2.2 Hydrocephalus in a rat model of Meckel Gruber syndrome with a TMEM67 mutation

Joon W. Shim^{1,2,3}, Paul R. Territo⁴, Stefanie Simpson¹, John C. Watson¹, Lei Jiang³, Amanda A. Riley⁴, Brian McCarthy⁴, Scott Persohn⁴, Daniel Fulkerson⁵ and Bonnie L. Blazer-Yost^{1*}

¹Department of Biology, Indiana University - Purdue University Indianapolis, IN 46202, USA.

²Department of Medicine, Boston University School of Medicine, Boston, MA 02118, USA.

³Biomedical Engineering Program, Weisberg Division of Engineering, College of Information Technology and Engineering, Marshall University, Huntington, WV 25755, USA. ⁴Department of Radiology and Imaging Sciences, Indiana University School of Medicine, Indianapolis, IN 46202, USA.; ⁵Department of Neurological Surgery, Indiana University School of Medicine, Indianapolis, IN 46202, USA. Correspondence and requests for materials should be addressed to B.B.-Y. (email: bblazer@iupui.edu)

2.3 Abstract

Transmembrane protein 67 (TMEM67) is mutated in Meckel Gruber Syndrome type 3 (MKS3) resulting in a pleiotropic phenotype with hydrocephalus and renal cystic disease in both humans and rodent models. The precise pathogenic mechanisms remain undetermined. Herein it is reported for the first time that a point mutation of TMEM67 leads to a gene dose-dependent hydrocephalic phenotype in the Wistar polycystic kidney (Wpk) rat. Animals with TMEM67 heterozygous mutations manifest slowly progressing hydrocephalus, observed during the postnatal period and continuing into adulthood. These animals have no overt renal phenotype. The TMEM67 homozygous mutant rats have severe ventriculomegaly as well as severe polycystic kidney disease and die during the neonatal period. Protein localization in choroid plexus epithelial cells indicates that aquaporin 1 and claudin-1 both remain normally polarized in all genotypes. The choroid plexus epithelial cells may have selectively enhanced permeability as evidenced by increased Na⁺, K⁺ and Cl⁻ in the cerebrospinal fluid of the severely hydrocephalic animals. Collectively, these

results suggest that TMEM67 is required for the regulation of choroid plexus epithelial cell fluid and electrolyte homeostasis. The Wpk rat model, orthologous to human MKS3, provides a unique platform to study the development of both severe and mild hydrocephalus.

2.4 Introduction

Hydrocephalus may be congenital or develop as a consequence of trauma, infection, venous occlusion, tumors, or intracranial hemorrhage resulting in cerebrospinal fluid (CSF) overproduction, malabsorption, or mechanical blockage of flow. Hydrocephalus is observed in approximately 1 in 1000 births but may occur at any age including a poorly understood “normal pressure hydrocephalus” found in the elderly (1). Depending on severity and duration, hydrocephalus may cause developmental delay, progressive neurological decline, blindness, impaired motor function, urinary incontinence, dementia, or death.

The classic but oversimplified definition of hydrocephalus describes two types, communicating and obstructive (2-3). In communicating hydrocephalus, the connections between the ventricles are open, but there is excess fluid resulting from an imbalance of CSF secretion, movement and/or absorption (4-6). Obstructive hydrocephalus results from a mechanical blockage of the circulation of CSF (7). Hydrocephalus is commonly treated by surgical placement of a shunt to divert the CSF (7) or an endoscopic third ventriculostomy (ETV) to create a channel bypassing a site of obstruction. More recently a growing number of infants are treated with an ETV and choroid plexus cauterization (8).

Ciliopathies are a spectrum of genetic disorders where proteins found in the primary cilia are mutated. The primary cilium is a cellular appendage on the apical membrane of polarized cells that functions as a mechano- or chemo-receptor and also plays a role in the formation of left-right asymmetry during development (9). The most common of the ciliopathies is polycystic kidney disease (PKD). Other ciliopathies such as nephronophthisis (NPHP), Joubert syndrome (JS), Meckel-Gruber Syndrome (MKS), and Bardet Biedl Syndrome (BBS), all have central nervous system defects (10-11). The cilia in these diseases show abnormalities, including truncation,

elongation or diminished numbers. How different ciliary phenotypes result in functional defects of the nervous system remains poorly characterized.

The Wpk rat, carrying a single point mutation in the transmembrane protein 67 (TMEM67), is a genetic model of hydrocephalus and PKD that is orthologous to human MKS type 3 (MKS3) (12-13). TMEM67 is one of a complex of co-localized proteins that, when mutated, cause MKS or JS (14-17). In renal tissue, and mouse embryonic fibroblasts, TMEM67 localizes in the plasma membrane and in the area of the ciliary transition zone, a region between the basal body and axoneme. TMEM67 has been characterized as one of the proteins that serve as a “filter” controlling protein movement into the primary cilium (14, 18). In Wpk rats, the TMEM67^{-/-} homozygous animals have renal cystic disease with severe hydrocephalus and survive for approximately three weeks (12). The heterozygous animals have no renal phenotype and breed normally in the first year.

The current studies are designed to compare the genotype and phenotype of Wpk rats and extend the characterization of cerebral abnormalities. The hydrocephalus is a communicating form of the disease as evidenced by an open cerebral aqueduct of Silvius in both the homozygous and heterozygous genotypes. During post-natal development of the homozygous hydrocephalic animals, the disease becomes severe with bilateral fusion of lateral ventricles. While the anatomical structure and polarity of the choroid plexus epithelial cells remain intact in the homozygous pups, there is an altered barrier function and electrolyte transport across the choroid plexus epithelia. The heterozygous (TMEM67^{+/-}) rats have midline malformations and mild hydrocephalus that does not appear to impair normal physiological functions until after the first year of life. The latter is, to our knowledge, the first description of an animal genetic model of slowly progressing hydrocephalus. These models are unique in that they avoid the necessity of intracranial injection of sclerotic or hemorrhagic agents to induce the disease. Both the heterozygous and homozygous rat models may be useful for detailed physiological, behavioral and pharmacological studies.

2.5 Results

Identification of the TMEM67/MKS3 heterozygous mutation using dCAPS markers. The Wpk rat was previously shown to have a single C to T substitution within exon 12 of the TMEM67/MKS3 gene that converts a proline to a leucine in the polypeptide (13). Although this mutation reduces the transcript level in kidney as determined by RNA gel blotting, there was little or no change in TMEM67/MKS3 RNA in brain tissues reported previously, (13) reducing the utility of RNA gel blotting as a genotyping tool for these studies. Moreover, to our knowledge, neither DNA blotting nor PCR methods for detecting the mutant allele had been previously developed. To overcome this limitation, we used a PCR-based method involving dCAPS markers (19). We designed mismatched primers flanking the mutation to create a cleavage site for MwoI only in the wild type (WT) allele (Figure 2.1a). However, amplification of rat genomic DNA with the dCAPS primers generated several PCR products in addition to the 51 bp target because of related sequences in rat genomic DNA. Therefore, nested PCR was used to first amplify a 157 bp region containing the target sequence (Figure 2.1b), followed by a second amplification using the dCAPS primers (Figure 2.1c). After MwoI digestion, the PCR product from WT animals generates two closely migrating fragments just below the 30 bp marker (Figure 2.1d, TMEM67^{+/+}; n=98). In contrast, the product from homozygous mutant animals was uncleaved, migrating near the 50 bp marker (Figure 2.1d, TMEM67^{-/-}; n=72). Heterozygotes were identified by the presence of the 51 bp product as well as the MwoI digestion products (Figure 2.1d, TMEM67^{+/-}; n=234). The dCAPS genotyping correlated well with the cerebral phenotypes described below. This technique provides the ability to unambiguously characterize the heterozygous animals for the first time and determine potential cerebral changes that result from a diminished TMEM67 protein expression.

Neonatal development of the Wpk model. The hydrocephalus in the TMEM67^{-/-} homozygous animals is severe, resulting in cranial doming (Figure 2.2a, b, d). At post-natal (P) day 17, the head dimensions of the homozygous animals were significantly increased over the control animals when measured in vertical (palate to cranial cap) or horizontal (biparietal) orientation (Figure 2.2d). The homozygous pups had a significantly reduced body weight at P12, P17, and P19 as compared to WT and died postnatally prior to weaning age (Figure 2.2a, c). The renal consequence of the TMEM67 mutation presented as severely cystic kidneys in the homozygous pups while both heterozygous and WT animals had normal kidneys (Figure 2.2e, g). These results are consistent

with the previous reports on the non-cystic and cystic Wpk rat model (12, 13, 20) but represent the first depiction a phenotype in heterozygous animals. As the animals age to adulthood, the renal phenotype of the heterozygous animals remains normal (Figure 2.2f). Unlike whole body and kidney, heart weight did not show a significant difference in the homozygous animals as compared with WT controls at P17 and the hematocrits were also normal (data not shown).

To substantiate the initial findings and to further characterize the heterozygous animals, a second cohort was examined at post-natal day 15 (Figure 2.2e, g). As in the first cohort, the homozygous animals showed a statistically significant decrease in body weight at P15. There was no difference between the WT and heterozygous animals. The brains and kidneys of these animals were also collected and weighed. Whether the kidney weights or the brain weights were expressed as organ weight or as organ weight as a percentage of body weight, the homozygous pups were statistically increased over the other two genotypes. The WT and heterozygous animals were the same in all parameters (Figure 2.2g).

Cerebral phenotype of the neonatal Wpk rats. To determine and compare ventricular volumes in the Wpk rats of all three genotypes, the pups were scanned using MRI at two postnatal time points. At P7-8, volumes of the lateral ventricle for WT, heterozygotes, and homozygotes were 1.5 ± 0.6 , 6.7 ± 1.8 and 71.9 ± 9.2 μl . After a further 10 days of maturation (P17-18), the respective lateral ventricle sizes were 2.6 ± 0.3 , 16.7 ± 5.4 and 491.2 ± 61.9 μl , respectively (Figure 2.3). Interestingly, the fold change in lateral ventricular volume during neonatal aging (P7-8 to P17-18) for WT (1.7X), heterozygous (2.5X) and homozygous (6.8X) animals was gene dosage dependent and significantly different between genotypes. Measurements in these young rats displayed the same order of magnitude as a previous report on basal cistern kaolin-injected hydrocephalus, in which ventricular volume was quantified in adult female rats (21).

Cerebral characteristics in the TMEM67^{+/-} rats. A sac-like protrusion was found during sectioning of early postnatal brains of the heterozygous animals suggesting an abnormality in the parietal to occipital lobe. In a coordinate, relatively caudal to the center of the brain where the pineal gland was seen, the heterozygous animals showed an elevated left hemisphere (V2MM; secondary visual cortex mediomedial area) as compared to that of sibling WT animals at P0. Interestingly,

homozygous rats did not show the asymmetry at this coordinate but, rather, the presence of a gap between two hemispheres with remnants of thrombotic membrane suggestive of venous sinus thrombosis (Figure 2.4a). In a more caudal coordinate where the aqueduct was present, the brains from the heterozygous animals retained the elevated height in the left hemisphere (ECIC; external cortex of the inferior colliculus) as compared to that of WT at P0 (Figure 2.4b).

Primary cilia are involved in tissue patterning during development; therefore, to determine potential effects of ciliary defects in the brain, the ependyma was examined using scanning electron microscopy of the brain in a sagittal orientation. At birth (P0), mono-cilia were detected in WT and heterozygous animals with occasional presence of ciliary tuft in the ventricular surface. In the homozygous ependyma, however, the mono-cilia (primary cilia) appears markedly longer than those of the heterozygous or WT controls (Fig. 4c). In agreement with a previous report (12), at latter time points (P8 and thereafter), the ventricular surface was covered with tufts of cilia, which were very similar in WT and homozygous rats (data not shown). To quantify the ciliary phenotype of the ependyma revealed in the SEM, the cilia length was measured by 5 independent, blinded observers who were naïve to the experimental protocol. A representative count by one observer and the mean values of all the observers are shown in Figure 2.4d. The results were confirmed in two separate experiments using immunofluorescent images of anti-Arl13b stained cilia (images not shown). The results of the latter experiment were tabulated and the averages are compared with the measurements of the SEM experiments (Figure 2.4d). Both sets of experiments indicated that the cilia of *TMEM67^{-/-}* was significantly longer than other genotypes.

Because the midline protrusion in the heterozygous animals was not visible on the external surface of the skull, we assessed the forebrain part of the head including extra-axial space (EAS) that subsumes subdural and subarachnoid space. Strikingly, formation of hemorrhage in the dorsomedial surface within the EAS along the midline was detected in the heterozygous animals with an increase in size in dorsomedial EAS as compared to that of WT. At P1, the external hemorrhage in the EAS appeared as a bilateral protrusion with respect to the midline in the forebrain (Figure 2.5a, solid arrow). At P18, there was no residual indication of hemorrhage but a protrusion similar to that observed in Figure 2.4a was observed in the brains of these animals (Figure 2.5b, solid arrow).

The ventricular enlargement in the homozygous animals became progressively worse with age, severely compromising other brain tissue by P18, the age when the affected animals show signs of terminal disease and were sacrificed for humane reasons. The serial sections confirmed ventriculomegaly with fusion of both ventricles (n=23), whereas the heterozygous animals exhibited mild enlargement of the lateral ventricle (n=8) (Figure 2.5b). The asymmetric lateral ventricle and the midline protrusion in the heterozygous rat were observed starting at P8 until around P360 (n=7).

Communication of CSF in the TMEM67^{-/-} brain. To determine the type of hydrocephalus occurring in the Wpk rat, we examined the caudal CSF space and circumventricular organ at the midline. The SCO did not show a significant change at P0 (Figure 2.6a). The cerebral aqueduct remained open in all genotypes during neonatal development and into adulthood (Figure 2.6a). To further substantiate the finding of communicating hydrocephalus indicated by the open aqueducts, a dye extravasation study was performed on all genotypes by injecting Evans blue in the cisterna magna of Wpk rats at P18. Blue dye leakage suggests that there was no obstruction along the CSF circulation including aqueduct and ventricles in either the homozygous or heterozygous rats (Figure 2.6b). However, the Evans blue trait along the aqueduct and cistern of the homozygous brains was less intense than that of heterozygous and WT brains. Taken together, the Evans blue dye injection through the cisterna magna visualized in sagittal orientation supports the histological observation in coronal serial sections that communicating hydrocephalus is present in the TMEM67 homozygous mutant rats.

Cerebral phenotype in adult TMEM67^{+/-} rats. To determine if the mild hydrocephalus that is present in pre-weaning animals continues through adulthood, brain scans and analysis of MRIs were performed to compare WT and heterozygous animals at 8 months of age. There is a statistically significant difference in the size of lateral ventricles between the WT and heterozygous animals (Figure 2.7). Interestingly, the asymmetry of the ventriculomegaly in the heterozygous animals continues into adulthood. Eight of eight (100%) of the heterozygous (TMEM67^{+/-}) rats developed ventriculomegaly at age 8 months as compared to the age-matched WT (n=10). All animals were included in the analysis and there was no overlap in ventricular volume between the WT and heterozygous animals (Figure 2.7).

Choroid plexus epithelium and barrier function. The choroid plexus epithelial cells are responsible for the nature of the blood-choroid plexus barrier. In addition, polarization of membrane proteins is necessary for vectorial osmolyte transport. To further characterize these epithelial cells in the disease state, the polarization of relevant membrane proteins was examined. Aquaporin 1, a water channel present in the choroid plexus was localized primarily to the apical plasma membrane in plexuses derived from new-born WT and homozygous pups. This localization was maintained in the homozygous animals at 15 days of life (Figure 2.8a)

Claudin 1, considered a barrier claudin, is a tight junction protein important for maintenance of transepithelial permeability (22, 23). Claudin 1 staining is similar in the newly born WT and homozygous pups but decreased in intensity after 15 days in the homozygous animals (Figure 2.8b). However, despite the decrease in intensity, the claudin-1 polarity to the apical junctions is maintained in the older pups.

Taken together, the localization studies indicate that the cells are viable and that a major transport protein as well as a junctional complex protein are appropriately polarized, albeit, with possible changes in quantitative expression levels.

The vascular permeability of the TMEM67 mutant brains was assayed to address changes in barrier function in animals with hydrocephalus (24, 25) Intracardial injection of Evans blue demonstrated that blue dye extravasation was significantly increased in brains from homozygous as compared to WT animals. Interestingly, we noted that Evans blue leakage was detected in the choroid plexus of the TMEM67^{-/-} rats (arrows, Figure 2.9a). To examine leakiness of the vasculature in the cerebral cortex, we administered intracardial Evans blue dissolved in saline. The area of Evans blue dye extravasation excluding the ventricular surface was measured which eliminated the confounding effect of dye leakage in the ventricles including the choroid plexus. Dye leakage in the cerebral cortex of the homozygous rats excluding ventricles was significantly elevated ($p=0.002$; Kruskal-Wallis with Dunnett's post hoc tests) as compared to WT animals (Figure 2.9 a-d).

Minor changes in vascular leakage and/or a change in the epithelial permeability of the blood-CSF barrier might be expected to have functional consequences manifested in the composition of the

CSF. Of the major electrolytes found in the CSF of late-stage hydrocephalic rats compared to control animals. Na^+ , K^+ and Cl^- are all statistically elevated in the hydrocephalic animals (Figure 2.9e).

2.6 Discussion

Hydrocephalus is a serious disease that can occur at any age and can arise from a multitude of causes. Regardless of cause, the main treatment is surgical intervention to divert excess CSF to other areas of the body and/or ablation of the choroid plexus to decrease CSF production. Development of pharmacological interventions has been hampered, in part, by a lack of physiologically relevant animal models, particularly those that demonstrate a more slowly progressing form of the disease and live long enough to allow a reasonable course of drug treatment.

The TMEM67 homozygous rat is an orthologous model of MKS3 and demonstrates many of the characteristics of the human disease including severe polycystic kidney disease and brain abnormalities (12, 13, 20). Like the homozygous rats, the human patients with MKS die in the perinatal or neonatal period (10). In the course of the current studies, we made the fortuitous observation that the heterozygous breeders had a mild form of hydrocephalus that appears to adversely affect the animals at approximately one year of age when they begin to show moderate signs of stress like failure to groom. Because of the difficulties in genotyping animals with a single nucleotide mutation, previous studies failed to distinguish WT from heterozygous animals and breeders were classified as heterozygous when they produced off-spring with neonatal hydrocephalus and grossly enlarged kidneys (12, 20). Accurate genotyping of the heterozygous Wpk animals by combining a nested PCR and dCAPS approach allowed us to genotype the animals shortly after birth and provided the ability to characterize the heterozygous animals in the neonatal period. Particularly important in this regard is the ability to distinguish differences in the ventricular volumes of all three genotypes as early as post-natal day 7-8 by MRI.

Due to both the severe hydrocephalus and cystic renal disease, homozygous pups succumb to the disease in the first few weeks of life. There is a statistically significant decrease in weight gain as early as post-natal day 12. At post-natal day 15, the kidney and brain weights of the homozygous

animals are significantly increased while, interestingly, the heterozygous animals are indistinguishable from WT in both parameters. In the homozygous animals, it has been reported that the disease results in fatality by 4-6 weeks (20). In the current studies, these animals were humanely sacrificed at or before post-natal day 18. Of interest for future studies is the finding that, while heterozygous animals maintain a hydrocephalic state through adulthood, there is no evidence of cystic kidney disease in the adult animals.

Both genotypes appear to express a communicating form of hydrocephalus. This is indicated by the open cerebral aqueduct on Silvis in both the neonatal and adult animals. In addition, Evan's Blue injection into the cisterna magna at P18 suggests that there was no obstruction along the CSF circulation including aqueduct and ventricles in either the homozygous or heterozygous rats. These results are consistent with a previous report (26) using a mouse model of a different ciliopathy, BBS, where the authors also found a communicating form of hydrocephalus after Evan's Blue injection.

In interpreting the MRI results of the adult animals, it is important to note that Wistar rats have a high degree of spontaneous ventriculomegaly. In a study by Tu et al., the incidence of enlarged ventricles was 19% (27). In the current study, no animals were excluded from analysis and no increased ventricular size was detected in any of the WT adults (n=10) that were analyzed by MRI. In addition, there was no overlap in the size of the lateral ventricles when comparing adult WT and heterozygous animals of the same age.

The TMEM67 gene appears to be related not only to ventricular size but also to regulation of cilia length and midline morphogenesis. An elongated ciliary phenotype has been reported in primary cilia of extra-cerebral tissues from patients with Meckel syndrome (11) and in Wpk rats (28). Studies of at least two other in vivo ciliopathy models of polycystic kidney disease (jck and cpk mice), have also reported the unusually long primary cilia in the kidney and bile duct (29, 30). In the ventricles, primary cilia are virtually impossible to measure after P0 because the animals develop tufted motile cilia which obscure the primary cilia within a day after birth. Previously published studies have shown that there is no difference in the tufted cilia between the WT and homozygous animals (12). However, the renal cilia length has been published for the WT and

homozygous rats (28). In the kidney, one does not have the confounding variable of tufted, motile cilia. Tammachote and colleagues reported a statistically significant increase in the number of cilia with lengths greater than 3 μM in the homozygous animals. It should be noted that in the previous report (28), genotyping was not done so the unaffected animals would be a mixture of WT and heterozygous pups. The current results are entirely consistent with the previous studies. In the homozygous animals, the primary cilia are statistically longer than those of the heterozygous or WT animals and are also longer than 3 μM . An entirely new finding is that the cilia from WT and heterozygous animals are not statistically different.

Hemorrhage in the brain is a primary causal factor in the development of communicating hydrocephalus (25, 31-33). Dorsomedial hemorrhage seen at P1 in the TMEM67 heterozygous rat and appears to be linked to midline malformation in the current study. Heterozygous pups (n=3) showed dorsomedial hemorrhage in the extra-axial space adjacent to SAS. There was no evidence of hemorrhage after P7 and, interestingly, there was also no evidence of hemorrhage in the homozygous animals. The role of hemorrhage and its possible association with mild hydrocephalus needs further investigation.

One potential cause of aberrant fluid homeostasis in ciliopathies is the mislocalization of polarized proteins in barrier epithelial cells responsible for electrolyte and fluid movement (34, 35). However, we find no evidence of mislocalization in the current studies. The choroid plexus water channel aquaporin 1 shows a predominately apical expression in both the WT and homozygous animals at birth and this polarity is maintained at P15. Likewise, claudin-1, a junctional protein important for maintenance of epithelial barrier function (23) shows an apical distribution, localized to the apical junctional complexes in both the WT and homozygous pups at birth. At day 15, the claudin-1 is still localized predominately on the apical side of the epithelia of the homozygous animals, albeit with a decreased intensity.

Thus, a junctional protein important for epithelial cell polarization, as well as a transport protein with a defined polarity in choroid plexus epithelia, maintain normal distributions. Despite the maintenance of normal cellular polarity, the Evan's Blue studies indicate an enhanced dye leakage

across the choroid plexus. Taken together these findings suggest a controlled increase in transepithelial permeability.

The endothelial cells of the choroid plexus have been characterized as a fenestrated capillary. Therefore, they form an area of the vasculature that is leaky to small molecular weight compounds. Under normal conditions it is the epithelial cells of the choroid plexus, a high resistance epithelial monolayer, that form the blood-CSF barrier. Under normal conditions, polarized electrolyte transport across the epithelium results in CSF that contains a higher concentration of Cl^- and a lower concentration of K^+ than plasma (4, 36). Na^+ concentrations are approximately equal in these two extracellular fluids. It follows, therefore, that if the development of hydrocephalus in the rat model is due to a non-specific increase in permeability across the epithelial cell barrier, the resulting CSF would have a composition more similar to a plasma filtrate. In this scenario, the Cl^- concentration would decrease and the K^+ concentration increases while the Na^+ concentration would be relatively unchanged. Surprisingly, this is not the case in the severely hydrocephalic animals where all three electrolytes are higher in the CSF compared to WT. These results further substantiate a controlled and specific increase in electrolyte secretion across the choroid plexus epithelial cells and into the CSF.

From these results, the development of the hydrocephalus could be predicted to be due to the increased osmotic gradient, which would cause fluid accumulation in the CSF. Substantial further investigation is necessary to determine which transporters may be primary in this altered transepithelial transport. However, it is interesting to note that renal cystic development in ciliopathies has been shown to be primarily due to an aberrant regulation of transepithelial Cl^- transport (37, 38). Since the transporters responsible for maintaining of K^+ and Cl^- gradients can be modulated by a variety factors including inflammatory cytokines, pressure, osmolarity, hormones, neuromodulators and intracellular signaling components, these proteins are important targets for regulating CSF production.

Based on the current findings, the TMEM67 homozygous rat is a good model of MKS as it demonstrates encephalocele-like changes, midline malformation and renal cystic disease (13-18, 39, 40). In addition, the characterization of the TMEM67^{+/-} phenotype elucidates a novel and

potentially useful model of more slowly progressing hydrocephalus. In the first year of life, the heterozygous animals groom themselves, reproduce normally and care for their young. However, at approximately one year of age, the animals start to exhibit signs of stress. They become unkempt in appearance and, on occasion, we have noted that the eyes seem to bulge. By 13 months of age, many of the animals have to be sacrificed for humane reasons, well before the expected life span of WT rats (~2 years). MRIs conducted to compare WT and heterozygous animals at 8 months of age, when the animals are still healthy, indicated that the hydrocephalus present at P18 is maintained chronically over the life of the TMEM67^{+/-} animals. These studies represent the first demonstration of hydrocephalus in the heterozygous Wpk rats and as such makes them unique as a slowly progressing hydrocephalic model. These studies also highlight the importance of further studies to elucidate the factors that control electrolyte transporters in the choroid plexus barrier epithelial cells and are likely to be important pharmaceutical targets in the control of CSF production.

2.7 Methods

Generation of a derived cleaved amplified polymorphic sequences (dCAPS) marker for the Wpk mutation. To detect WT and mutant alleles of the Wpk rat TMEM67 gene, a derived cleaved amplified polymorphic sequences (dCAPS) approach was employed (19). We located the region containing the point mutation in the Wpk rat in chromosome 5 (RefSeq NC_005104) and TMEM67 mRNA sequences (RefSeq NM_001107916) from NCBI. The C to T substitution in the Wpk mutant (13) occurs at nucleotide 1186 in exon 12 within the TMEM67 mRNA. The sequence containing the mutation did not lie within any known restriction site, making it impossible to design a traditional CAPS marker. Therefore, a dCAPS approach was adopted using MwoI restriction enzyme since all point mutations except A to T can be converted into a marker for MwoI (19). The Wpk/TMEM67 dCAPS forward primer was 5'-CCTGGCTGACTTTCCCAGTG-3' and reverse primer was 5'-GTATATTCCAGGTAAATATCAGCAAACACA-3'. The 3'-end of the dCAPS forward primer was directly 5' to the mutation site. The reverse primer was 3' to the point mutation ('Reverse' in Figure 2.1a) in the intron immediately following the exon containing the point mutation. The mismatched G at the 3'-end of the forward primer and the mismatched GC near the 3'-end of the reverse primer create the left- and right-hand GC dinucleotides within the

MwoI site after PCR. In preliminary amplifications, the dCAPs primer pair generated several discrete PCR products with rat genomic DNA because of the presence of closely related target sequences in the genome. This complication was alleviated by using nested PCR. The forward and reverse primers for nested PCR were 5'-GCTATGAGAGAGCAGGGGAG-3' and 5'-AACTCCTGGCTGACTTTCCC-3', respectively (Figure 2.1 a). Nested PCR provided a PCR product of 157 bp (Figure 2.1b) to use as a template for subsequent amplification with the dCAPS primers (Fig. 1c). Total DNA for PCR analysis was isolated from tail clips using QIAamp DNA Kit (Qiagen).

Nested PCR was carried out in 20 μ l containing 25 ng genomic DNA following the manufacturer's instructions (GoTaq®Green Master Mix). Cycling conditions were: denaturation at 95°C for 2 min, followed by 30 cycles of denaturation at 95°C for 30 sec, annealing at 49.5°C for 15 sec, and extension at 72°C for 30 sec. The dCAPS PCR was performed in 20 μ l reactions containing 2 μ l of amplified products from the nested PCR with the following cycling conditions: 95°C for 5 min (denaturation), followed by 30 cycles at 95°C for 15 sec (denaturation), 44°C for 15 sec (annealing), and 72°C for 5 sec (extension). PCR products were digested with MwoI (New England Biolabs) in total reaction volumes of 50 μ l by adding 10 μ l of PCR product to 5 μ l of the 10X CutSmart buffer (1:10 dilution) containing 5 units of MwoI (34 μ l H₂O, 10 μ l PCR product, 5 μ l 1X CutSmart buffer, and 1 μ l MwoI). The samples were then incubated at 60°C for 1 h. Following digestion, the samples were separated by electrophoresis on vertical 15% polyacrylamide gels in 1X Tris/boric acid/EDTA (TBE) buffer and visualized by staining with ethidium bromide. Two different size markers of 50 bp DNA ladder (New England Biolabs, NEB#B7025) and 10 bp DNA ladder (Invitrogen/ThermoFisher, SM1313) were used for the nested PCR, and the PCRs pre- or post-MwoI digestion, respectively.

Animal procedures. The Wpk rats on a Wistar background were bred as previously described (12, 13, 20). Neonatal pups (postnatal day 0 to 18; P0 to P18), both male and female were randomly assigned to be used based on genotype. For the adult rat radiological study, TMEM67^{+/-} rats at the age of 8 months were used (n=8) as compared to the WT controls (n=10). At the time of sacrifice, the body weights were measured and the animals were anesthetized with an overdose of sodium pentobarbital (150 mg/kg body weight). Blood was collected via cardiac puncture and the carcass

was flushed with saline and perfused intracardially with 4% paraformaldehyde (PFA). Kidneys and hearts were removed and weighed. Biparietal and vertical (palate to cranial cap) head measurements were taken with Vernier calipers (Manostat, Merenschwand, Switzerland). In animals that were not perfused, the CSF was collected with 25-gauge needle through cisterna magna in a sagittal position and transferred to the freezer (-80 C°) prior to electrolyte analysis.

Rodent use and procedures conformed to the National Institutes of Health (NIH) guidelines and were approved by the Institutional Animal Care and Use Committees at Indiana University Purdue University Indianapolis and the Indiana University School of Medicine. Both male and female animals were used.

Electrolyte analysis. CSF was collected from terminally anesthetized normal and homozygous pups aged 15-20 days. In the case of the hydrocephalic animals, each n was from an individual animal. For the normal animals, CSF was pooled from 4-6 animals for each determination. Ionic composition of Na⁺, Cl⁻, and K⁺ was quantified and osmotic concentration [mOsM] in the CSF was determined. The electrolyte quantification was performed at the IU Health Pathology Laboratories of the Indiana University School of Medicine.

Magnetic resonance imaging (MRI). On day P7-8 and P17-18, rat pups were briefly removed from their litter, sedated with 5% isoflurane (balance medical oxygen) and anesthesia maintained with 1-2% isoflurane (balance medical oxygen). Adult animals (P240 + 3 days) were lightly sedated with 2% isoflurane. High resolution T2-weighted (T2W) MRI images were acquired using a 3T clinical MRI scanner (MAGNETOM Trio, Siemens Healthcare, Erlangen, Germany) outfitted with a dedicated 4 channel rat head coil and bed system (RAPID MR, Columbus, OH). Images were acquired using a 3D SPACE sequence with the following acquisition parameters: (TA: 5.5min; TR: 2080ms; TE: 162ms; FS: On; Ave: 2; Flip Angle: 150; Slice Thickness 0.2mm; Matrix: 192x192; FOV: 35mmx35mm) yielding 0.18 x 0.18 x 0.2mm resolution images. Volumes of interest (VOI) on lateral ventricles were determined from threshold-based image segmentation of native CSF contrast, and images were quantified for lateral ventricular volumes using Analyze 12.0 (AnalyzeDirect, Overland Park, KS).

Histology. Rats were terminally anesthetized with sodium pentobarbital and intracardial perfusion was conducted with saline followed by 4% paraformaldehyde (PFA). Harvested brains and kidneys were immersed in 30% sucrose in PBS at 4C° for 2-3 days or when cryo-protected tissue has sunken down to the bottom of the dish. The tissue in sucrose solution was briefly washed with PBS and further placed in a square mold with optimal cutting temperature (O.C.T.) compound (Tissue-Tek) at -170 C° using dry ice and isopentane (Fisher Scientific), in a rectangular aluminum tray. Snap-frozen molds containing tissue specimen were kept at -80 C° until cryo-sectioning (25). Following the rostral-caudal axis in the rat brain atlas (41), 2 mm rostral to the bregma (bregma +2.0 mm) was identified during sectioning and labeled 'start of the lateral ventricle or SLV'. The selection of slides for comparison among genotypes was based on the distance from the SLV. 2 mm caudal to SLV corresponds to the bregma in controls (P18). In massively hydrocephalic sections, however, the volume of the brains was higher than that of controls. Therefore, serial sections were obtained prior/post the bregma target of interest to determine the identical anatomical location for the sections from control and hydrocephalic brains. Appearance of third ventricles, dorsal and ventral hippocampus, aqueduct, SCO, the fourth ventricle and cerebellum during coronal sectioning formed secondary references to the SLV in the sections from hydrocephalic brains as compared to the control. During cryosectioning, 20 µm thickness was applied at -23 C°. Selected serial sections were stained with hematoxylin alone or hematoxylin and eosin. Stained sections were imaged with a light microscope (M420, Heerbrugg, Switzerland), and images were captured using Kodak camera (DC290, Rochester, NY). In assessing CSF circulation, sterile filtered 1% Evan's Blue (4 µl/g body weight) in PBS was injected to cisterna magna using a 25-gauge needle at about 6 µl/sec (21). To examine barrier function within the central nervous system, 1% Evan's Blue (4 µl/g body weight) in PBS was injected intracardially using a 25-gauge needle, prior to 4% PFA perfusion.

Hematoxylin stain. Frozen sections were air dried at room temperature for 10 min. Sections were stained in hematoxylin solution (Surgipath 01522) for 1 min. Sections were then washed with ultrapure water or Milli-Q® (MQ) water for 4 min (twice), acidic alcohol solutions for 5 min, and MQ water for 4 min. Sections were then immersed in ammonia water (or sodium bicarbonate) 5-6 times slowly, MQ water for 4 min, and graded ethanol (EtOH) in the following order: 80 %

EtOH for 4 min, 95 % EtOH for 1 min (three times), 100 % EtOH for 1 min, 100 % EtOH for 3 min, Xylene for 5 min, and mounted with Permount medium (Fisher Scientific).

Hematoxylin and eosin stain. Sections were allowed to come to room temperature then stained with hematoxylin (Poly Scientific #s212A) for 3 minutes. Stained sections were rinsed with deionized water before washing in tap water for 5 minutes. Slides were dipped in acid ethanol (1 mL concentrated HCl + 400 mL 70% ethanol in water) 8-12 times, rinsed twice in tap water for 1 minute each, then rinsed in deionized water for 2 minutes. Sections were then stained with eosin for 30-45 seconds and dehydrated with three 5 minute washes in 95% ethanol, followed by three 5 minute washes in 100% ethanol, and finally three 15 minute washes in Xylene. Slides were then coverslipped with Permount mounting media (Fisher Scientific #SP15-100) and allowed to dry overnight.

Immunofluorescence. Slides were incubated with primary antibodies diluted in blocking solution overnight at 4°C, rinsed, and incubated with the secondary antibodies for 1 h at room temperature. Primary antibodies were rabbit anti-claudin 1 or anti-aquaporin 1 (1:100 dilution; Abcam) and anti-Arl13b (1:100, Proteintech). The secondary antibody was Alexa Fluor dye-conjugated goat anti-rabbit IgG (diluted 1:1000; Invitrogen). For nuclear staining 4',6-diamidino-2-phenylindole (DAPI) 500 ng/ml (Sigma) was used. Confocal images were taken on a Leica TCS SP8 high speed multiphoton and confocal imaging system. For low magnification fluorescence micrographs, a Nikon 90i microscope with Spot RT cooled CCD camera was used.

Scanning electron microscopy (SEM). The specimens were fixed with the appropriate aldehyde fixative for a minimum of 2 hours. They were then rinsed with PBS and post fixed with 1% osmium tetroxide in 0.1M Phosphate Buffer for 2 hours. Post fixation and rinsing with PBS, the specimens were dehydrated through a series of ethyl alcohols then chemically dried using HMDS (hexamethyldisilazane, Electron Microscopy Sciences, Fort Washington, PA). The schedule was as follows: 2 parts 100% ethyl alcohol/1-part HMDS for 15 minutes, 1 part 100% ethyl alcohol/2 parts HMDS for 15 minutes, then 2 changes for 15 minutes each with 100% HMDS. After HMDS depletion, the specimens were allowed to air-dry in a hood overnight, mounted on aluminum stubs with adhesive tabs, and sputter coated for 3 minutes using a Polaron (Energy Beam Sciences,

Agawam, MA). The specimens were viewed on a JEOL 6390LV (Peabody, MA) scanning electron microscope and digital images were taken.

Image Analysis. To quantify Evans blue leakage in the brain, images of coronal sections were analyzed using NIH ImageJ. Briefly, micrographs showing hematoxylin or H&E stained sections were processed through line measure function. For the assay of barrier functions, photographs with Evans blue extravasation were processed through sharpen, edge detection, binarization, and pixel count. This enabled the calculation of pictorial elements or blue dye stained areas of the brain (with albumin to which Evans blue binds). Serial sections with 100 μm interval involving forebrain, midbrain, and hindbrain from three animals per genotype were used. To quantify cilia length, blinded observers who did not have information on genotypes were asked to measure the cilia length as exemplified or indicated with arrows (Figure 2.4). Using ImageJ, the known scale bar (5 μm) was used as an input and the line or curve measurement function was used to quantify the length of mono-cilia.

Statistical analysis. Statistical analyses were performed using SigmaPlot (version 11, Systat Software Inc.) and Prism (GraphPad version 7). Normality of data distribution was tested using the F-test for unequal variance. Normally distributed data were analyzed using Student's t-test and Tukey's post-hoc test for pair-wise comparison after ANOVA when comparing two or three groups respectively. Non-normally distributed data were analyzed using the nonparametric Mann-Whitney test and Kruskal-Wallis with Dunnett's post hoc tests when comparing two and three data groups, respectively. Data were expressed as average \pm standard error of the mean (S.E.) and were considered significant at the $p \leq 0.05$ level.

Data Availability. All data generated or analyzed during this study are included in this published article.

2.8 Acknowledgements

These studies were funded by an Indiana University Collaborative Research Grant from the Office of the Vice President for Research, Indiana University, an Indiana Institute of Biomedical Imaging

Sciences Research Development Grant from the Department of Radiology and Imaging Sciences, Indiana University School of Medicine and an Innovator Award from the Hydrocephalus Association. The authors are grateful to Prof. Larry Benowitz and Dr. Joseph Madsen, Harvard Medical School, Boston, MA, USA for critical reading of this manuscript. We thank Daniel Preston, Ayodamola Otun and Caleb Danko for technical support and Chris Konz, Vickie Birge and Julie Nigro for expert oversight of the rat colony at the IUPUI School of Science. J.W.S. was supported by NIH 5T32HL007224-42 (Dr. Victoria M. Bolotina). We thank H. Painter, R. Raines, K. Kammer, I. McKnight, and H. White for conducting the blinded measurements of ciliary length.

2.9 Author Contributions

J.W.S. and B.B-Y. designed the experiments, analyzed the data, and wrote the manuscript. J.W.S. and S.S. conducted and analyzed experiments. L.J., A.A.R., B.M., S.P., and P.R.T. conducted and analyzed the rat brain scans using MRI. J.C.W. provided expertise in nested PCR, designed primers for dCAPs markers, and wrote part of the methods section. D.F. provided expertise in pediatric neurological disorders, analyzed experiments and edited the manuscript.

Competing financial interests: The authors declare no competing interests.

Figure 2.1. Characterization of the TMEM67 genotype in the Wpk rat. (a) Design of dCAPs genotyping approach. Primers for nested PCR are labeled Nested F and Nested R. MwoI indicates the sequence and location of the MwoI site created during PCR with the upstream and downstream dCAPs primers (labeled Forward and Reverse, respectively). The WT genomic sequence is labeled WT and the mutant sequence is labeled TMEM67^{-/-}. The C→T mutation in the Wpk mutant is marked in red. (b) Polyacrylamide gel analysis of nested PCR products obtained from genomic DNA from (left to right) WT, heterozygous, or homozygous mutant rats. The expected product size was 157 bp. The left lane contains DNA length markers. Note that in the first lane to the left, a 50 bp DNA ladder (50 – 1350 bp) was used as a standard with 50 to 150 bp markers indicated (c) A polyacrylamide gel as in (b) except that the nested PCR products were amplified with the dCAPs primers (see a). The expected product size was 51 bp. (d) A polyacrylamide gel as in (c) except that the dCAPs PCR products were digested with MwoI prior to electrophoresis. MwoI digestion of the dCAPS product from the WT allele is expected to produce two unresolved bands migrating slightly faster than the 30 bp marker. MwoI is not expected to cleave the dCAPs product from the mutant allele. Note that in the first lane from the left of both gels(c and d), a 10 bp DNA ladder (10-150) was used as a standard with the 20 to 50 bp markers indicated.

a)

Nested F 5'-AACTCCTGGCTGACTTTCC

MwoI GCNNNNNNNGC

Forward 5'-CCTGGCTGACTTTCCAGTG

WT ...aaactcctggctgactttcccagtcctgtgtttatgatatttacctggaatatactgatg...ctcccctgctctctcatagc...

TMEM67^{-/-} ...aaactcctggctgactttcccagtcctgtgtttatgatatttacctggaatatactgatg...ctcccctgctctctcatagc...

Reverse ACACAAACGACTATAAATGGACCTTATATG-5'

Nested R GAGGGGACGAGAGAGTATCG-5'

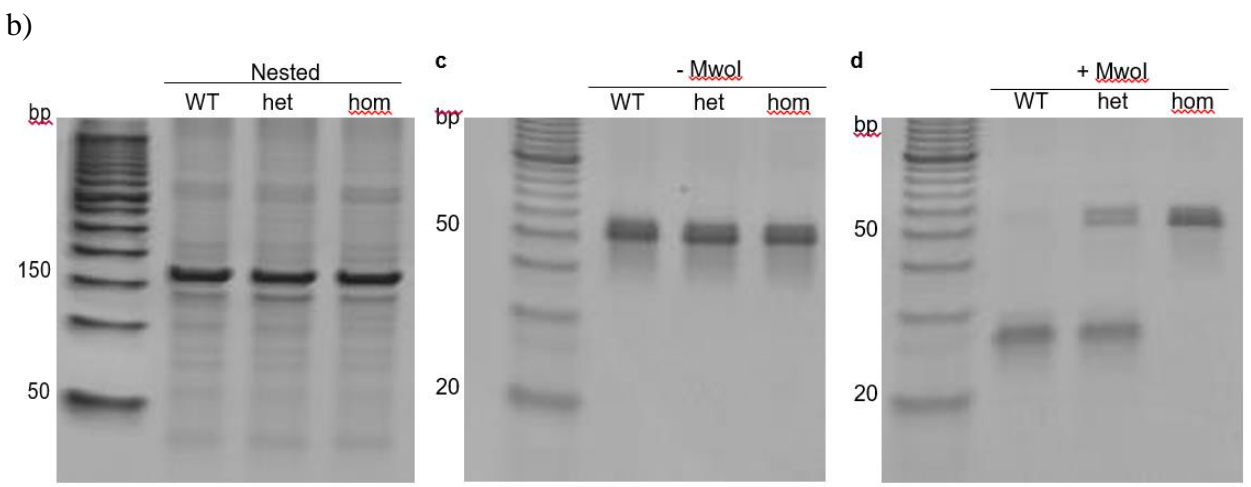


Figure 2.1 Characterization of the TMEM67 genotype in the Wpk rat.

Figure 2.2. Correlation of phenotypic and genotypic characteristics in the Wpk rat. (a) TMEM67^{-/-} Wpk rat displaying a dome-shaped head with reduced body size compared to a WT littermate at P15. (b) Typical cranial doming at P17 in the Wpk homozygous rat as compared with a sibling WT animal. (c) Comparison of body weights of WT and TMEM67^{-/-} rats from postnatal day 0 to 21 (P0-P21). The TMEM67^{-/-} mutants had a significantly reduced body weight at P12 (p=0.012), P17 (p=0.015), and P19 (p=0.01) as compared to WT. The homozygous animals were humanely sacrificed at day 19. (d) Measurement of head sizes of WT and homozygous mutant rats at P17. Head sizes in the homozygous animals were significantly increased over the control animals when measured in vertical (palate to cranial cap) (p=0.006) or horizontal (biparietal) orientation (p=0.007). Numbers in parentheses at the base of the columns indicate the number of animals measured. (e) Representative renal phenotypes of the WT, TMEM67^{+/-} and TMEM67^{-/-} rats at P0 (hematoxylin stain) and P15 (hematoxylin and eosin stain). (f) Representative adult renal phenotypes of the WT and TMEM67^{+/-} and TMEM67^{-/-} rats at P389 and P460 (hematoxylin and eosin stain). (g) Body weight, kidney weight, brain weight, and related organ weight as a percentage of body weight. At the time of sacrifice (P15), body weight and organ weight were determined and the organ weight as a percentage of the total body weight was calculated. The numbers of animals analyzed are indicated on the graphs. Scale bars, 1 mm (b, e-f). Single (*), double (**), triple (***) , and quadruple (****) asterisks denote p<0.05, p<0.01, p<0.005, and p<0.0001, respectively.

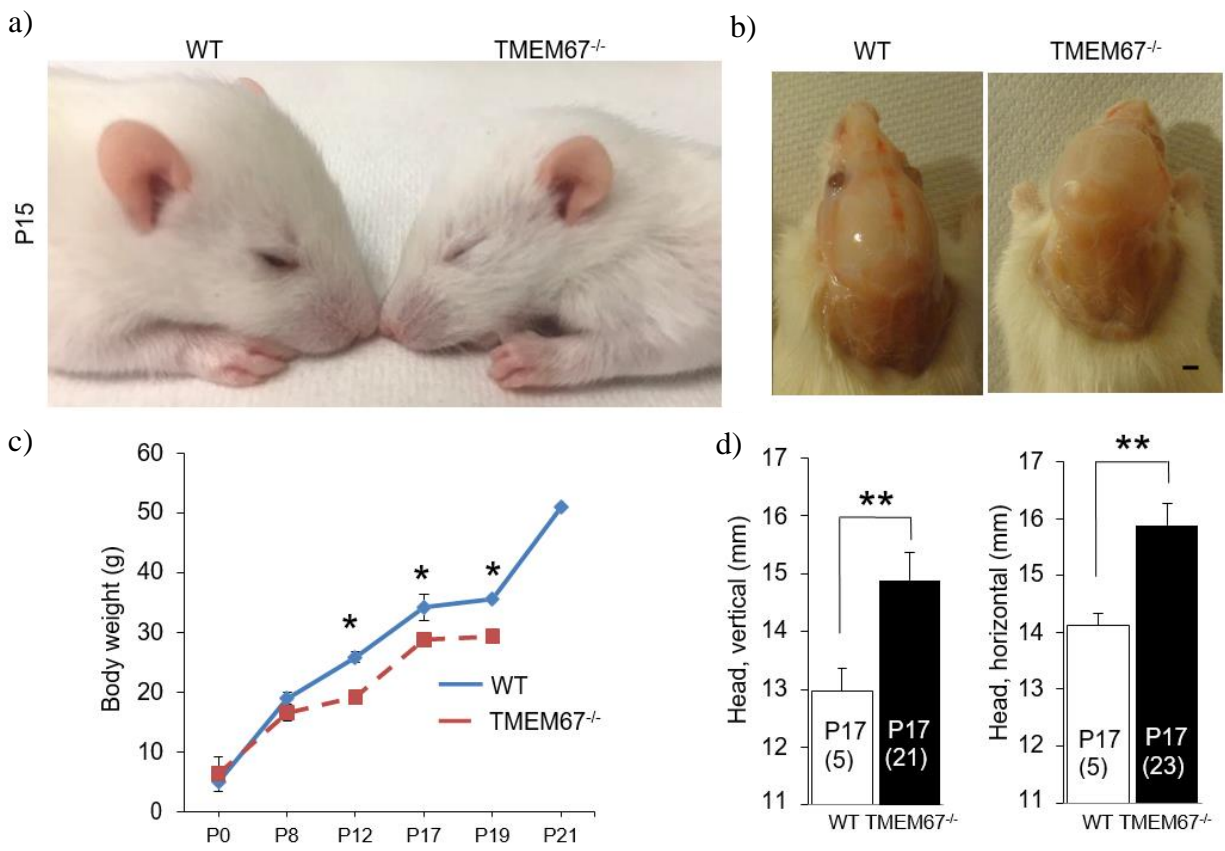


Figure 2.2 Correlation of phenotypic and genotypic characteristics in the Wpk rat.

Figure 2.2 continued

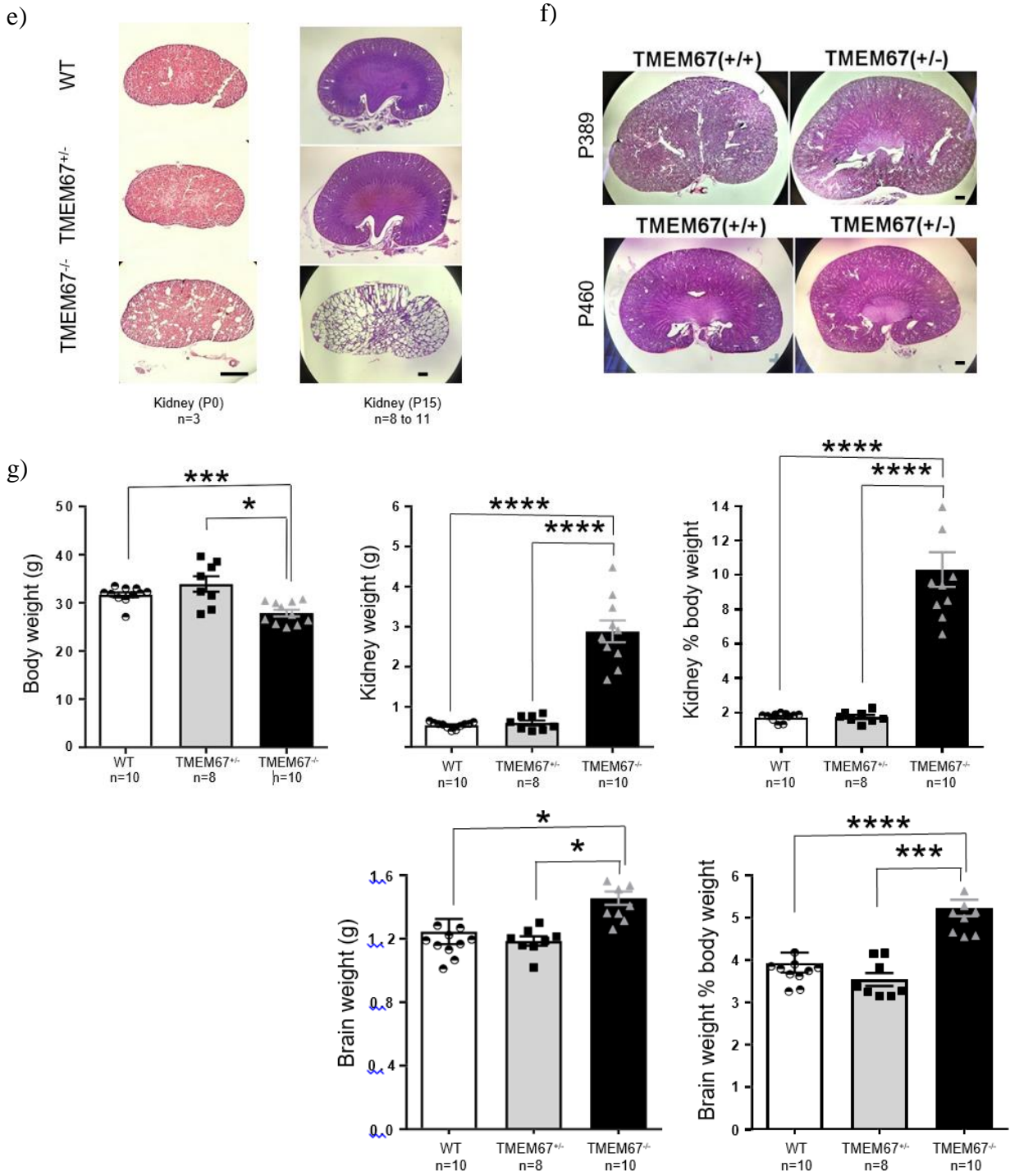


Figure 2.3. Magnetic Resonance Imaging (MRI) of the three genotypes of the pre-weaning Wpk rat model with TMEM67 mutations. (a) Head scan of Wpk rats at P7-8 in coronal, sagittal, and transverse orientation with 3 dimensional reconstructions of lateral ventricle (LV; yellow). (b) Head scan of Wpk rats at P17-18 in coronal, sagittal, and transverse orientation with 3 dimensional reconstructions of the LV (yellow). A bar graph summarizing the quantitative data of the lateral ventricles per genotype is shown in the lower right corner. Note that the heterozygous animals (middle) show intermediate size in LV volume. n= 4 to 6 per genotype. Asterisks denote *, $p < 0.05$, **, $p < 0.01$, and ***, $p < 0.001$, respectively.

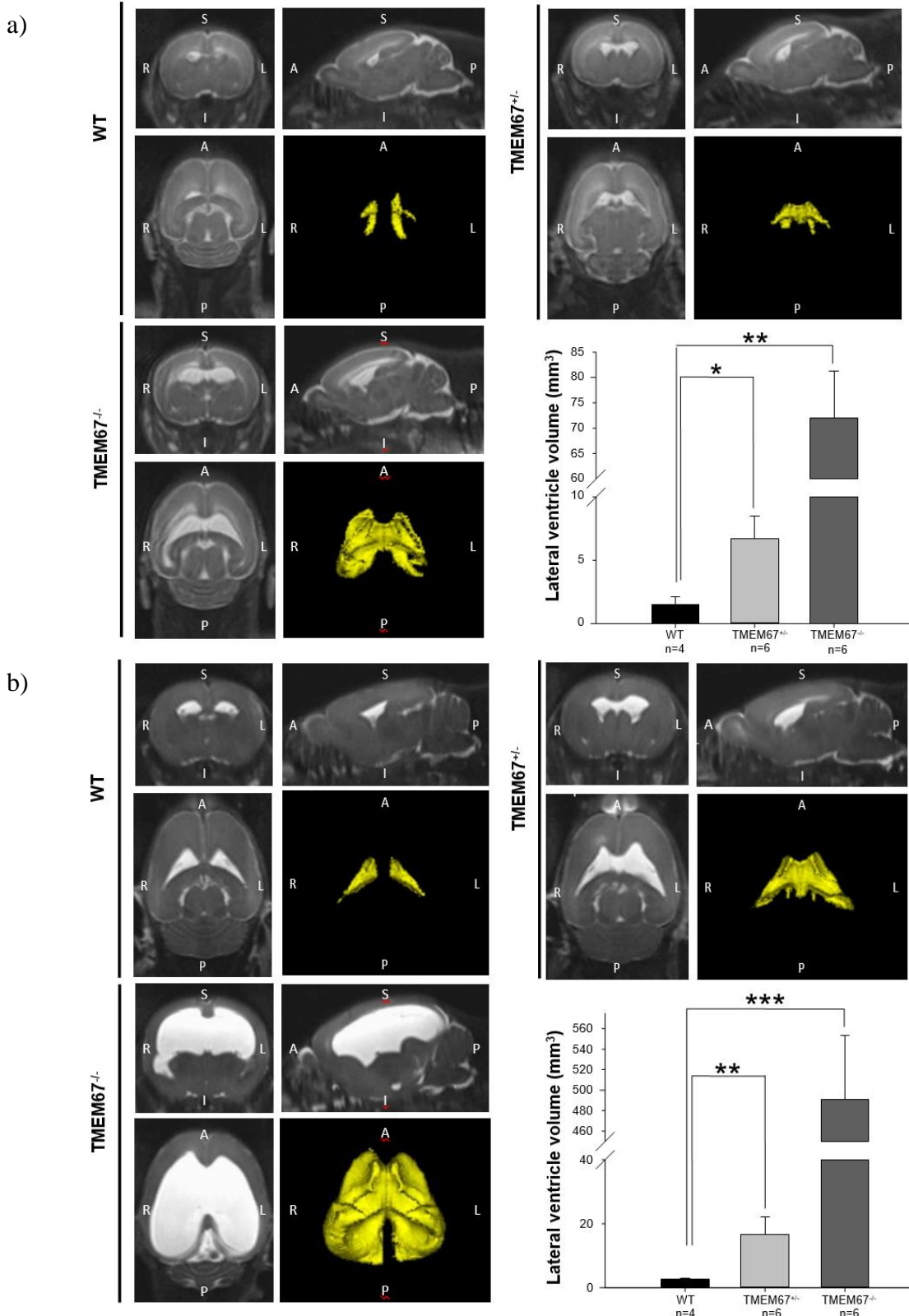


Figure 2.3 MRI of the three genotypes of juvenile Wpk rat model with TMEM67 mutations.

Figure 2.4. Midline malformation and ciliary phenotype at birth in the *TMEM67^{+/-}* rats. (a) Twenty μm (thickness) sections of dorsal cerebral cortex along the midline in the hindbrain. Note that a sac-like protrusion (double arrowheads) is found in the left hemisphere of *TMEM67^{+/-}*. At P0 a wide gap is detected between two hemispheres in *TMEM67^{-/-}* as compared to WT. Red arrows indicate usual location of pineal gland. In *TMEM67^{-/-}*, a bloody membrane was observed. The single arrowhead indicates the subcommissural organ (SCO). (b) A sac-like protrusion in the occipital lobe of *TMEM67^{+/-}* (double arrowheads) as compared with WT at P0. Aq denotes aqueduct. Note that aqueduct is open in all genotypes at birth. $n=3$ per genotype (a representative section per genotype is shown in a-b; hematoxylin and eosin stain). (c) Scanning electron micrographs displaying primary cilia on the striatal side of the ependyma in WT, *TMEM67^{+/-}* and *TMEM67^{-/-}* at P0. (d) 5 blinded observers measured cilia length as indicated with arrows. The scattered plot of the representative measurement by an observer (left), the scattered plot of the combined measurement by five observers (middle), and the bar graph showing the combined measurement of the SEM and IF using anti-Arl13b staining of cilia (not shown) are presented in the lower panel. Asterisk denotes *, $p<0.05$ (as compared to WT and *TMEM67^{+/-}*, respectively). Two animals per genotype. Scale bars, 1 mm (a-b), 2 μm (c), and 5 μm (d)

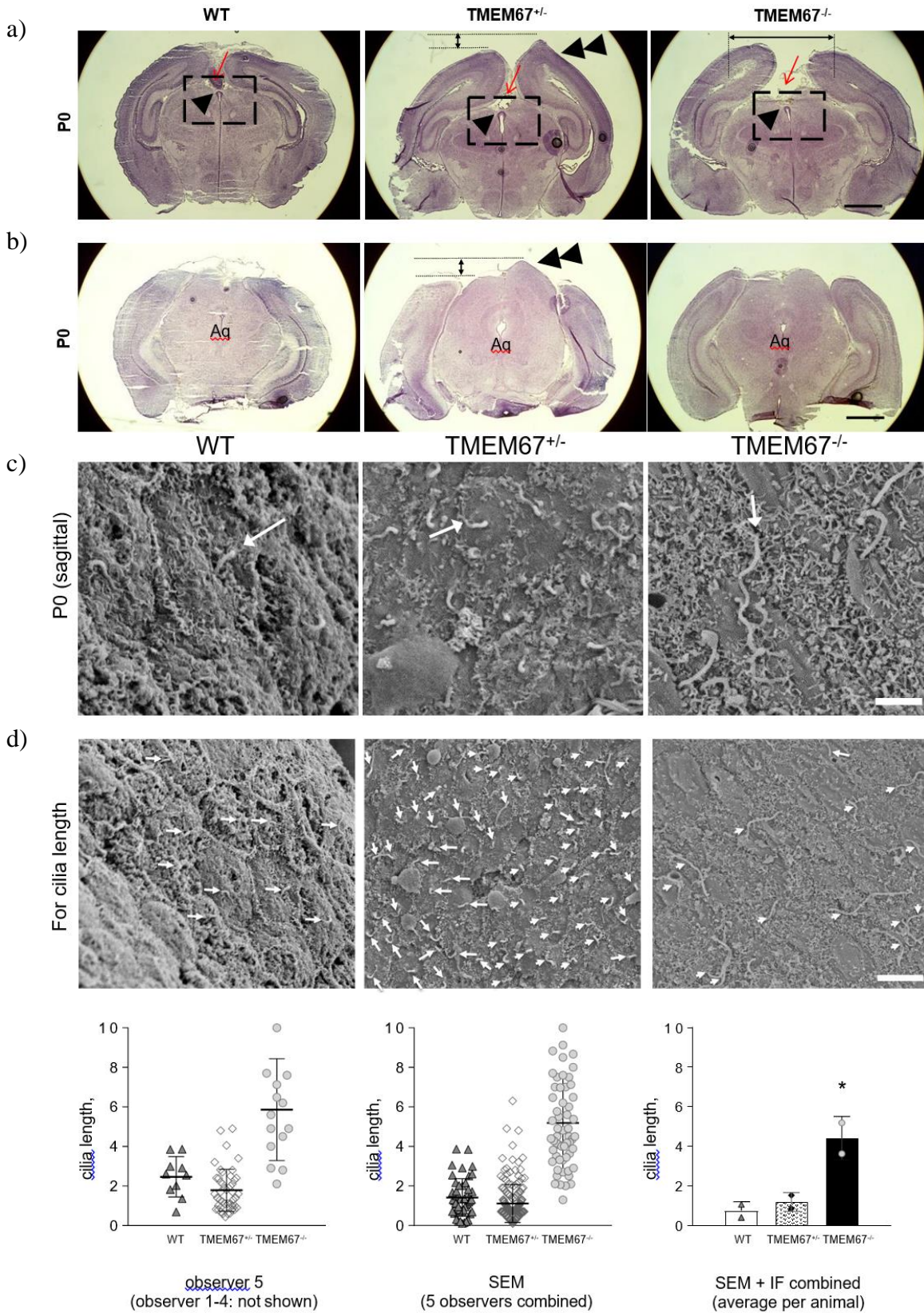


Figure 2.4 Midline malformation and ciliary phenotype at birth in the TMEM67^{+/-} rats.

Figure 2.5. Hemorrhage at birth and neonatal ventriculomegaly. (a) Hemorrhage in the TMEM67 heterozygous mutant brains at birth. The left panel demonstrates a representative serial section of a WT (TMEM67^{+/+}) rat from the forebrain (sincipital) to hindbrain (occipital) at postnatal day 1 (P1). The subsequent three panels show three different animals with TMEM67^{+/-} alleles exhibiting hemorrhage (solid arrows) adjacent to the venous sinus within extra-axial space adjacent to the subarachnoid space at P1. Similar results were obtained for n = 3 animals per genotype. (b) Representative cerebral phenotype of the TMEM67^{+/+}, TMEM67^{+/-}, and TMEM67^{-/-} animals at P18, respectively. Note that mild ventriculomegaly was observed in the TMEM67^{+/-} (n=8; 4 left enlarged, 2 right enlarged, 2 both sides) while bilateral dilation with fusion of lateral ventricles was seen in the TMEM67^{-/-} rats (n=23). Arrow indicates a protrusion on the dorsomedial surface of the cerebral cortex in the TMEM67^{+/-} rat. Scale bars, 1 mm (a-b)

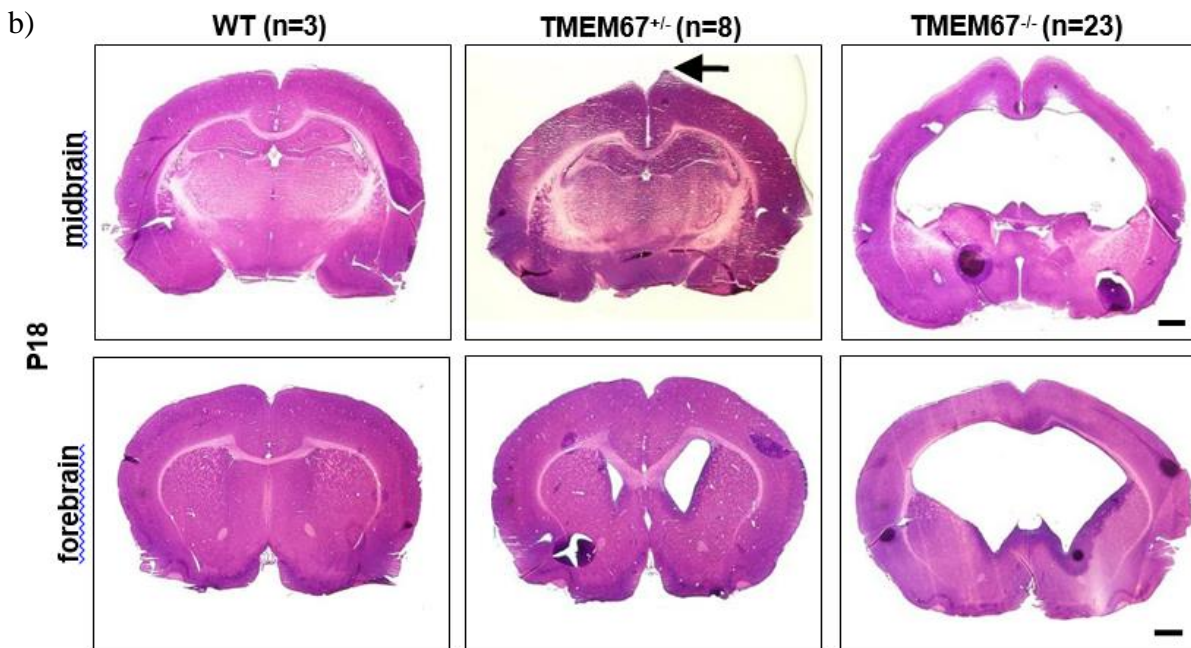
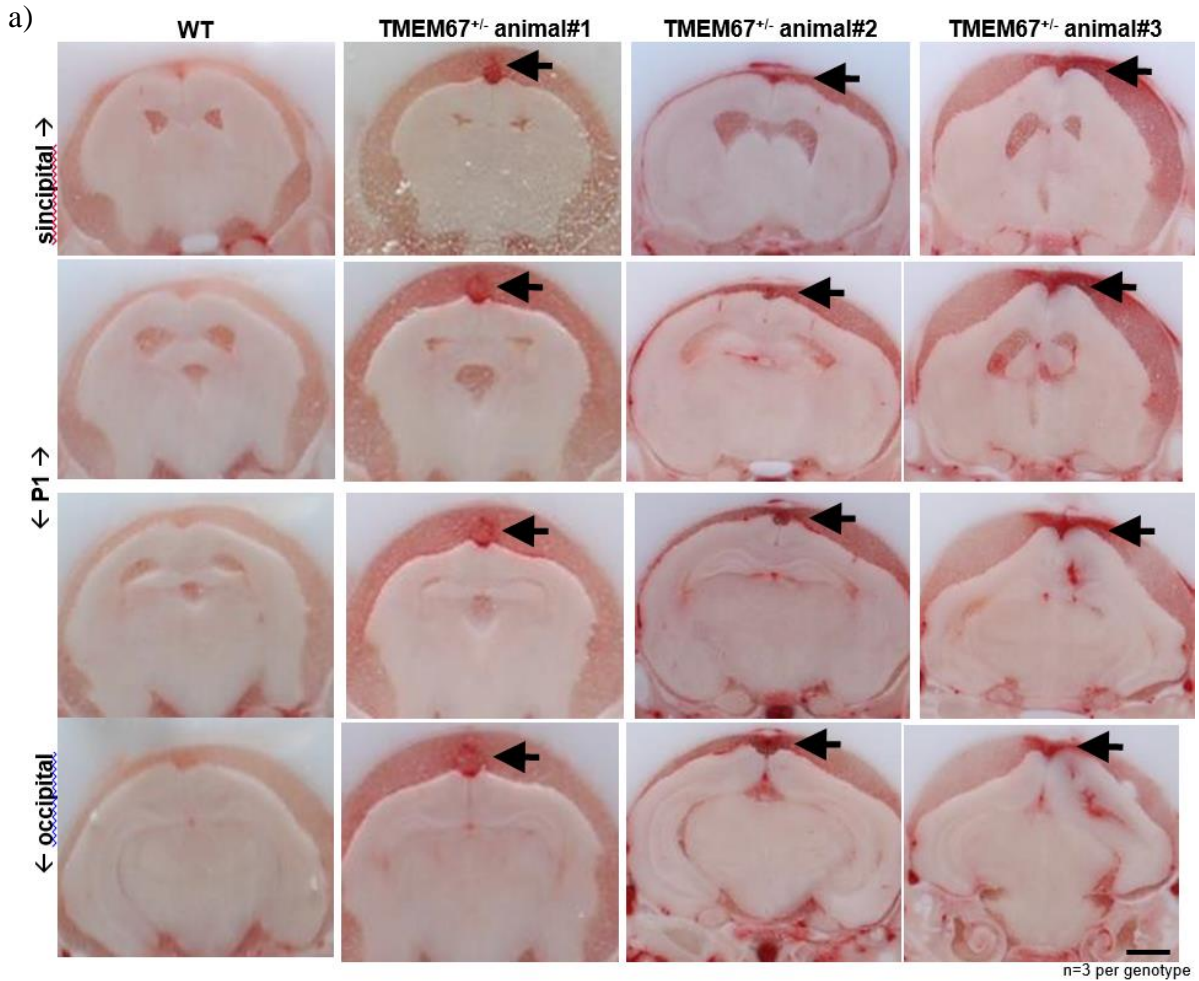


Figure 2.5 Hemorrhage at birth and neonatal ventriculomegaly.

Figure 2.6. Communicating hydrocephalus (a) Representative depictions of the aqueducts of the TMEM67^{+/+}, TMEM67^{+/-}, and TMEM67^{-/-} rats at P0, P8 and P15. Note that the aqueduct is open (arrow with “aq”) in TMEM67^{-/-}. Approximate coordinates from the bregma are indicated based on the rat brain atlas. The images are representative of n = 3 animals of each genotype and age. (b) Sagittal sections injected with Evans Blue to determine continuity (communication) or discontinuity (obstruction) of the CSF flow. Dye leakage along the CSF circulation including lateral ventricle, third ventricle, aqueduct and fourth ventricle was visualized by the cisterna magna injection of Evans blue in TMEM67^{+/+}, TMEM67^{+/-}, and TMEM67^{-/-} rats at P18. 3V and aq. denote third ventricle and aqueduct, respectively. Scale bars, 250 μ m (a) and 1 mm (b). The images are representative of n = 3 at each genotype

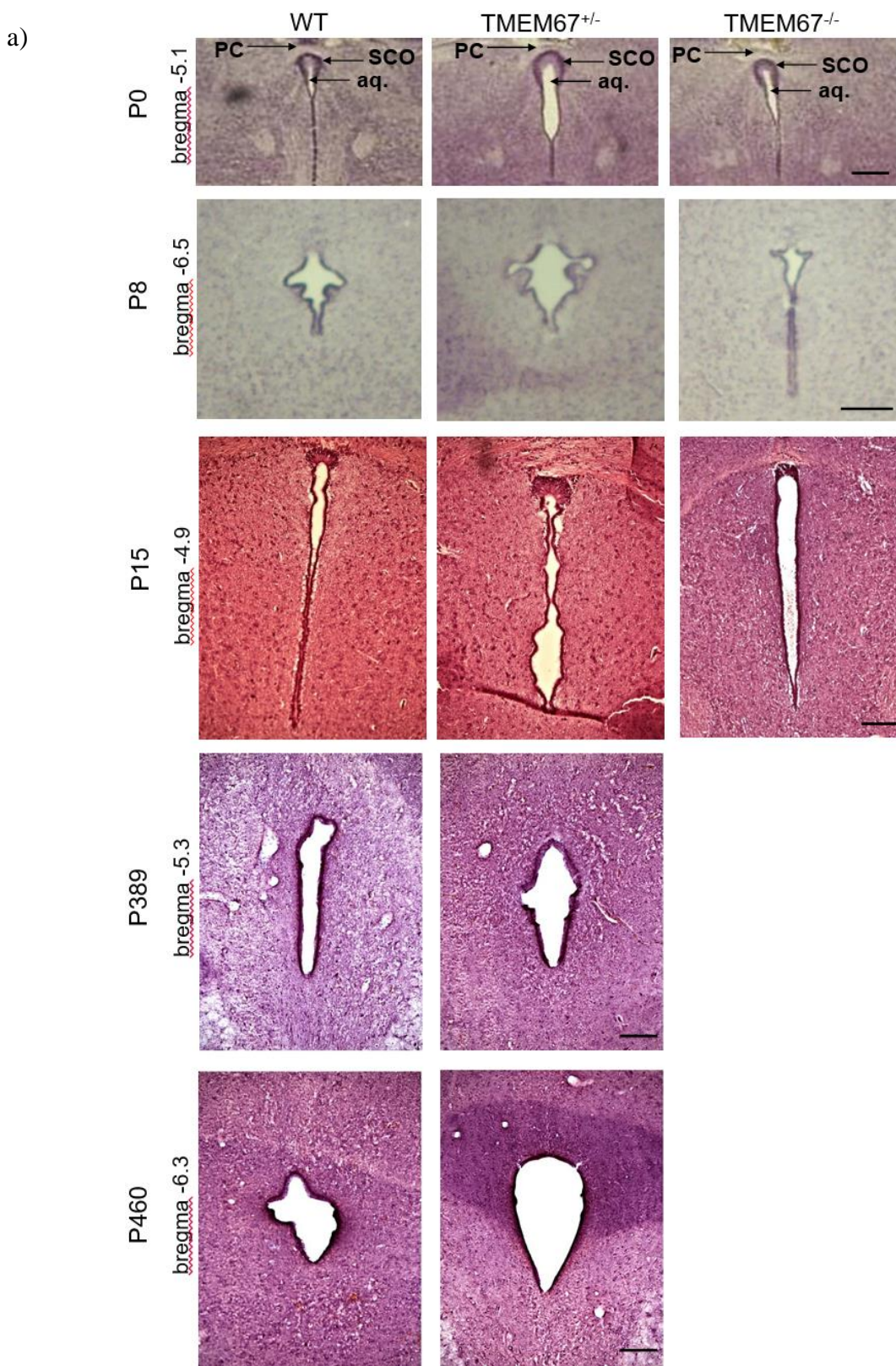
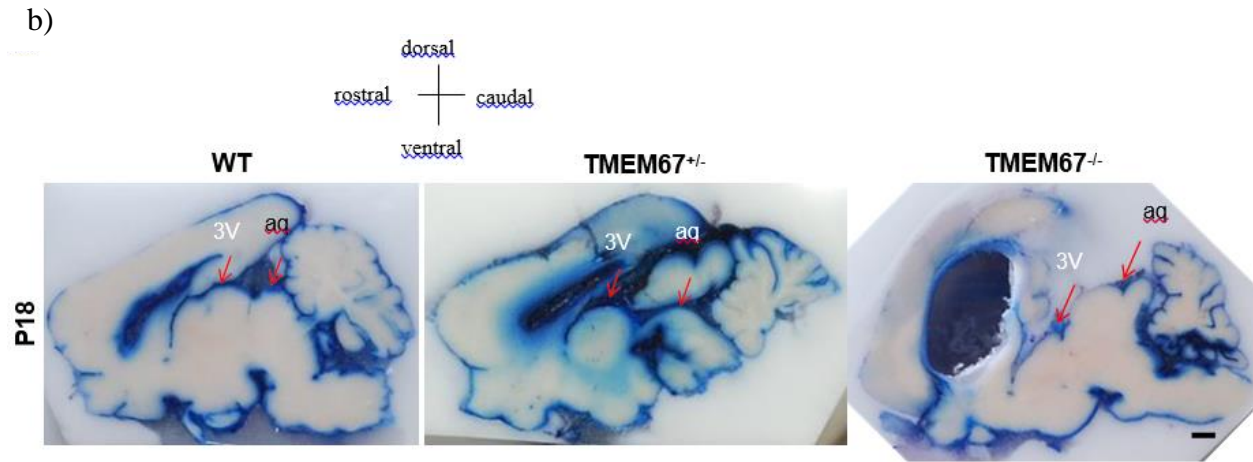


Figure 2.6 Communicating hydrocephalus.

Figure 2.6 continued



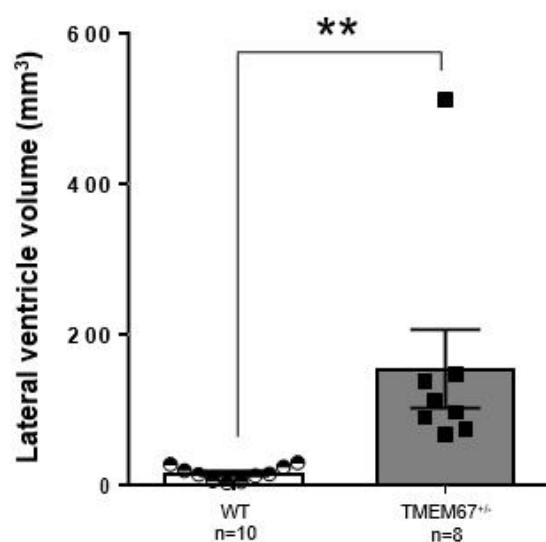
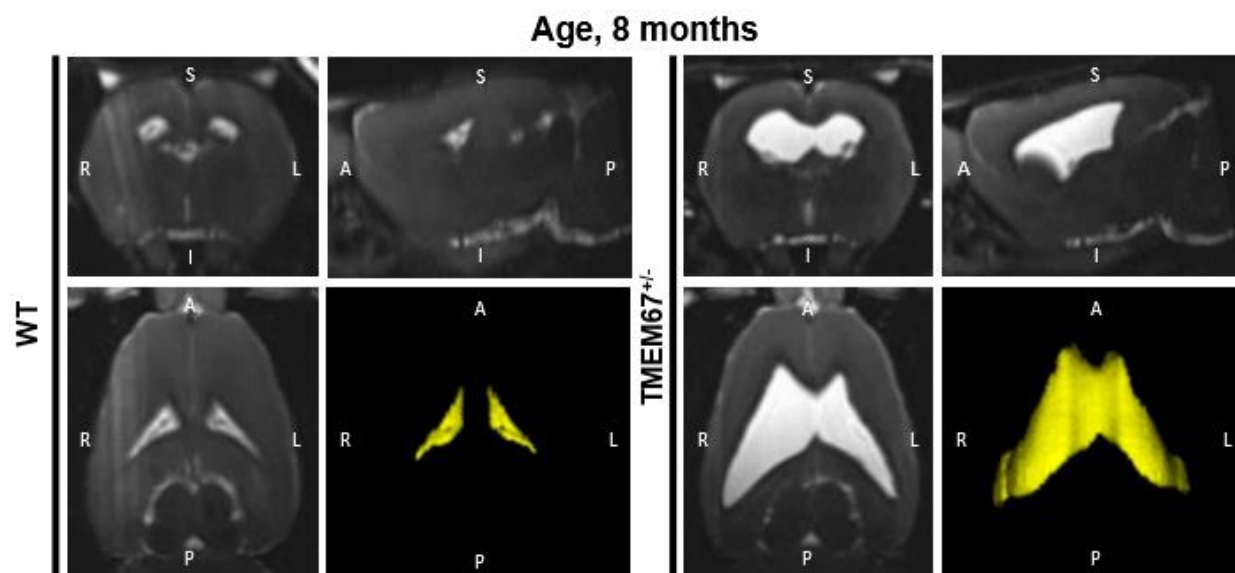


Figure 2.7 MRI of WT and TMEM67^{+/-} Wpk rats at 8 months of age.

Magnetic Resonance Imaging (MRI) of the WT and heterozygous (TMEM67^{+/-}) Wpk rats at 8 months of age. Head scan of Wpk rats at P240 + 3 days of age in coronal, sagittal, and transverse orientation with 3 dimensional reconstructions of lateral ventricle (LV; yellow). A bar graph with scattered dots summarizing the quantitative data of the lateral ventricles per genotype is shown in the third panel. Numbers of animals scanned are indicated at the bottom of each column. Double asterisks (**) denote $p < 0.01$.

Figure 2.8. Immunofluorescence of membrane proteins in the Wpk choroid plexus. Brain tissue was sectioned at 20 μm and incubated with primary antibody for the water channel, aquaporin 1, or the tight junction protein, claudin-1 (1:100 antibody dilutions). Protein expression is shown in WT and hydrocephalic rats at birth (P0) and P15. DAPI staining allows for visualization of nuclei. Negative (-) controls were incubated with secondary antibodies (1:1000 dilution, AlexaFluor goat anti-rabbit IgG). Images were taken on a Leica TCS SP8 (upright high-speed multiphoton and confocal imaging system) at 20x magnification. Scale bars = 50 μm . These images represent an n of at least 3 for each genotype and age.

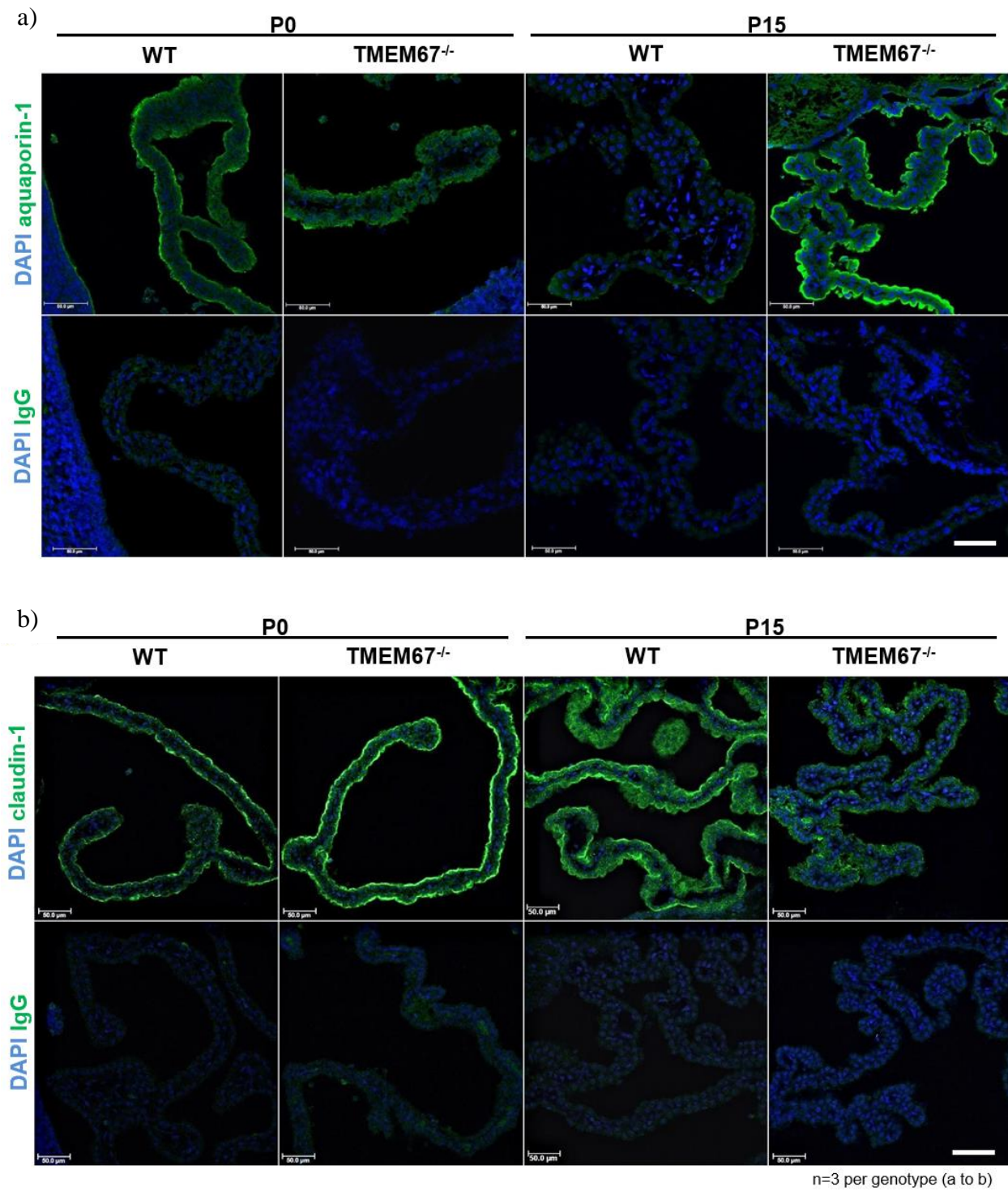


Figure 2.8 Immunofluorescence of membrane proteins in the Wpk CP.

Figure 2.9. Evans blue leakage in the brain after intracardial injection of the dye. (a) Representative coronal sections displaying Evans blue leakage in all three genotypes of the Wpk rat. Arrows indicate blue dye leakage in the choroid plexus in the lateral ventricles of a TMEM67^{-/-} brain. The images are representative of n = 3 at each genotype. (b) Magnified image of Evans blue leakage in the cerebral cortex, from dashed rectangles shown in a. (c) Binary image of Evans blue positive pixels quantified in the cerebral cortex obtained from b. (d) Box plot exhibiting statistical analysis of Evans blue leakage along the vasculature of the cerebral cortex as exemplified on images in c. Note that Evans blue binds to albumin. Evans blue injection indicates a trend towards a dose-dependent increase of the dye extravasation in the cerebral vessels. Serial sections (n=21-29) from three animals per genotype were used. AU, arbitrary unit. Asterisks denote *, p<0.05. Scale bars, 10 μm (a) and 1 mm (b). (e) Ionic composition of the CSF from TMEM67 rats: Bar graphs demonstrating an osmotic concentration in milliosmolar (mOsM) of sodium (Na⁺), chloride (Cl⁻), and potassium (K⁺) in the CSF of WT and TMEM67^{-/-} rats, postnatal day 15-20. Each bar represents 6 determinations. In the case of the homozygous animals, each determination was from the CSF of a single individual. For the normal animals, CSF from 4-6 individuals was pooled to obtain sufficient material for each determination. Statistical significance from the left to the right. p=0.0103 (CSF Na⁺); p=0.0013 (CSF Cl⁻); p=0.041 (CSF K⁺) by unpaired t test. Single and double asterisks denote p<0.05 and p<0.01, respectively. Scale bars, 1 mm (a) and 500 μm (b)

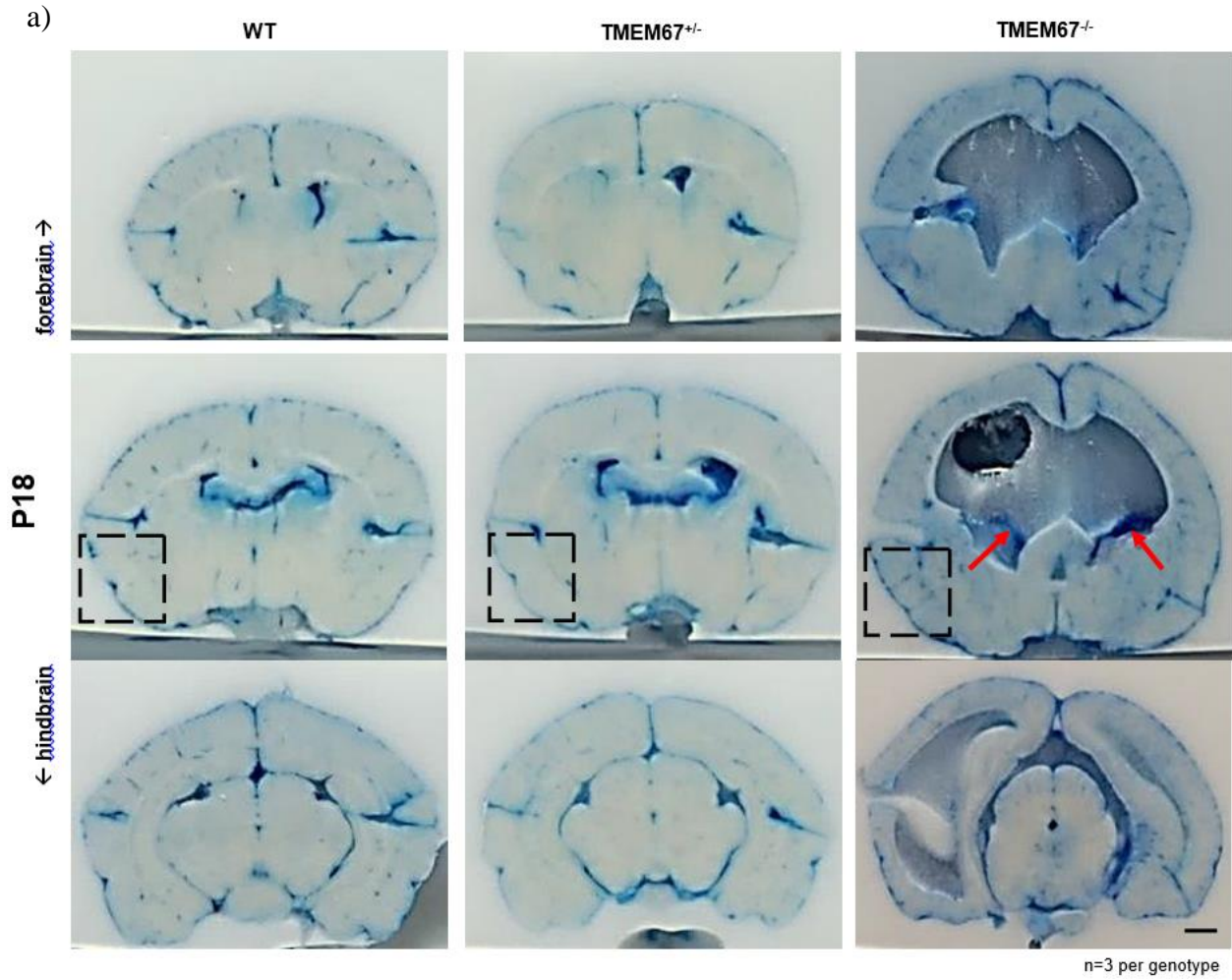
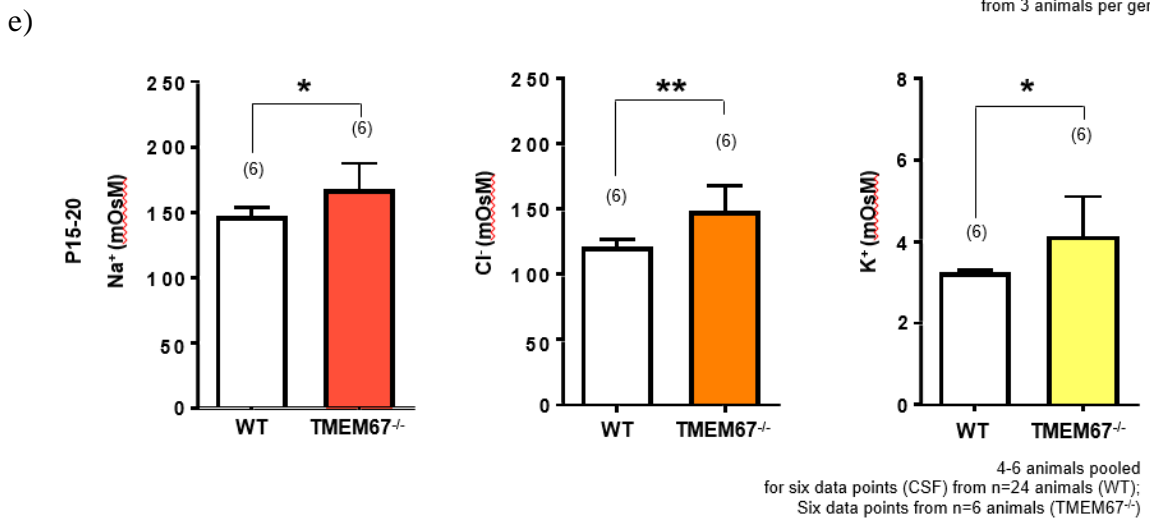
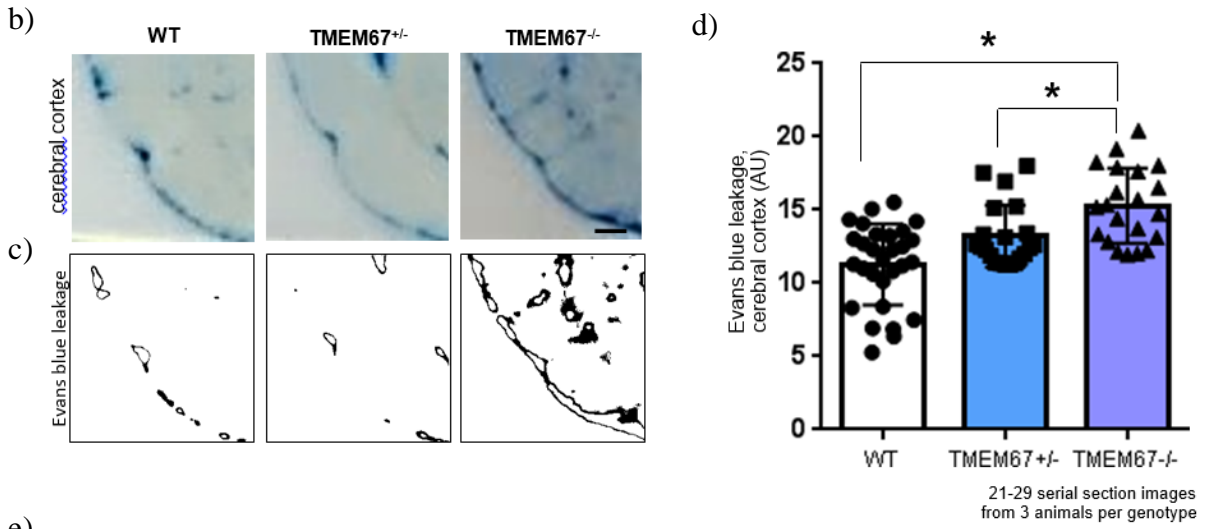


Figure 2.9 Ventricular Evans blue leakage and CSF ionic composition from TMEM67 rats.

Figure 2.9 continued



2.10 References

1. Jaraj, D., Rabiei, K., Marlow, T., Jensen, C., Skoog, I., and Wikkelsø, C. (2015). Mortality and dementia in untreated iNPH: a 25-year follow-up of a population-based cohort. *Fluids And Barriers Of The CNS*, 12(Suppl 1), O7.
2. Huh, M., Todd, M., and Picketts, D. (2009). SCO-ping out the mechanisms underlying the etiology of hydrocephalus. *Physiology*, 24(2), 117-126.
3. Ortloff, A., Vío, K., Guerra, M., Jaramillo, K., Kaehne, T., and Jones, H. et al. (2013). Role of the subcommissural organ in the pathogenesis of congenital hydrocephalus in the HTx rat. *Cell And Tissue Research*, 352(3), 707-725.
4. Johanson, C., Duncan, J., Klinge, P., Brinker, T., Stopa, E., and Silverberg, G. (2008). Multiplicity of cerebrospinal fluid functions: New challenges in health and disease. *Cerebrospinal Fluid Research*, 5(1).
5. McAllister, J. (2012). Pathophysiology of congenital and neonatal hydrocephalus. *Seminars In Fetal And Neonatal Medicine*, 17(5), 285-294.
6. Jiménez, A., Domínguez-Pinos, M., Guerra, M., Fernández-Llebrez, P., and Pérez-Fígares, J. (2014). Structure and function of the ependymal barrier and diseases associated with ependyma disruption. *Tissue Barriers*, 2(1), e28426.
7. Tully, H., and Dobyns, W. (2014). Infantile hydrocephalus: A review of epidemiology, classification and causes. *European Journal Of Medical Genetics*, 57(8), 359-368.
8. Stone, S., and Warf, B. (2014). Combined endoscopic third ventriculostomy and choroid plexus cauterization as primary treatment for infant hydrocephalus: a prospective North American series. *Journal Of Neurosurgery: Pediatrics*, 14(5), 439-446.
9. Praetorius, H., and Spring, K. (2005). A physiological view of the primary cilium. *Annual Review Of Physiology*, 67(1), 515-529.
10. Harris, P., and Torres, V. (2009). Polycystic kidney disease. *Annual Review Of Medicine*, 60(1), 321-337.
11. Avasthi, P., and Marshall, W. (2012). Stages of ciliogenesis and regulation of ciliary length. *Differentiation*, 83(2), S30-S42.
12. Gattone, V., Tourkow, B., Trambaugh, C., Yu, A., Whelan, S., and Phillips, C. et al. (2004). Development of multiorgan pathology in the wpk rat model of polycystic kidney disease. *The Anatomical Record*, 277A(2), 384-395.

13. Smith, U., Consugar, M., Tee, L., McKee, B., Maina, E., and Whelan, S. et al. (2006). The transmembrane protein meckelin (MKS3) is mutated in Meckel-Gruber syndrome and the wpk rat. *Nature Genetics*, 38(2), 191-196.
14. Garcia-Gonzalo, F., Corbit, K., Sirerol-Piquer, M., Ramaswami, G., Otto, E., and Noriega, T. et al. (2011). A transition zone complex regulates mammalian ciliogenesis and ciliary membrane composition. *Nature Genetics*, 43(8), 776-784.
15. Sang, L., Miller, J., Corbit, K., Giles, R., Brauer, M., and Otto, E. et al. (2011). Mapping the NPHP-JBTS-MKS protein network reveals ciliopathy disease genes and pathways. *Cell*, 145(4), 513-528.
16. Williams, C., Li, C., Kida, K., Inglis, P., Mohan, S., and Semenc, L. et al. (2011). MKS and NPHP modules cooperate to establish basal body/transition zone membrane associations and ciliary gate function during ciliogenesis. *The Journal Of Cell Biology*, 192(6), 1023-1041.
17. Barker, A., Renzaglia, K., Fry, K., and Dawe, H. (2014). Bioinformatic analysis of ciliary transition zone proteins reveals insights into the evolution of ciliopathy networks. *BMC Genomics*, 15(1), 531.
18. Abdelhamed, Z., Wheway, G., Szymanska, K., Natarajan, S., Toomes, C., Inglehearn, C., and Johnson, C. (2013). Variable expressivity of ciliopathy neurological phenotypes that encompass Meckel–Gruber syndrome and Joubert syndrome is caused by complex de-regulated ciliogenesis, Shh and Wnt signalling defects. *Human Molecular Genetics*, 22(7), 1358-1372.
19. Michaels, S., and Amasino, R. (1998). A robust method for detecting single-nucleotide changes as polymorphic markers by PCR. *The Plant Journal*, 14(3), 381-385.
20. Nauta, J., Goedbloed, M. A., Van Herck, H., Hesselink, D.A., Visser, P., Willemsen, R., Van Dokkum, R.P.E., Wright, C.J., and Guay-Woodford, L.M. (2000). New rat model that phenotypically resembles autosomal recessive polycystic kidney disease. *Journal of the American Society of Nephrology*, 11(12), 2272-2284.
21. Wagshul, M., McAllister, J., Rashid, S., Li, J., Egnor, M., and Walker, M. et al. (2009). Ventricular dilation and elevated aqueductal pulsations in a new experimental model of communicating hydrocephalus. *Experimental Neurology*, 218(1), 33-40.

22. Steinemann, A., Galm, I., Chip, S., Nitsch, C., and Maly, I. (2016). Claudin-1, -2 and -3 are selectively expressed in the epithelia of the choroid plexus of the mouse from early development and into adulthood while claudin-5 is restricted to endothelial cells. *Frontiers In Neuroanatomy*, 10.
23. Günzel, D., and Yu, A. (2013). Claudins and the modulation of tight junction permeability. *Physiological Reviews*, 93(2), 525-569.
24. Shim, J., Sandlund, J., Han, C., Hameed, M., Connors, S., and Klagsbrun, M. et al. (2013). VEGF, which is elevated in the CSF of patients with hydrocephalus, causes ventriculomegaly and ependymal changes in rats. *Experimental Neurology*, 247, 703-709.
25. Shim, J., Sandlund, J., and Madsen, J. (2014). VEGF: A potential target for hydrocephalus. *Cell And Tissue Research*, 358(3), 667-683.
26. Carter, C., Vogel, T., Zhang, Q., Seo, S., Swiderski, R., and Moninger, T. et al. (2012). Abnormal development of NG2+PDGFR- α + neural progenitor cells leads to neonatal hydrocephalus in a ciliopathy mouse model. *Nature Medicine*, 18(12), 1797-1804.
27. Tu, T., Turtzo, L., Williams, R., Lescher, J., Dean, D., and Frank, J. (2014). Imaging of spontaneous ventriculomegaly and vascular malformations in Wistar rats: Implications for preclinical research. *Journal Of Neuropathology & Experimental Neurology*, 73(12), 1152-1165.
28. Tammachote, R., Hommerding, C., Sindera, R., Miller, C., Czarnecki, P., and Leightner, A. et al. (2009). Ciliary and centrosomal defects associated with mutation and depletion of the Meckel syndrome genes MKS1 and MKS3. *Human Molecular Genetics*, 18(17), 3311-3323.
29. Sohara, E., Luo, Y., Zhang, J., Manning, D., Beier, D., and Zhou, J. (2008). Nek8 regulates the expression and localization of polycystin-1 and polycystin-2. *Journal Of The American Society Of Nephrology*, 19(3), 469-476.
30. Muchatuta, M., Gattone, V., Witzmann, F., and Blazer-Yost, B. (2009). Structural and functional analyses of liver cysts from the BALB/c-cpk mouse model of polycystic kidney disease. *Experimental Biology And Medicine*, 234(1), 17-27.
31. Yung, Y., Mutoh, T., Lin, M., Noguchi, K., Rivera, R., and Choi, J. et al. (2011). Lysophosphatidic acid signaling may initiate fetal hydrocephalus. *Science Translational Medicine*, 3(99), 99ra87-99ra87.

32. Robinson, S. (2012). Neonatal posthemorrhagic hydrocephalus from prematurity: pathophysiology and current treatment concepts. *Journal Of Neurosurgery: Pediatrics*, 9(3), 242-258.
33. Shim, J., Sandlund, J., Hameed, M., Blazer-Yost, B., Zhou, F., Klagsbrun, M., and Madsen, J. (2016). Excess HB-EGF, which promotes VEGF signaling, leads to hydrocephalus. *Scientific Reports*, 6(1).
34. Wilson, P. (2011). Apico-basal polarity in polycystic kidney disease epithelia. *Biochimica Et Biophysica Acta (BBA) - Molecular Basis Of Disease*, 1812(10), 1239-1248.
35. Tissir, F., Qu, Y., Montcouquiol, M., Zhou, L., Komatsu, K., and Shi, D. et al. (2010). Lack of cadherins Celsr2 and Celsr3 impairs ependymal ciliogenesis, leading to fatal hydrocephalus. *Nature Neuroscience*, 13(6), 700-707.
36. Damkier, H., Brown, P., and Praetorius, J. (2013). Cerebrospinal fluid secretion by the choroid plexus. *Physiological Reviews*, 93(4), 1847-1892.
37. Terryn, S., Ho, A., Beauwens, R., and Devuyt, O. (2011). Fluid transport and cystogenesis in autosomal dominant polycystic kidney disease. *Biochimica Et Biophysica Acta (BBA) - Molecular Basis Of Disease*, 1812(10), 1314-1321.
38. Blazer-Yost, B. (2015). ADPKD channels: The polycystins. *Ion Channels And Transporters Of Epithelia In Health And Disease*, 747-771.
39. Vierkotten, J., Dildrop, R., Peters, T., Wang, B., and Ruther, U. (2007). Ftm is a novel basal body protein of cilia involved in Shh signalling. *Development*, 134(14), 2569-2577.
40. Leightner, A., Hommerding, C., Peng, Y., Salisbury, J., Gainullin, V., and Czarnecki, P. et al. (2013). The Meckel syndrome protein meckelin (TMEM67) is a key regulator of cilia function but is not required for tissue planar polarity. *Human Molecular Genetics*, 22(10), 2024-2040.
41. Paxinos, G., and Watson, C. (2004). *The rat brain in stereotaxic coordinates* (pp. 40-367).

CHAPTER 3. ACTIVATION OF TRPV4 STIMULATES ION FLUX IN PCP-R CELLS

3.1 Preface

The following journal article, of which I am co-first author, was submitted to the *American Journal of Physiology: Cell Physiology* in December of 2017 and accepted in May of 2018. In this article, I contributed by conducting the electrophysiology experiments with the inhibitor of two of the three IK isoforms, TRAM34 (Figures 10-11). For this experiment, I tested two different concentrations of TRAM34 in order to determine whether IK was necessary for TRPV4-mediated ion flux and whether the IK channel was the TRAM34-sensitive or -insensitive form. Higher concentrations of TRAM34 showed that our cells contained the TRAM34-insensitive isoform.

Additional data I provided for this article included the immunofluorescence experiments on the PCP-R cells untreated and treated with the TRPV4 agonist, GSK1016790A (Figure 6). These images show the protein claudin-1 in the junctional complexes of the cells. From this, we were able to conclude that the cell line not only grows as a monolayer, but also that the junctional complexes are not affected by the activation of TRPV4 via its agonist. Negative controls were included to further confirm our conclusions.

Further contributions I provided included performing statistical analysis on all electrophysiology experiments. This analysis involved running Student's t-tests on all data points compared to either the experimental group's control or another experimental group within the same data set. The data point was deemed significant if the $p < 0.02$.

Finally, I was involved in the formatting and revisions of this article. In regard to formatting, I designed and formatted the immunofluorescence and RT-PCR figures and formatted all electrophysiology figures published. I also assisted with the design of the CP epithelia diagram (Figure 12). Furthermore, during the revision process, I drafted and revised answers to reviewer comments and questions as well as revised the manuscript in accordance with reviewer suggestions. I was also thoroughly involved in reviewing and editing the manuscript in preparation for submission and publication.

3.2 Activation of TRPV4 Stimulates Transepithelial Ion Flux in a Porcine CP Cell Line

Daniel Preston^{1*}, Stefanie Simpson^{1*}, Dan Halm², Alexandra Hochstetler¹, Christian Schwerk³, Horst Schrotten³, Bonnie L. Blazer-Yost¹

1. Department of Biology, Indiana University-Purdue University at Indianapolis, Indiana

2. Neuroscience, Cell Biology and Physiology, Wright State University, Dayton, Ohio

3. Mannheim Medical Faculty, University of Heidelberg, Childrens Hospital, Mannheim, Germany

* These authors contributed equally to the research

Running Title: The TRPV4 Hub Protein in Choroid Plexus

Corresponding Author

Bonnie L. Blazer-Yost

Indiana University-Purdue University Indianapolis

Biology Department, SL 358

723 West Michigan Street

Indianapolis, IN 46202

Tel: 317-278-1145; Fax: 317-274-2846

email: bblazer@iupui.edu

Keywords: Ca²⁺-activated K⁺ channels, epithelial conductance, blood-choroid plexus barrier, IK, TRAM34

D.P., S.S. and A.H. performed the electrophysiological experiments and calculated the results; D.P. conducted the RT-PCR experiments; S.S. performed the confocal imaging; D.H. provided intellectual input regarding the calculation and interpretation of conductance measurements; C.S. and H.S. provided the PCP-R cell line and advice regarding the culturing of the cells; B.B.Y. designed the experiments, approved the final data presentation and wrote the manuscript.

3.3 Abstract

The choroid plexus (CP) epithelium plays a major role in the production of cerebrospinal fluid (CSF). A polarized cell line, the porcine choroid plexus – Riems (PCP-R) line, that exhibits many of the characteristics of the native epithelium, was used to study the effect of activation of the transient receptor potential vanilloid 4 (TRPV4) cation channel found in the PCP-R cells as well as in the native epithelium. Ussing-style electrophysiological experiments showed that activation of TRPV4 with a specific agonist, GSK 1016790A, resulted in an immediate increase in both transepithelial ion flux and conductance. These changes were inhibited by either of two distinct antagonists, HC067047 or RN1734. The change in conductance was reversible and did not involve disruption of epithelial junctional complexes. Activation of TRPV4 results in Ca^{2+} influx, therefore, we examined whether the electrophysiological changes were the result of secondary activation of Ca^{2+} -sensitive channels. PCP-R cells contain two Ca^{2+} -activated K^+ channels, the small conductance (SK) 2 and the intermediate conductance (IK) channels. Based on inhibitor studies, the former is not involved in the TRPV4-mediated electrophysiological changes while one of the three isoforms of the IK channel (KCNN4c) may play a role in the apical secretion of K^+ . Blocking the activity of this IK isoform with TRAM34 inhibited the TRPV4-mediated change in net transepithelial ion flux and the increased conductance. These studies implicate TRPV4 as a hub protein in the control of CSF production through stimulation by multiple effectors resulting in transepithelial ion and subsequent water movement.

3.4 Introduction

The choroid plexus (CP), formed by a tufted capillary surrounded by an epithelial monolayer, is thought to be responsible for the majority of cerebrospinal fluid (CSF) production. CSF cushions and protects the brain, substantially reducing the effective weight of the organ. CSF also serves as a medium to deliver nutrients, effectors and immune modulators as well as to remove toxins including β -amyloid (6, 22, 27, 36). In addition, CSF contributes to more subtle functions that are dependent on minor changes in electrolyte composition such as modulating sleep/wake cycles and neuronal excitability (10).

The CP is among the most secretory of the organ systems, with approximately 2 grams of tissue producing in excess of 0.5 liters of CSF per day in an adult human (7, 22, 34). The capillary bed that serves as the source of the major components of the CSF is lined with a fenestrated endothelium, therefore, producing a plasma filtrate based primarily on molecular size. The CP epithelium that surrounds the capillaries forms the blood-CSF barrier and is the basis for the selectivity that is responsible for the unique composition of the CSF by the regulated movement of electrolytes and water (7, 22, 34). Notably, in addition to a pH differential in which CSF is slightly more acidic (pH 7.27) compared to the interstitial fluid (pH 7.46), there are differences in electrolyte composition between the CSF and the plasma (22). Transporters and regulatory proteins present in the CP epithelial cells are responsible for creating and maintaining these crucial compositional differences. As recently reviewed (22), the major electrolyte transporters and aquaporins present in the CP have been elucidated, and their polarization within the epithelial membranes is well established. Other, less well-documented transporters remain to be identified. The effectors that control the expression and activation of these CP transport proteins remain largely unknown. Because the composition and volume of the CSF is not static but varies on a diurnal basis (10), understanding the complex mechanisms controlling the production of CSF is crucial for understanding critical brain functions in both health and disease.

Transient receptor potential vanilloid 4 (TRPV4) is one member of a family of mechano- and osmotic-sensitive channels found in multiple cell types, including the CP (16, 21, 33). When activated, TRPV4 acts as a non-specific cation channel that allows the influx of Ca^{2+} into cells. In several tissues, TRPV4 serves as a hub protein that coordinates multiple internal and external signals with the activation of electrolyte and water channels in a tissue-specific manner (9). TRPV4 has been shown to have direct effects on transport proteins in the brain including aquaporin-4 in astrocytes (5), and the Ca^{2+} -activated Cl^- channel, TMEM16A, in primary cultures of CP cells (30). In the hippocampus, TRPV4 was elevated 8 hours after traumatic brain injury and the increased expression was dependent on NKCC1 (18), a co-transporter which is also found in the apical membrane of native CP epithelia (35). Calcium influx through TRPV4 has also been shown to stimulate Ca^{2+} -sensitive K^+ channels in a tissue-specific manner. Ca^{2+} -sensitive K^+ channels fall into three categories: BK (big conductance; $\text{K}_{\text{Ca}1.1}$); IK (intermediate conductance; $\text{K}_{\text{Ca}3.1}$; $\text{K}_{\text{CNN}4}$); or SK1, SK2, SK3 (small conductance; $\text{K}_{\text{Ca}2.1}$, 2.2, 2.3) channels (28). In

endothelial cells of smaller resistance arteries and arterioles, low intraluminal pressure stimulates TRPV4 causing localized Ca^{2+} sparklets which activate IK channels and reduce arteriole tone (2). In these resistance arteries, activation of the TRPV4 did not stimulate SK channels although the SK channel $\text{K}_{\text{Ca}2.3}$ is present in the endothelial cells. In freshly isolated cerebral myocytes, there are indications that TRPV4 forms a Ca^{2+} signaling complex with ryanodine receptors and BK channels that elicits smooth muscle hyper-polarization and arterial dilation (11). TRPV4 activation also resulted in the secondary activation of the BK channel in a high resistance mammary epithelial cell line (23). TRPV4 has been identified on the apical membrane of native CP epithelia (24, 30) and in primary CP cell lines (20, 30).

The complexity of the CP *in vivo* makes studying the regulation of electrolyte transporters challenging. Unfortunately, most *in vitro* primary cultures of CP epithelial cells exhibit a very low transepithelial electrical resistance (TER) that is inconsistent with the barrier function of these epithelia *in vivo*. In addition, a low transepithelial resistance poses technical difficulties when measuring permeability changes that may be part of an effector response. Continuous cell lines recently established in one of our laboratories (H.S. and C.S.) are, to our knowledge, the only lines described that exhibit a moderate to high TER (25, 26). The porcine choroid plexus – Riems (PCP-R) cell line expresses tight junction components, including claudin-1, claudin-3, ZO-1 and occludin, and develops a high transepithelial resistance when grown on permeable supports indicating the formation of a barrier epithelium (25). In the current studies, the PCP-R line was used to examine the physiological effects of TRPV4 stimulation on the permeability of the epithelial monolayer and on activation on electrogenic transepithelial ion flux.

3.5 Materials and Methods

Cell Culture: The PCP-R cell line was derived from primary cultures of porcine choroid plexus (25). PCP-R cells were grown in DMEM containing 4.5 g/L glucose, 3.7 g/L NaHCO_3 , 24 mM HEPES, 10% fetal bovine serum, 100 U/ml penicillin, 100 mg/ml streptomycin and 5 $\mu\text{g/ml}$ insulin. Cells were grown in a 75 cm^2 flask until confluent (typically 7-10 days). For electrophysiology experiments, cells were trypsinized and seeded onto a permeable, 0.4 μm pore diameter, filter support (EMD Millipore, Billerica, MA) at 50% confluent density in PCP-R media and placed

inside a 6-well plate (Corning, Corning, NY). The bottom of each well was bathed in 2 ml of PCP-R media, and 1.5 ml of the media containing cells was placed on the top of the filter. PCP-R media was replaced thrice weekly.

Electrophysiology: For electrophysiological analyses, PCP-R cells were cultured on 6-well, Transwell filters for 9-12 days. Ussing-style electrophysiological techniques were used to monitor TER/conductance as well as changes in electrogenic transepithelial ion flux. Filters were excised, mounted in Ussing chambers, and connected to a DVC-1000 Voltage/Current Clamp (World Precision Instruments) with voltage and current electrodes on either side of the membrane. Each half of the chamber contains a tapered fluid compartment with fittings for voltage electrodes (close to the epithelial membrane) and current electrodes (at the opposite end of the chamber). Each fluid chamber was water jacketed to maintain a constant temperature (37°C). The cells were bathed in serum-free media. Media were circulated in the chambers and oxygenated by means of a 5% CO₂/O₂ gas lift. The spontaneous transepithelial potential difference was measured and clamped to zero, and the resultant short-circuit current (SCC) was monitored continuously as a measurement of net transepithelial ion flux. As per convention, a positive deflection in the SCC is either anion secretion (from blood to CSF) or cation absorption (CSF to blood) and a negative deflection indicates the opposite. TER is recorded every 200 seconds throughout each experiment by applying a 2 mV pulse and using the resulting deflection in the SCC to calculate the TER and conductance by Ohm's law. Cultures that showed basal TERs of less than 500 Ω.cm² were not used. Conductances were also calculated from the change in SCC during the voltages pulses as $\Delta I/\Delta V$. In all cases, the graphs shown in each panel represent a series of control and experimental cultures that were grown and analyzed in parallel.

Immunostaining: PCP-R cells were grown to confluency on Transwell filters (9-12 days). Cells were treated with diluent or the TRPV4 agonist GSK101679A for 10 minutes and then immediately fixed with 4% paraformaldehyde in PBS. For immunohistochemistry, the fixed cells were washed and incubated overnight with anti-claudin-1 primary antibody (Abcam ab15098; 1:200 dilution) diluted in blocking solution (PBS, 1% goat serum, 1% BSA, 0.1% sodium azide) at 4°C. The cells were then washed and incubated with secondary antibody. The secondary antibody was Alexa Fluor dye-conjugated goat anti-rabbit (Jackson ImmunoResearch 111-545-

144, 1:1000 dilution in blocking solution). For nuclear staining DAPI (500 ng/ml; Sigma D9542) was used. Confocal images were taken on a Leica TCS SP8 (upright high-speed multiphoton and confocal imaging system).

RT-PCR: PCP-R cells were grown as a monolayer in a 75 cm² flask in PCP-R media until confluent. Total RNA was isolated using the RNeasy mini kit (Qiagen, Hilden, Germany), according to the manufacturer's supplementary protocol for animal cells grown in a monolayer. 5 µg of total RNA was transcribed to cDNA using the Superscript IV First-Strand Synthesis System (Invitrogen, Carlsbad, CA) according to the manufacturer's protocol using both random hexamers and oligo-dT primers. Specific primers were designed using Primer3Plus according to mRNA sequences obtained from Ensembl and verified using the NCBI database. cDNA was then used for PCR utilizing GoTaq Green Master Mix (Promega, Madison, WI) and 10 µM forward and reverse primers (IDT, Coralville, IA) (Table 3.1) and the products separated on a gradient agarose gel to determine optimum annealing temperatures. A second PCR was carried out using only optimum annealing temperatures for each primer pair. Electrophoresis was carried out on a 1.5% agarose gel stained with ethidium bromide utilizing flanking 1 kb and 100 bp ladders and visualized under UV light using a ChemiDoc XRS imager (Bio-Rad, Hercules, CA). The primers used are shown in Table 3.1.

Statistics: All results shown are displayed as mean ± S.E.M. for the number of experiments indicated on the graphs. Indicated plot points on all figures were compared using Two-tailed Students *t*-test. P-values less than 0.02 were considered significant. All statistical analyses were performed using SigmaPlot 13.0.

3.6 Results

The PCP-R cell line develops a high resistance monolayer when grown on permeable supports with optimal resistances occurring 9-12 days post seeding (Figure 3.1). Addition of the TRPV4 agonist GSK1016790A to PCP-R cells causes an increase in transepithelial conductance indicating an increased permeability across the epithelial monolayer (Figure 3.2, top). Concurrently with the initiation of the conductance change is a stimulation of short circuit current (SCC) indicating net

electrogenic transepithelial ion flux composed of anion absorption (CSF to blood) and/or cation secretion (blood to CSF) (Figure 3.2, bottom). Although the conductance remains elevated, the net electrolyte flux returns to a level that is statistically equal to the basal level within 20-30 minutes after agonist addition. A 10 minute pre-treatment with either of two structurally unrelated TRPV4 antagonists, HC067047 or RN1734, completely blocked the increased permeability of the monolayer as well as the electrogenic ion flux (Figure 3.2). To determine the maximal concentration of the agonist which did not result in an irreversible change in conductance and ion flux, a dose response was performed using concentrations of 0.1, 1, 3, 5, and 10 nM GSK1016790A (Figure 3.3). When the TER of the epithelial monolayer falls below $100 \Omega \cdot \text{cm}^2$ or the conductance rises higher than 10 mS/cm^2 it is observed that the TER will continue to fall to unmeasurable levels and the experiment using this culture has to be discarded (data not shown).

A limited dose response was also performed for the TRPV4 antagonist RN1734 at concentrations of 5, 25, and 50 μM in order to determine the maximal inhibitory concentration (Figure 3.4). Interestingly, the agonist-induced conductance responses are immediately reversible upon the addition of a TRPV4 antagonist. This reversal is accompanied by a statistically significant change in the electrogenic flux (Figure 3.5).

To visualize how the TRPV4 agonist was affecting the junctional complexes, PCP-R cells grown on Transwell filter supports were treated with GSK1016790A or diluent for 10 minutes before fixation and staining with anti-claudin-1 antibody (Figure 3.6). During the incubations, the Ca^{2+} concentration was maintained by the use of serum-free media because changes in extracellular Ca^{2+} have profound effects on tight junctions and epithelial conductance (13,19). The untreated, agonist treated, and negative control (no primary antibody) cells were grown in the same 6-well Transwell plate and were treated, fixed, stained and imaged in parallel. No obvious difference was observed between the junctional complexes in any of the monolayers examined; rather all junctional complexes remained intact.

Stimulation of TRPV4 causes an influx of Ca^{2+} which is postulated to secondarily stimulate Ca^{2+} -activated channels. Therefore primers were designed to determine the presence of Ca^{2+} -activated K^+ channels in the PCP-R cell line. When negative results were obtained, a second primer pair

was designed to confirm the results (Table 3.1). The only Ca^{2+} -sensitive K^+ channels found in the PCP-R cell line were the intermediate conductance (IK; $\text{K}_{\text{Ca}3.1}$) and the small conductance (SK) 2 channels (Figure 3.7). As expected, TRPV4 is endogenously expressed in the cell line (Figure 3.7).

The RT-PCR results were followed by electrophysiological experiments. As expected from the PCR results, iberiotoxin, an inhibitor of big conductance potassium channels (BK; $\text{K}_{\text{Ca}1.1}$) had no effect on the TRPV4-stimulated conductance change or transepithelial ion flux (Figure 3.8). Unexpectedly, apamin, a pan-SK channel blocker, was also without effect on TRPV4-mediated ion flux or conductance changes (Figure 3.9). A similar lack of effect on either electrophysiological parameter was noted after pre-incubation with the more SK2-specific inhibitors tamapin, Lei-Dab, or scyllatoxin (data not shown).

Pre-treatment with low dose (1 μM) TRAM 34, an inhibitor of two of the three isoforms of IK, also termed Kcnn4 , had no effect on the subsequent response to TRPV4 agonist. However, increasing the TRAM 34 concentration to 50 μM resulted in an inhibition of both the increased conductance and short-circuit current (Figure 3.10). If a moderately high dose of TRAM 34 (25 μM) was added to the apical bathing media during the pre-incubation, the response to the TRPV4 agonist was completely inhibited; conversely if the same concentration was added only to the media bathing the serosal face of the tissue, there was a reduced inhibition of the ion flux accompanied by a substantial, but not complete, inhibition of the increased conductance (Figure 3.11).

3.7 Discussion

Choroid plexus cell line models should be expected to have a phenotype characteristic of epithelia that maintain controlled movement of electrolytes and fluid. In the initial description of the PCP-R cell line, the cultures developed a transepithelial resistance of 300-600 $\Omega\cdot\text{cm}^2$ after 6 days of culture on permeable supports depending on seeding density (25). In the current studies, additional days in culture resulted in monolayers that exhibited even tighter epithelia, more suitable for electrophysiological experiments.

In preliminary studies, TRPV4 antagonists decrease hydrocephalic development in a genetic rat model of the disease suggesting a role for TRPV4 in CSF secretion (8). As in the native CP (33), the PCP-R cells contain TRPV4 which can be activated by a specific TRPV4 agonist. The electrophysiological changes elicited by the TRPV4 agonist are inhibited by two structurally distinct and specific antagonists which underscores the specificity of the response.

The rapid and substantial increase in transepithelial conductance elicited in response to the TRPV4 agonist was unexpected and indicates a large change in transcellular permeability. The conductance plateaus at a high level indicating that the permeability remains increased even though the electrogenic ion flux returns toward basal levels by 20-25 minutes. Similar large conductance changes have previously been described in colonic epithelia, another epithelium capable of large secretory fluxes, after stimulation with prostaglandins (15). In the PCP-R cells, both the increased permeability and stimulated ion flux are immediately reversible by TRPV4 antagonists even after the initiation of a response.

TRPV4 has been previously reported to regulate the integrity of the blood-CSF barrier (20). However, these studies are difficult to compare to the current experiments because the starting resistances of the primary cultures used were low ($50-70 \Omega \cdot \text{cm}^2$) and treatment with 10 nM GSK1016970A caused a disintegration of the cell junctions within 10-20 minutes. Activation of TRPV4 by the phorbol ester 4α -PDD (4α -phorbol-12,13-didecanoate) also caused a decrease in transepithelial resistance (increased conductance) in a mammary epithelial cell line similar to the change seen in the PCP-R cells (23). In the latter phase of mammary cell response there was down-regulation of junctional claudins and frequent large breaks in the tight junction strands.

A dose response using the TRPV4 agonist GSK1016790A in the PCP-R cell line indicated that while 5 and 10 nM elicited stronger responses, treatment of PCP-R cells with 3 nM GSK1016970A caused no overt changes in the cell junctions and did not cause an irreversible disruption of the epithelial structure in confluent monolayers. To mimic a physiologically relevant response, 3 nM agonist was used in the majority of the experiments.

A dose response was performed using the TRPV4 antagonist RN1734, at concentrations of 5, 25 and 50 μM , clearly indicating that while concentrations of both 25 and 50 μM caused complete inhibition of the change in conductance, 50 μM had the more complete inhibition of the change in SCC with no adverse effects on cellular viability as measured by TER (conductance).

Claudin-1, endogenously present in both native CP (12, 14, 29) and the PCP-R cell line (25 and Figure 3.2), is considered a barrier claudin important for maintenance of transepithelial permeability (14). The immunolocalization of claudin-1 did not change after stimulation with GSK1016970A, a finding which is consistent with the rapid reversal of the TRPV4 agonist-mediated response by antagonist. Both findings suggest that, under our experimental conditions, the junctional complexes are not irreparably broken.

Taken together, our results are consistent with a change in transepithelial permeability that does not involve the breakdown of tight junctions, the dissociation of the epithelial cells, or a decrease in claudin-1 expression in the tight junctions. The reasons for the difference between the current studies and the previous reports showing a breakdown of junctional complexes is unknown but the agonist concentration may play a role. Over-activation of TRPV4 by exogenous agonists does have pathological consequences. For example, i.v. administration of GSK1016790A caused circulatory collapse in mice, rats and dogs due to endothelial barrier function failure (33). While the current studies did not explore the long term effects on the junctional complexes, it is important to consider the normal *in vivo* role of TRPV4. It is unlikely that the endogenous regulation of the channel will lead to catastrophic breakdown of tight junctions. GSK1016970A has been shown to have nanomolar potency with EC_{50}s between 1-5 nM in human, dog and bovine cellular assays and EC_{50}s of 10-18.5 nM in rodents (33). The PCP-R cells are exquisitely sensitive to the agonist with ~50% of cultures resulting in an irreversible change in conductance at both 5 and 10 nM. The maximum agonist concentration that does not result in an irreversible change in resistance/conductance appears to be 3 nM and we have chosen, therefore, not to use higher concentrations in the majority of the experiments.

When examining the transepithelial ion fluxes using short-circuit current electrophysiology, the initial direction of the TRPV4-mediated ion flux is consistent with anion absorption and/or cation

secretion. Given that the CP is, on a per gram basis, one of the most secretory epithelia in the body, it is likely that cation secretion accounts for the majority of the electrolyte flux within the first few minutes. Thereafter the net transport indicated by the SCC plateaus briefly and then reverses indicating a complex mixture of net electrogenic fluxes.

Although Na^+ secretion cannot be discounted, amiloride, an inhibitor of the epithelial Na^+ channel found in many high-resistance epithelia, did not block the TRPV4-mediated flux (data not shown). The role of other Na^+ transporters was not examined in these studies. TRPV4 is a cation channel that, when activated, transports Ca^{2+} into cells. The most likely candidate for the cation secretion was postulated to be K^+ channels, specifically Ca^{2+} -activated K^+ channels. The importance of Ca^{2+} -activated K^+ channels in CP epithelia has been recognized for over three decades (17) but the identification has remained elusive. RT-PCR of the PCP-R cells indicated the presence of SK2 and IK but not SK1 SK3, or BK. In agreement with these data an inhibitor of BK (iberiotoxin) did not block the TRPV4-stimulated changes in transepithelial ion flux or conductance in the PCP-R cell line. While the SK channels are differentially sensitive to apamin, 100 nM of this bee venom should have blocked the all three channels (32). However, pretreatment with apamin did not block the TRPV4-mediated ion flux or conductance change. Likewise, preincubation with tamapin, Lei-Dab7 or scyllatoxin, relatively specific inhibitors of SK2 (1, 32) did not inhibit GSK1016790A-stimulated electrogenic ion flux or conductance (data not shown). Thus, although SK2 appears to be present in the cell line, it is not involved in TRPV4 agonist-stimulated ion flux or conductance changes.

IK, also known as KCNN4, has recently been shown to have 3 isoforms in the rat. KCNN4a-specific transcripts were found in smooth muscle while KCNN4b and KCNN4c were expressed in epithelial cells (3). Interestingly, these latter two isoforms show a divergence in TRAM34 sensitivity as well as epithelial cell polarity. In intestinal cells, the IC_{50} for the inhibitory effect of TRAM34 on the KCNN4b isoform was in the sub-micromolar range while the IC_{50} for the KCNN4c isoform was approximately an order of magnitude higher in the low micromolar range (3, 4, 15). The KCNN4b isoform was localized to the basolateral membrane of intestinal cells where it was involved in K^+ absorption while the KCNN4c isoform was localized to the apical membrane where it is involved in K^+ secretion (4, 15, 28).

Low dose (1 μM) TRAM34 did not affect TRPV4-stimulated ion flux or conductance while 50 μM completely inhibited both parameters. These data are consistent with the involvement of the Kcnn4c isoform of the IK channel. A moderately high dose of TRAM34 (25 μM) completely inhibited TRPV4-mediated ion flux and conductance changes when added to the apical bathing media indicating an apical localization of this isoform as found in previous studies (4, 15, 28). However, addition of the same concentration of the inhibitor to the serosal bathing media partially inhibited TRPV4-mediated ion flux and substantially, but not completely, blocked the increase in conductance. These data indicate a relatively complex inhibitor effect that could be due to transepithelial permeability of the TRAM34 or to off-target effects of the inhibitor. In immune cells, micromolar concentration of TRAM-34 reduced lysophosphatidylcholine induced increases in intracellular calcium by inhibiting non-selective cation channels (24). Similar effects on non-selective cation channels, including TRPV4, cannot be ruled out in the current experiments. Figure 3.12 contains a diagram of the choroid plexus and the hypothesized placement of the IK channel based on the current studies. Additional experiments will be necessary to clarify additional components that are likely to be contributing to the electrophysiological responses.

In the 1980's, a series of elegant electrophysiological experiments by Wright and colleagues in *Necturus* CP showed that the apical membrane accounted for more than 90% of the K^+ conductance of the epithelial cells and suggested the presence of an apical Ca^{2+} -activated K^+ channel (17, 37). Our current studies are in agreement with this early work and suggest that the apical Ca^{2+} -activated K^+ channel is the KCNN4c isoform of IK.

In summary, we have shown that activation of TRPV4 stimulates a striking change in transepithelial permeability accompanied by a transepithelial ion flux. The effect of the TRPV4 agonist appears to be specific because the effect is blocked by two chemically distinct antagonists. The lack of permeability change after antagonist pre-incubation further indicates that the agonist is not having a nonspecific effect on the epithelial cell junctions. Agents that block the increase in conductance also block the electrogenic transepithelial ion flux. We hypothesize that the transepithelial ion flux is due to cation secretion because a preliminary study has indicated that TRPV4 antagonists are effective in decreasing the hydrocephalus in a model of the communicating form of the disease (8), thus suggesting that electrolyte flux into the CP is an integral component

of the response. A substantial portion of the transepithelial ion flux due to stimulation of a Ca^{2+} -activated K^+ channel, IK. The decreased sensitivity and the apical localization of the TRAM34 effect in the CP cells indicates that the form of IK found in the CP is KCNN4c. However, the sustained conductance change suggests that the response to TRPV4 stimulation is complex, likely involving electrogenic and electroneutral transporters. Further experimentation will be necessary to determine the exact nature of the osmolyte permeability and which transport effects are primary and which are secondary.

3.8 Acknowledgements

The authors would like to thank Dr. Nicolas Berbari for help in designing the RT-PCR primers.

3.9 Grants

These studies were supported by a Hydrocephalus Association/ Team Hydro Innovator Award; pilot funding from the Indiana University Collaborative Research Grant Funds of the Office of the Vice President for Research; and a Project Development Team within the ICTSI NIH/NCRR grant # ULITR001108.

3.10 Disclosures

None.

Table 3.1 Primer pairs used for the RT-PCR with corresponding product sizes (bp). To confirm the presence or absence of the gene of interest for the K⁺ channels, two different primer pairs were used. *Gapdh* was used as a positive control in all RT-PCR experiments.

<i>Sus Scrofa</i> gene	Protein	Primer Sequences 5' - 3'		Product Size (bp)
		Forward Primer	Reverse Primer	
<i>Kcnn1</i>	SK1	GGAAGAGGAAGAAGATGAGGAA	GAGAGGAAAGTGATGGAGATGA	801
	SK1	CTTCAGCATCTCCTCCTGGATC	TGGATGGCTTGGAGGAACTTAC	432
<i>Kcnn2</i>	SK2	AGAACCAGAATATCGGCTACAA	TAAAAGCATGACTCTGGCAATC	488
	SK2	TCTGATTGCCAGAGTCATGCTT	CACGTGCTTTTCTGCTTTGGTA	418
<i>Kcnn3</i>	SK3	AACACACAAAGCTGCTAAAGAA	TCTGGAGTGGGGAGTTTTATTT	466
	SK3	GGCGAGTACAAGTTCTTCTGGA	TAGCTTGCAGGAACTTCCTCTG	685
<i>Kcnn4</i>	IK	CTGGTTTGTGGCCAAGTTGTAC	TCCTACGCGTGTGTTTGTAGAA	419
	IK	ATCAGCATTTCACGTTCTTGC	TCCTACGCGTGTGTTTGTAGAA	799
<i>Kcnma1</i>	BK	ACTTGGAAGGAGTCTCAAATGA	ATCTGATCATTGCCAGGGATTA	445
	BK	TTACTGCAAGGCCTGTCATGAT	AAGGTCCGTATCAGGGTAAGGA	990
<i>Trpv4</i>	TRPV4	AGATTGGGATCTTTTCAGCACAT	AGCAAGTAGACCAGCAGGAAAC	724
<i>Gapdh</i>	GAPDH	TTTAACTCTGGCAAAGTGGAC	CATTGTTCGTACCAGGAAATGAG	884

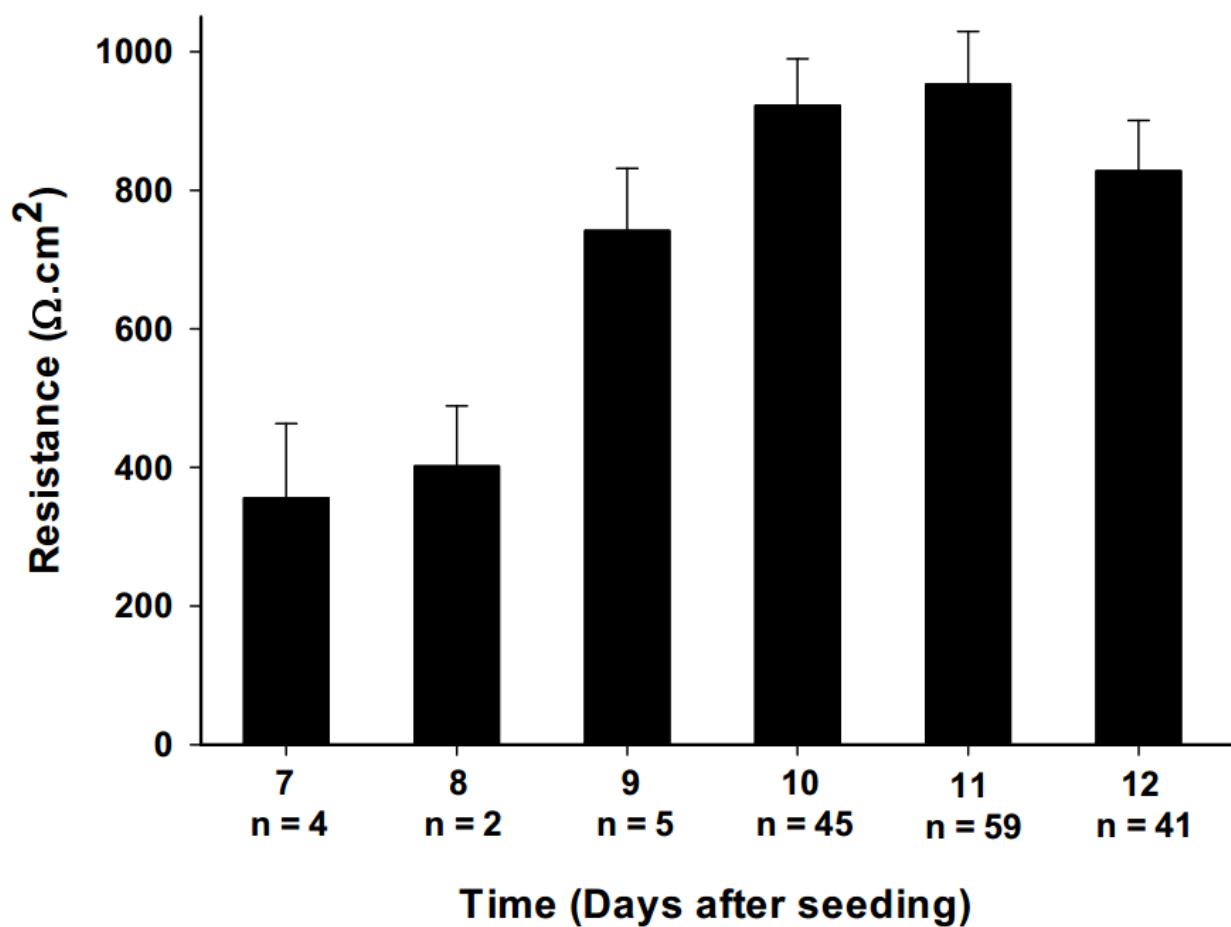


Figure 3.1 Development of transepithelial resistance of the PCP-R cell line.

Development of transepithelial resistance of the PCP-R cell line after seeding on Transwell supports. The bars are a composite of control values from multiple electrophysiological experiments conducted over a two-year period. In each case the resistance was measured just before the addition of an electrolyte transport effector, i.e., after the cells were mounted in the Ussing chambers and allowed to reach a stable baseline current. The bars represent the mean \pm S.E.M. for the number of experiments listed.

Figure 3.2: Effect of TRPV4 agonist and antagonists on transepithelial conductance and electrogenic ion flux in the PCP-R cell line. RN1734 or HC067047, specific TRPV4 antagonists were added to the PCP-R cultures indicated by the open circles and grey squares at time $T = -10$ minutes. At time 0, the TRPV4 agonist GSK 1016790A was added to all cultures. The symbols represent the means \pm S.E.M. for the number of experiments indicated on the graphs. SCC = short-circuit current. * indicates statistically significant differences between the two conditions ($p < 0.02$) as measured by Students *t-test*, paired data.

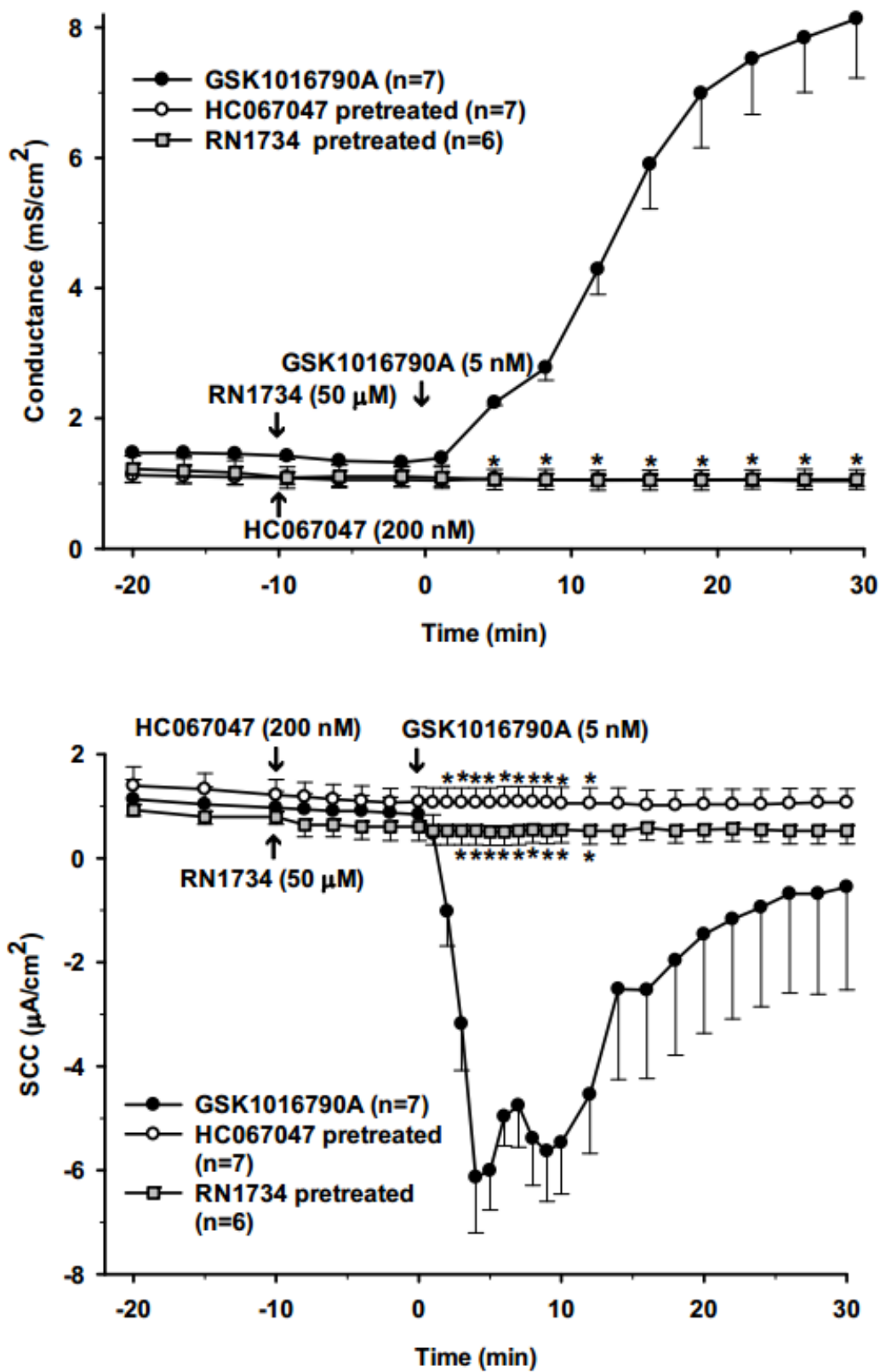


Figure 3.2 Effect of TRPV4 agonist and antagonists in the PCP-R cells.

Figure 3.3: Dose response for the TRPV4 agonist GSK1016790A effect on transepithelial conductance and ion movement in the PCP-R cell line. Concentrations of 0.1, 1, 3, 5, and 10 nM GSK1016790A were added to the PCP-R cultures at T = 0 minutes. Cell cultures whose resistance drops below $100 \Omega \cdot \text{cm}^2$ or the conductance rises higher than 10 mS/cm^2 were considered irreversibly altered by the agonist and were not included. The same experimental data were used for both graphs. Delta (Δ) SCC is defined as the difference in SCC between the value just before agonist addition and the value at the point of the maximal response. The symbols represent the means + S.E.M. for the number of experiments indicated on the graphs. SCC = short-circuit current.

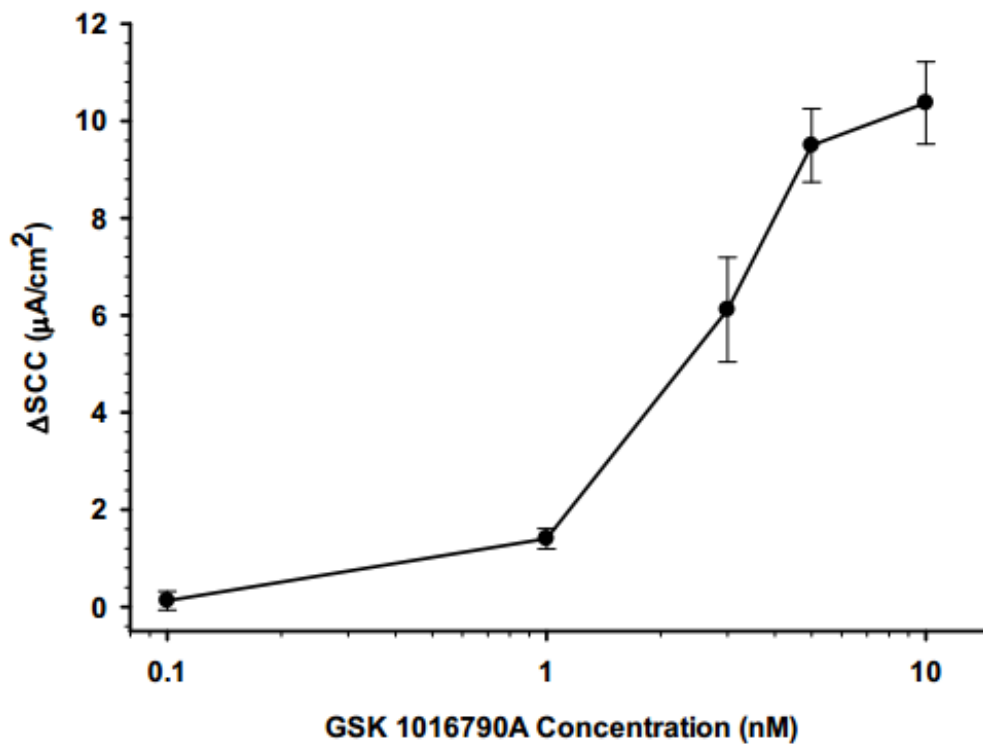
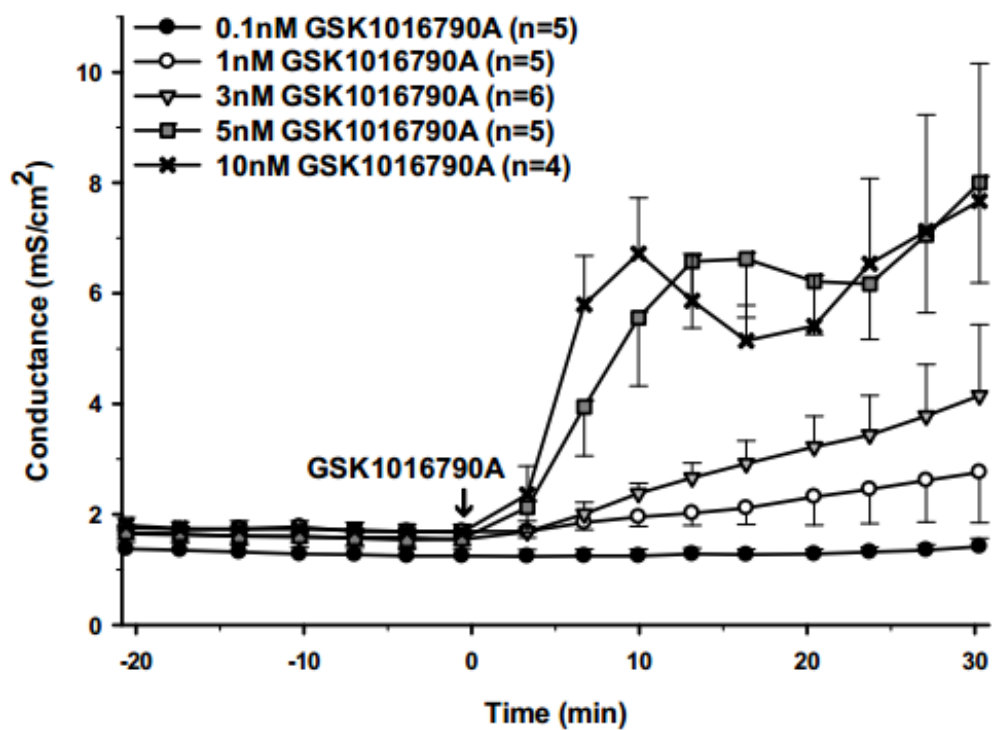


Figure 3.3 Dose response for TRPV4 agonist GSK1016790A in PCP-R cells.

Figure 3.4: Dose response for the TRPV4 antagonist RN1734 pre-treatment in the PCP-R cell line. Concentrations of 5, 25, and 50 μ M RN1734 were added to the PCP-R cultures at T = -10 minutes. At time 0, the TRPV4 agonist GSK1016790A was added to all cultures. The symbols represent the means + S.E.M. for the number of experiments indicated on the graphs. SCC = short-circuit current.

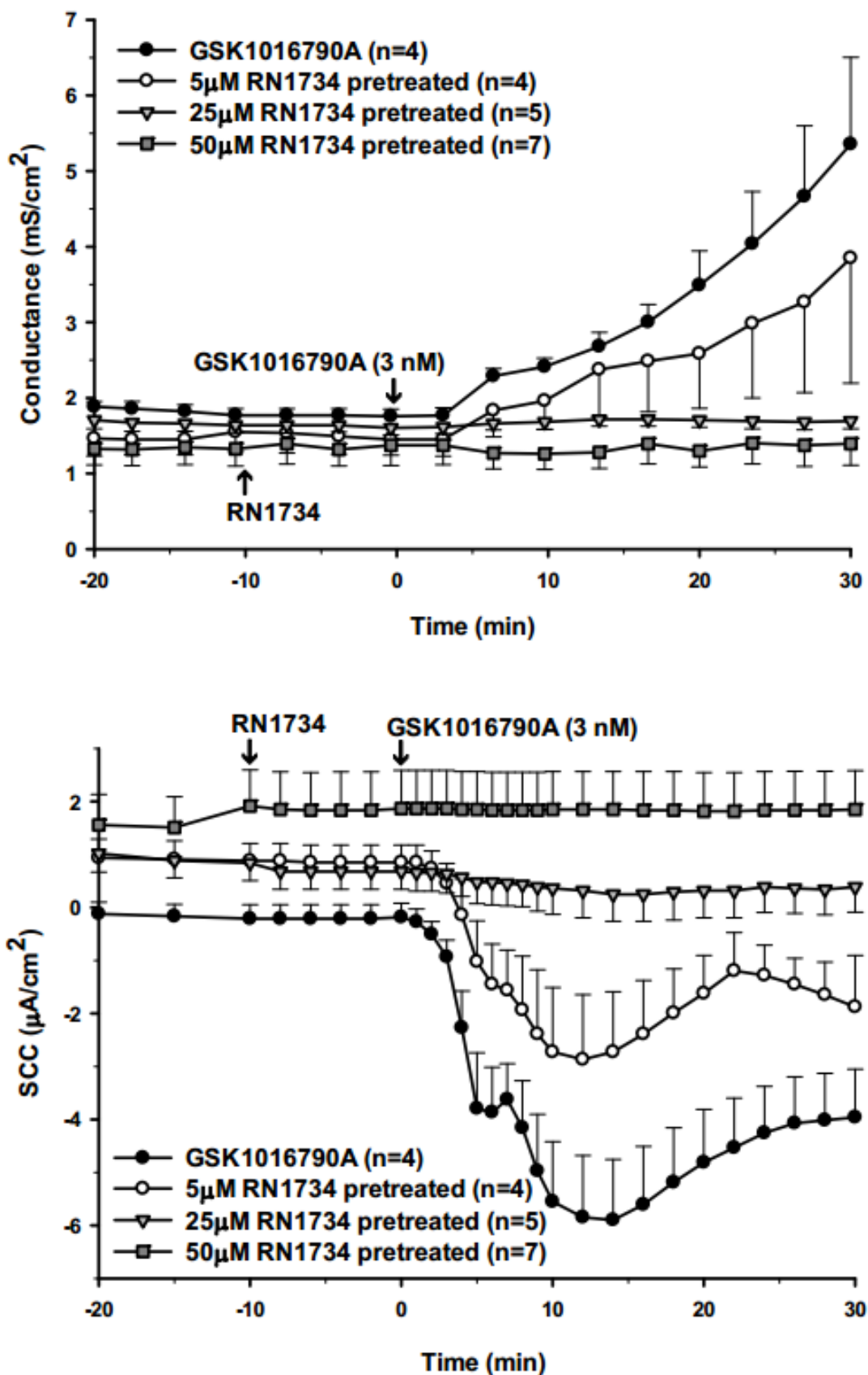


Figure 3.4 Dose response for TRPV4 antagonist RN1734 pre-treatment in PCP-R cells.

Figure 3.5: Reversibility of a TRPV4 agonist response by a TRPV4 antagonist. At time 0 the TRPV4 agonist GSK1016790A was added to all culture. RN 1734, a TRPV4 antagonist, was added to the cultures indicated by the open circles 15 minutes after the addition of the agonist. The symbols represent the means \pm S.E.M. for the number of experiments indicated on the graphs. SCC = short-circuit current. * indicates statistically significant differences between the two conditions as measured by a 2-tailed Student's t-test ($p < 0.02$).

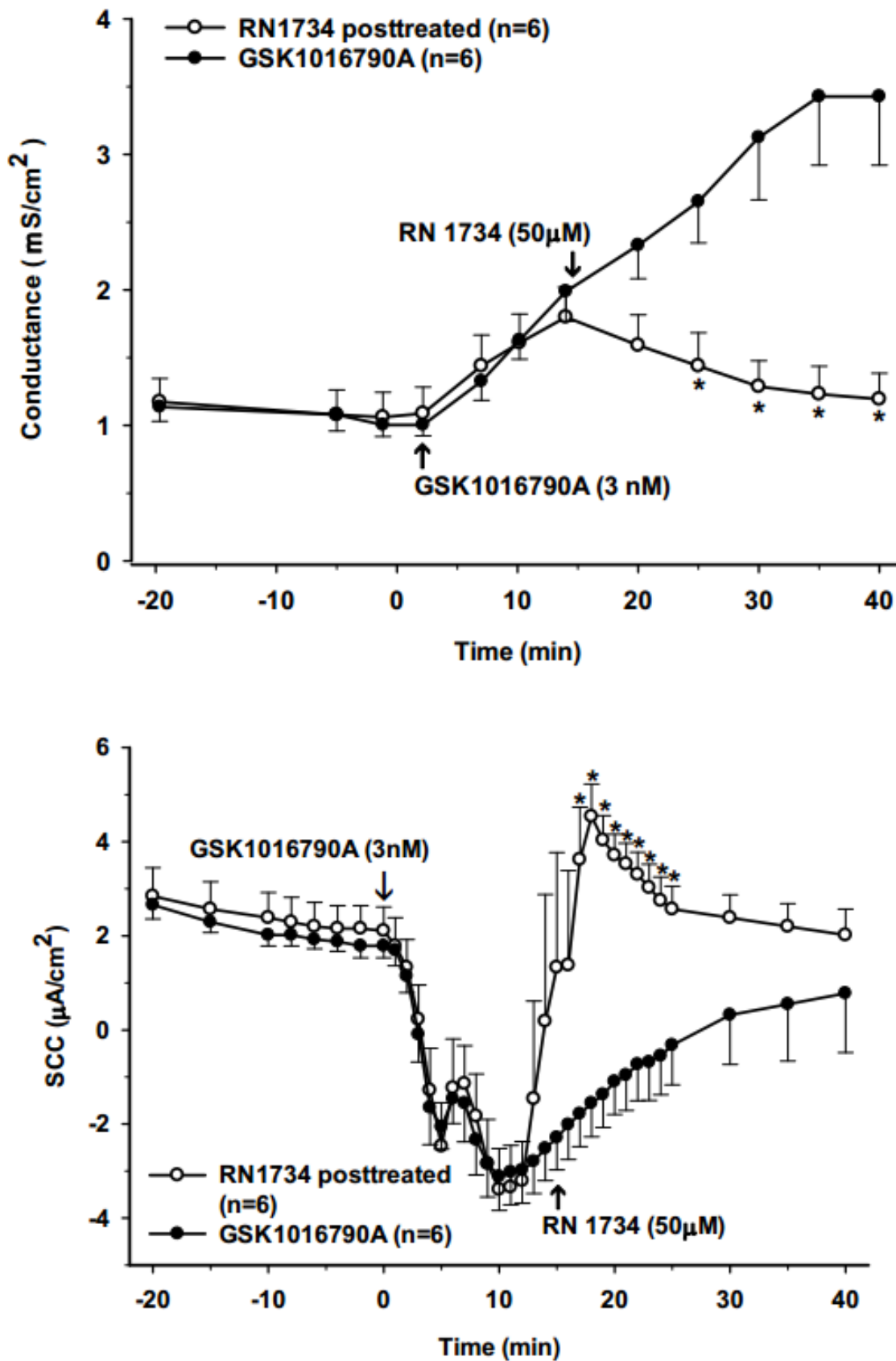


Figure 3.5 Reversibility of a TRPV4 agonist response by a TRPV4 antagonist.

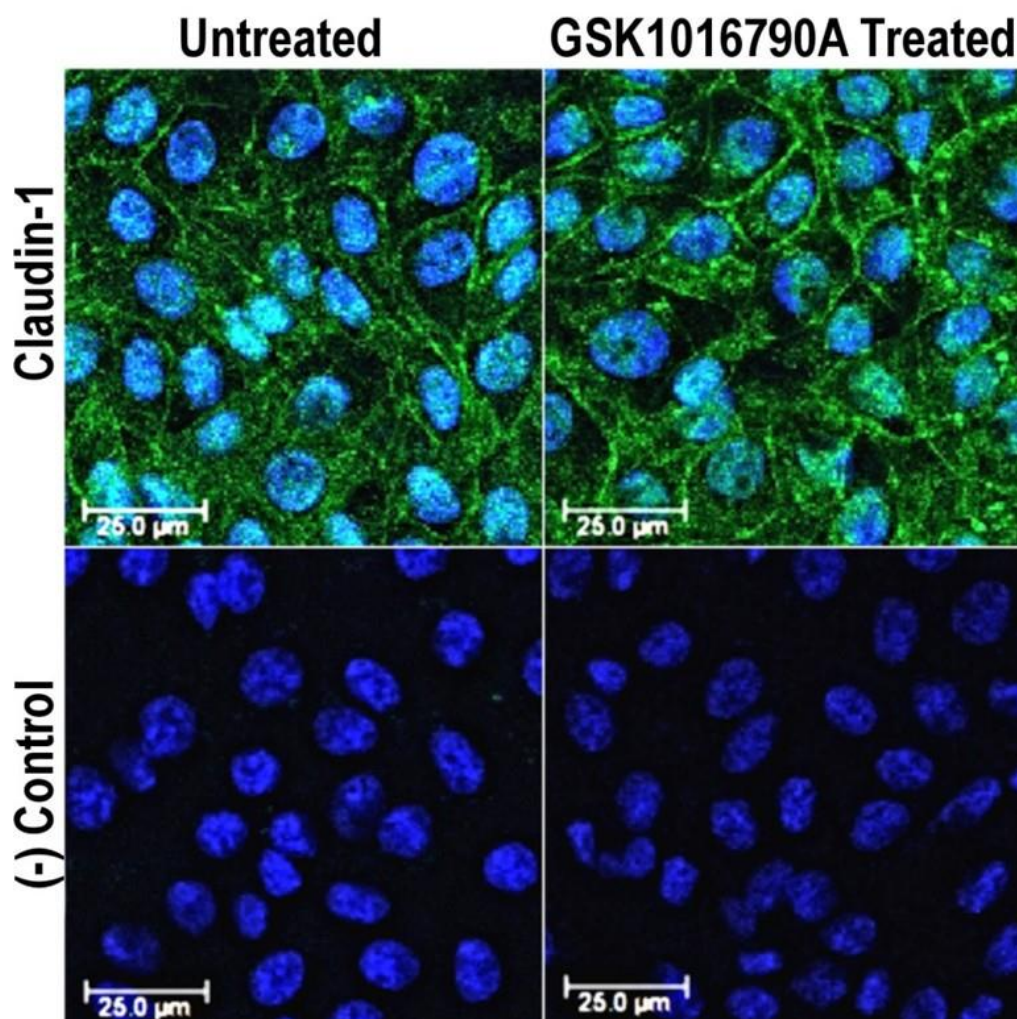


Figure 3.6 Immunohistological staining of claudin 1 in the PCP-R cell line.

Cells were stained with DAPI (blue) to visualize nuclei and anti-claudin-1 antibody (green) to show the presence of tight junctions. Treated cells were pre-incubated with TRPV4 agonist, GSK1016790A (3nM), for 10 minutes before fixation and staining. Negative control cells were stained with DAPI and secondary antibody only. This figure is representative of 4 independently conducted experiments. Scale bars represent 25μm.

Figure 3.7: RT-PCR of selected ion channels in the PCP-R cell line. Left hand gel shows the results of RT-PCR of Ca²⁺-activated K⁺ channels. The gel shows expression of only SK2 and IK among the calcium activated potassium channels. SK1, SK3 and BK were all notably absent. The second gel shows expression of TRPV4. For any channels not present, additional primer sets were utilized to confirm absence of the cDNA.

SK = small conductance K⁺ channel; IK = intermediate conductance K⁺ channel; BK = big conductance K⁺ channel; TRPV4 = transient receptor potential vanilloid 4; GAPDH = glyceraldehyde 3-phosphate dehydrogenase

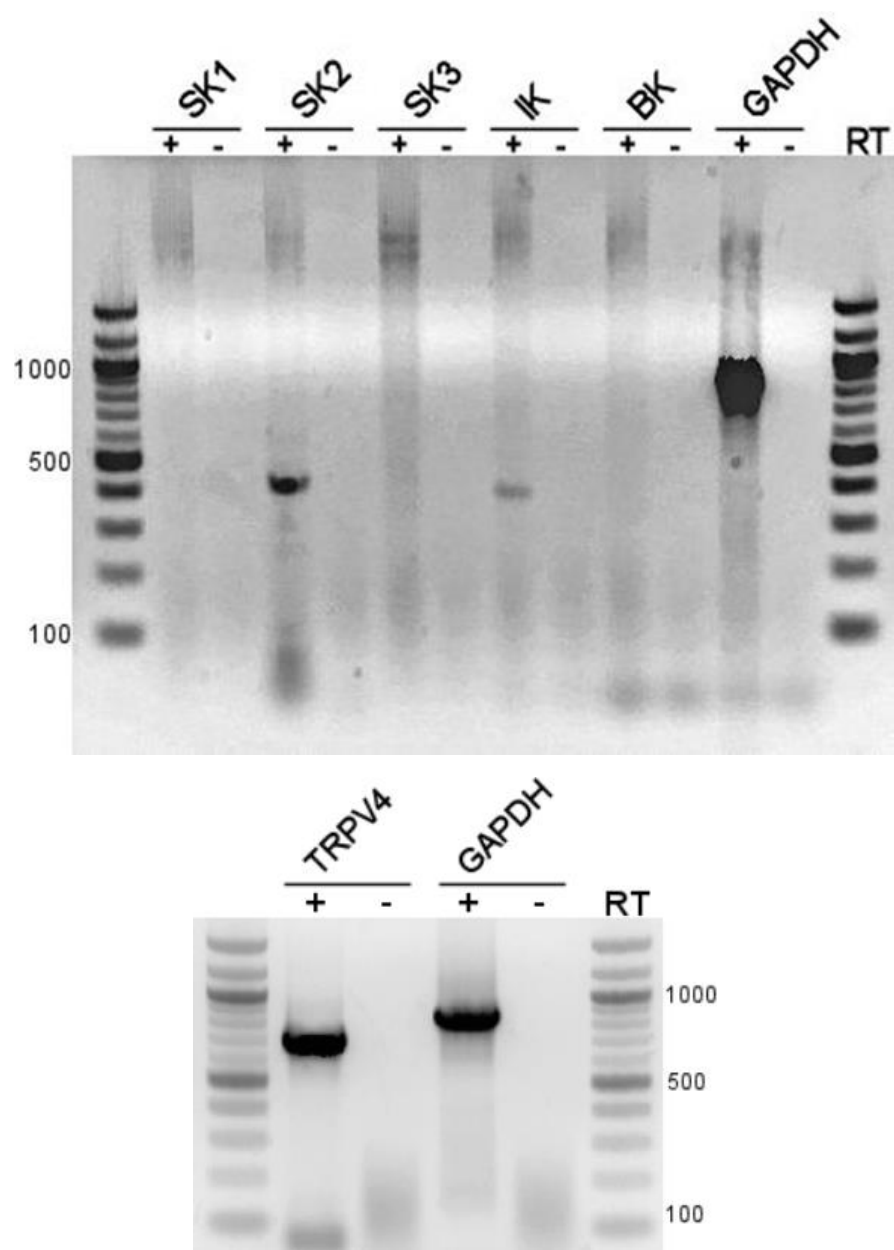


Figure 3.7 RT-PCR of selected ion channels in the PCP-R cell line.

Figure 3.8: Effect of pre-treatment with a BK channel inhibitor on TRPV4 agonist stimulated increases in transepithelial conductance and ion transport. Iberiotoxin, an inhibitor of big conductance potassium (BK) channel was added to the PCP-R cultures indicated by the open circles at time T = -10 minutes. At time 0, the TRPV4 agonist GSK 1016790A was added to all cultures. The symbols represent the means \pm S.E.M. for the number of experiments indicated on the graphs. SCC = short-circuit current.

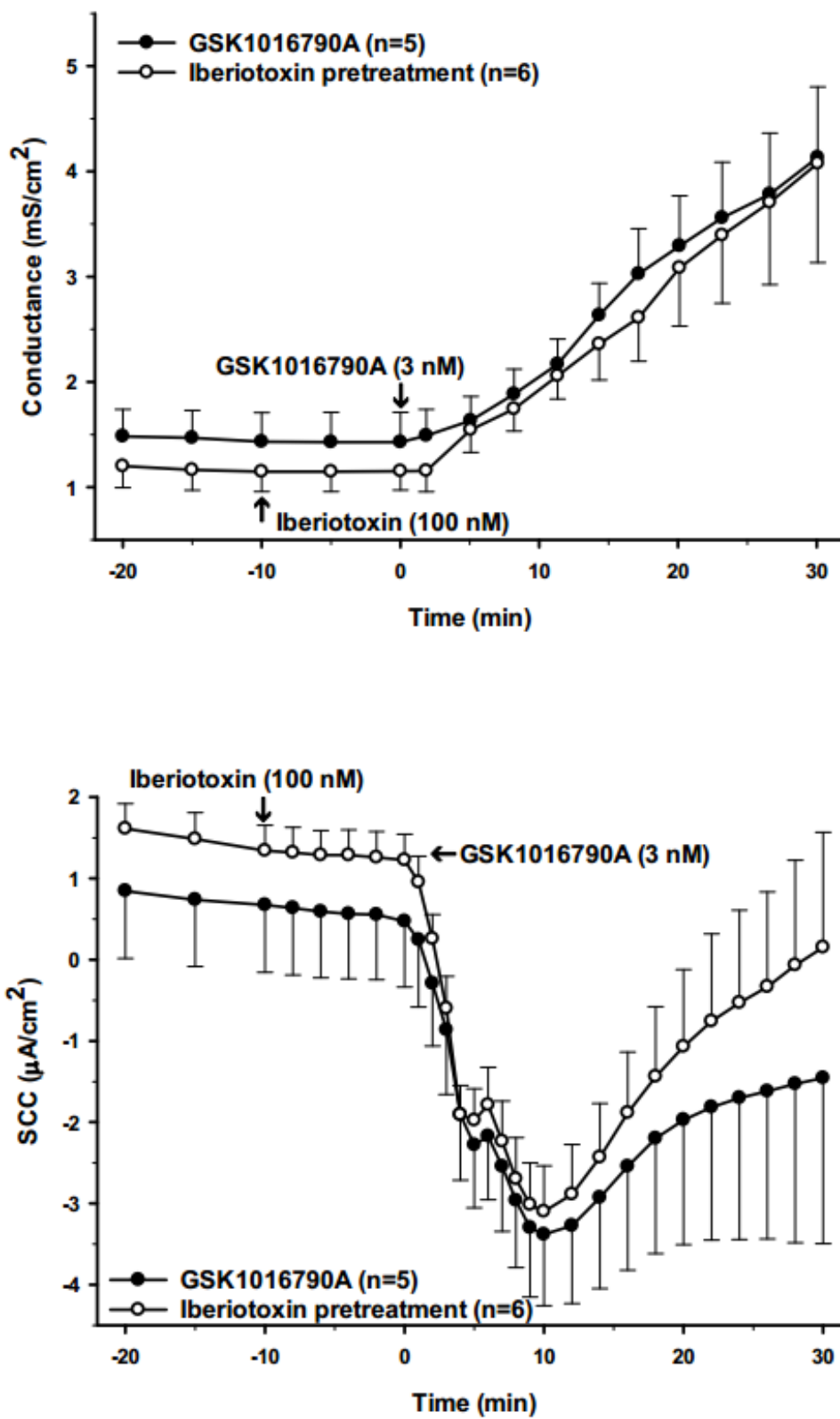


Figure 3.8 Effect of BK channel inhibitor on TRPV4-mediated responses.

Figure 3.9: Effect of pre-treatment with an inhibitor of SK channels on TRPV4 agonist stimulated increases in transepithelial conductance and ion transport. Apamin, an inhibitor of small conductance potassium (SK) channels, was added to the PCP-R cultures indicated by the open circles at time T = -10 minutes. At time 0, the TRPV4 agonist GSK 1016790A was added to all cultures. The symbols represent the means \pm S.E.M. for the number of experiments indicated on the graphs. SCC = short-circuit current.

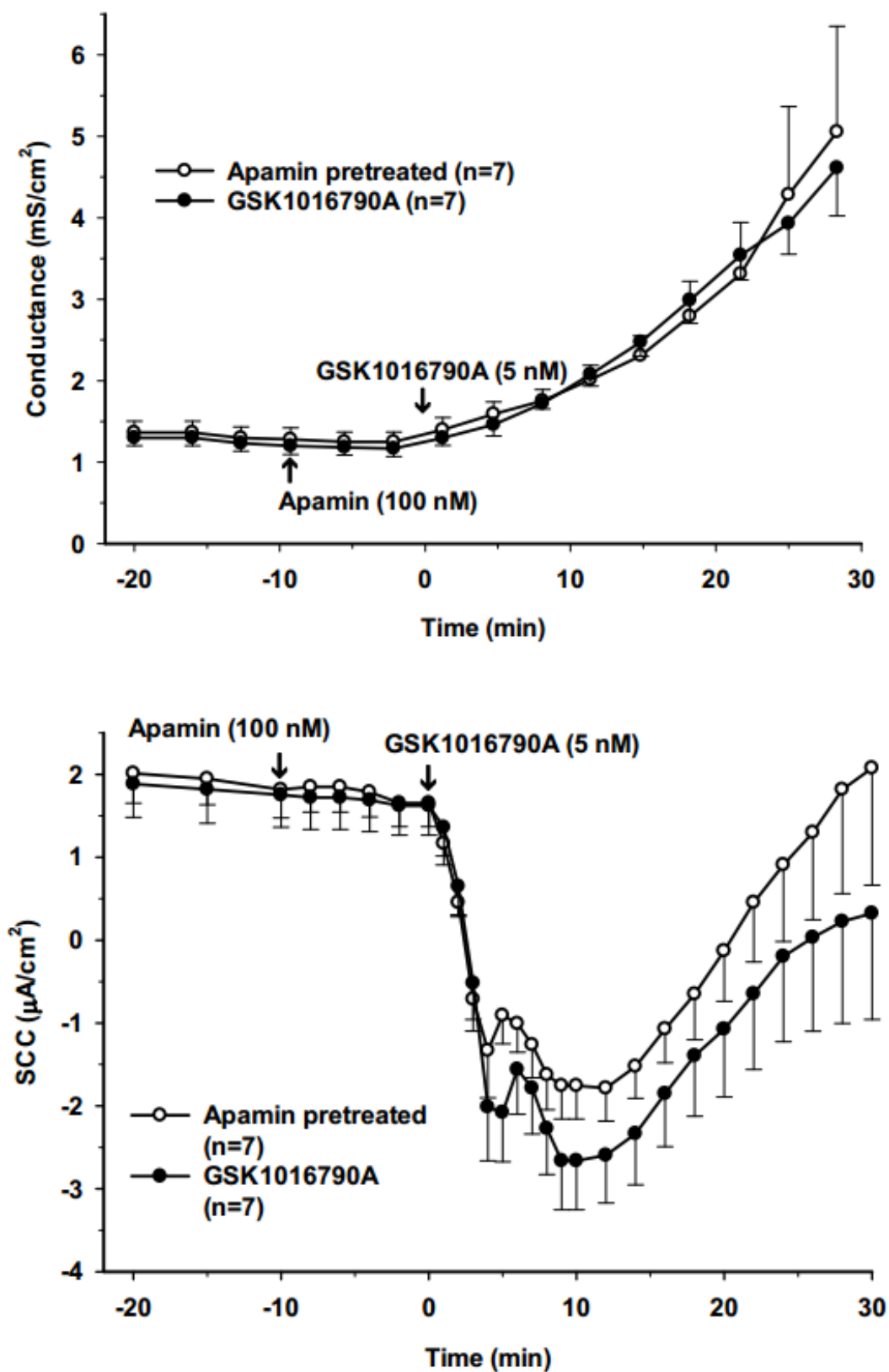


Figure 3.9 Effect of SK channel inhibitor on TRPV4-mediated responses.

Figure 3.10: Effect of pre-treatment with high and low doses of an IK channel inhibitor on TRPV4 agonist stimulated increases in transepithelial conductance and ion transport. TRAM34, an inhibitor of intermediate conductance potassium (IK) channels, was added bilaterally to the PCP-R cultures indicated by the open circles or inverted triangles at time T = -10 minutes. At time 0, the TRPV4 agonist GSK 1016790A was added to all cultures. The symbols represent the means \pm S.E.M. for the number of experiments indicated on the graphs. SCC = short-circuit current. The positive control data (GSK1016790A only) shown in this figure are the same data that are shown in figure 11. * indicates statistically significant differences between the experimental and control (solid circles) groups ($p < 0.02$) as measured by Students *t-test*, paired data. τ indicates statistically significant differences between the two experimental (open circles and inverted triangles) groups ($p < 0.02$) as measured by Students *t-test*, paired data.

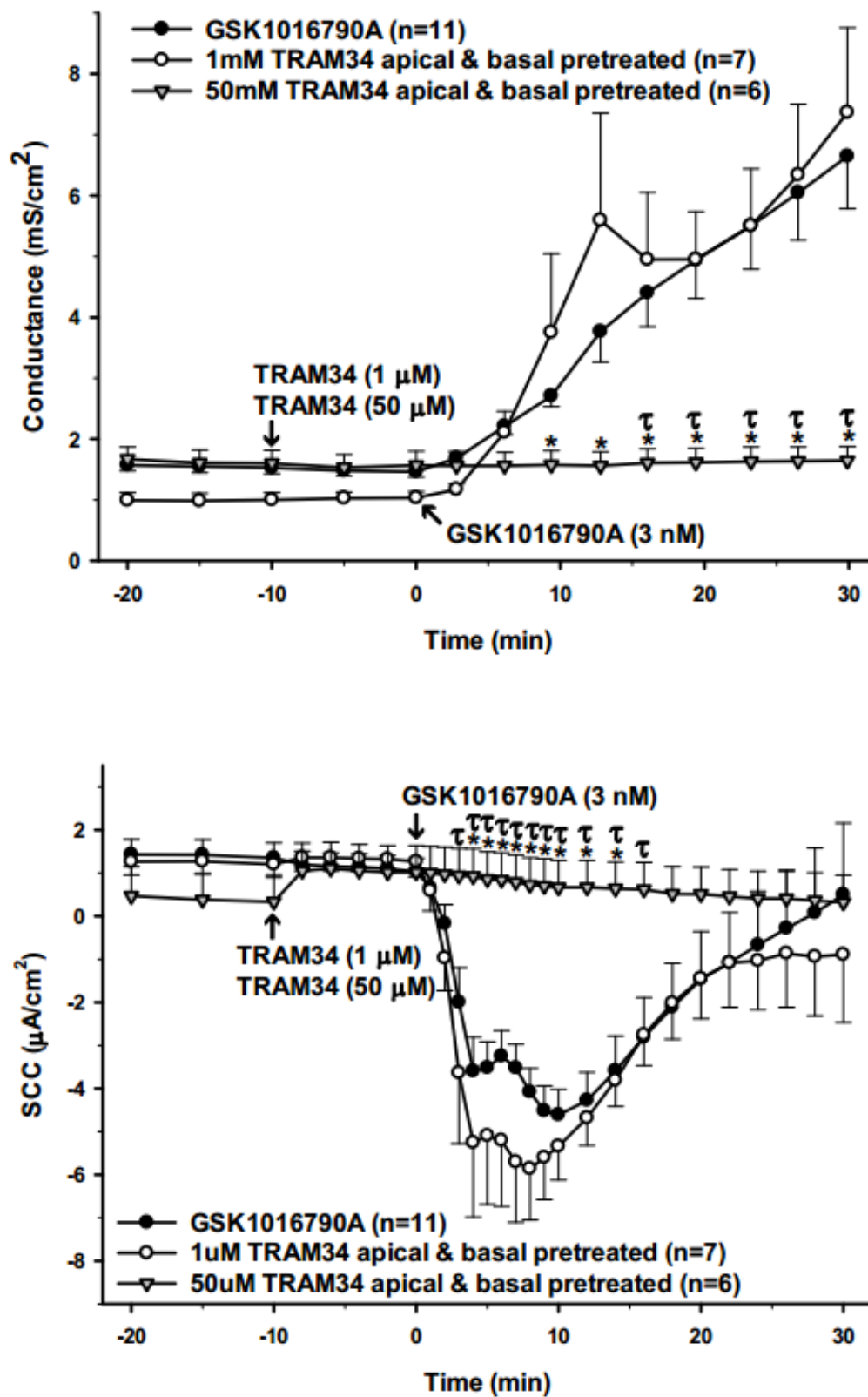


Figure 3.10 Effect of high/low doses of IK channel inhibitor on TRPV4-mediated responses.

Figure 3.11: Sidedness of the effect of an inhibitor of IK channels on TRPV4 agonist stimulated increases in transepithelial conductance and ion transport. TRAM34, an inhibitor of intermediate conductance potassium (IK) channels, was added to either the serosal or apical bathing media of the PCP-R cultures indicated by the open circles or inverted triangles at time $T = -10$ minutes. At time 0, the TRPV4 agonist GSK 1016790A was added to all cultures. The symbols represent the means \pm S.E.M. for the number of experiments indicated on the graphs. SCC = short-circuit current. The positive control data (GSK1016790A only) shown in this figure are the same data that are shown in figure 10. * indicates statistically significant differences between the experimental and control (solid circles) groups ($p < 0.02$) as measured by Students *t-test*, paired data. τ indicates statistically significant differences between the two experimental (open circles and inverted triangles) groups ($p < 0.02$) as measured by Students *t-test*, paired data.

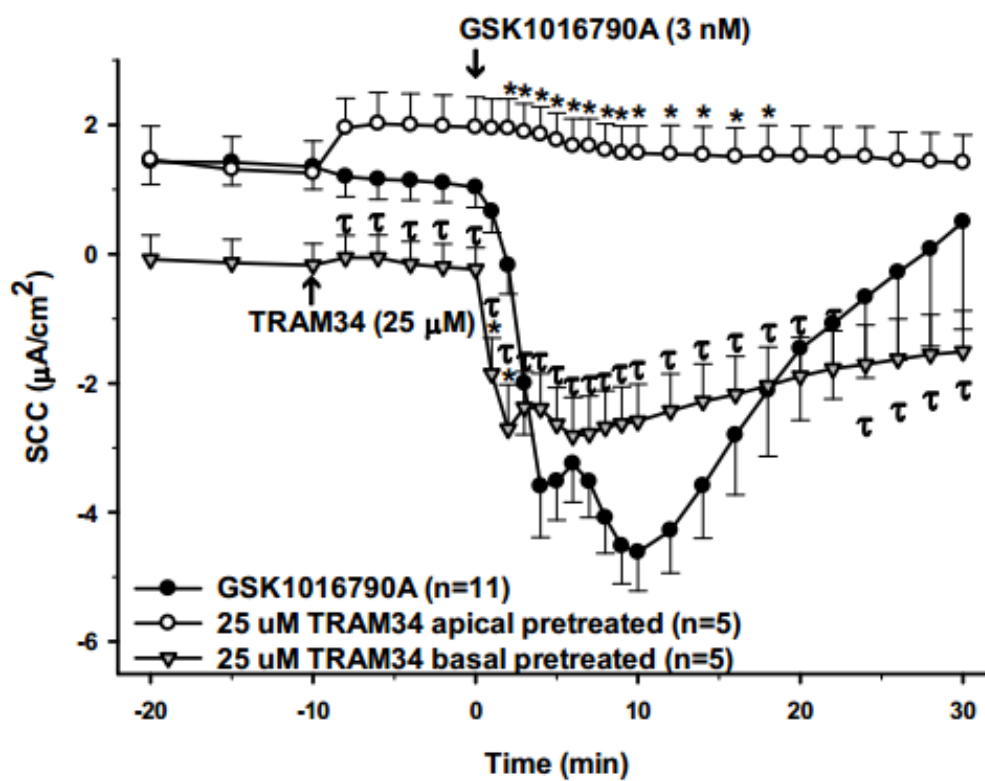
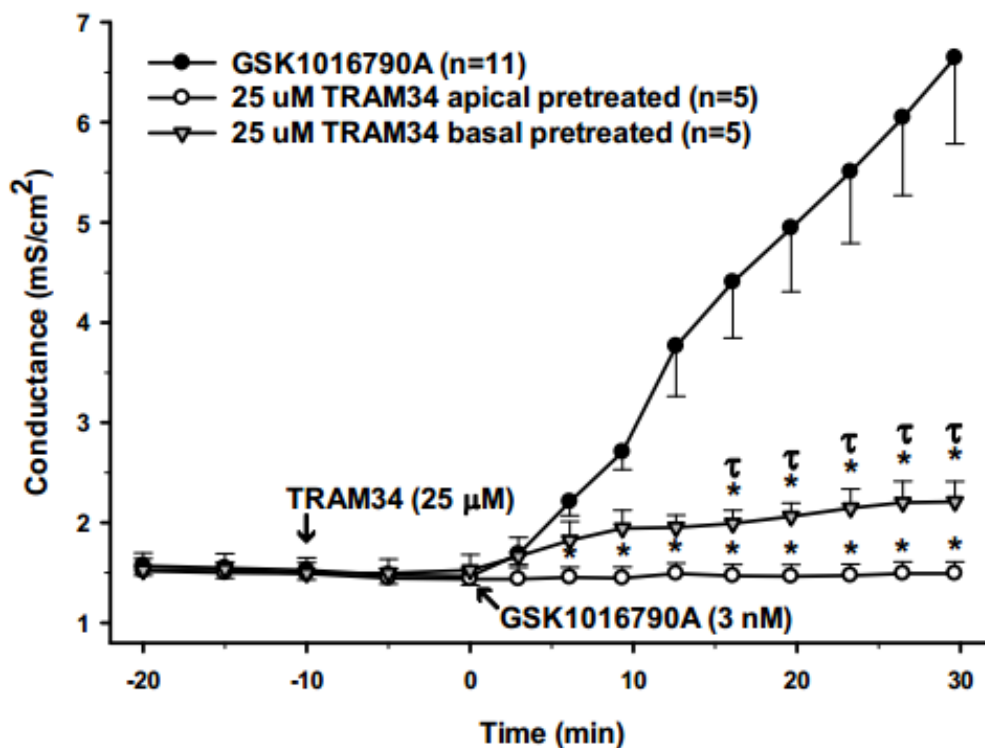


Figure 3.11 Sidedness of IK channel inhibitor on TRPV4-mediated responses.

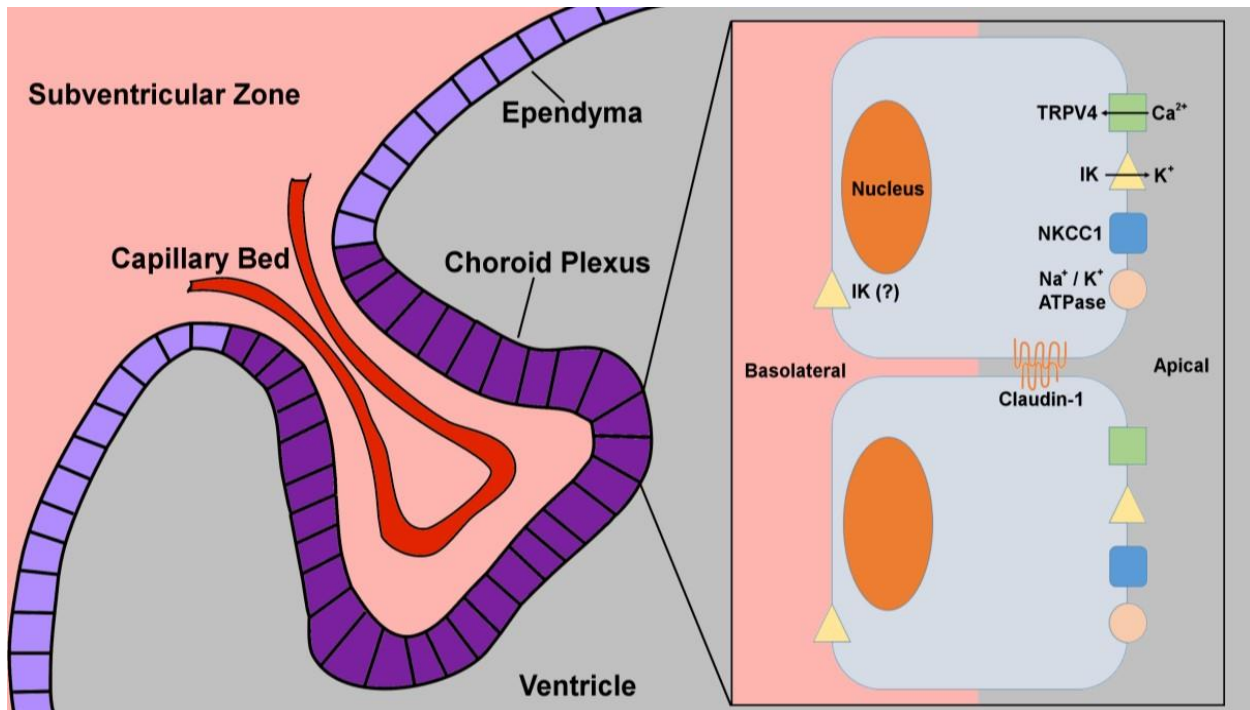


Figure 3.12 Diagram of selected transporters in the choroid plexus epithelia.

The left hand side of the diagram illustrates that the choroid plexus within the ventricle is continuous with the ependymal cells. Choroid plexus cells (dark purple) are increased in size compared to ependymal cells (light purple). On the right-hand part of the diagram, individual choroid plexus cells are shown as polarized with transporters on both the apical and basolateral membranes, and connected by tight junctional proteins.

3.11 References

1. Adelman, J., Maylie, J., and Sah, P. (2012). Small-conductance Ca^{2+} -activated K^+ channels: Form and function. *Annual Review Of Physiology*, 74(1), 245-269.
2. Bagher, P., Beleznai, T., Kansui, Y., Mitchell, R., Garland, C., and Dora, K. (2012). Low intravascular pressure activates endothelial cell TRPV4 channels, local Ca^{2+} events, and IK_{Ca} channels, reducing arteriolar tone. *Proceedings Of The National Academy Of Sciences*, 109(44), 18174-18179.
3. Barmeyer, C., Rahner, C., Yang, Y., Sigworth, F., Binder, H., and Rajendran, V. (2010). Cloning and identification of tissue-specific expression of KCNN4 splice variants in rat colon. *American Journal Of Physiology-Cell Physiology*, 299(2), C251-C263.
4. Basalingappa, K., Rajendran, V., and Wonderlin, W. (2011). Characteristics of Kcnn4 channels in the apical membranes of an intestinal epithelial cell line. *American Journal Of Physiology-Gastrointestinal And Liver Physiology*, 301(5), G905-G911.
5. Benfenati, V., Caprini, M., Dovizio, M., Mylonakou, M., Ferroni, S., Ottersen, O., and Amiry-Moghaddam, M. (2011). An aquaporin-4/transient receptor potential vanilloid 4 (AQP4/TRPV4) complex is essential for cell-volume control in astrocytes. *Proceedings Of The National Academy Of Sciences*, 108(6), 2563-2568.
6. Crossgrove, J., Li, G., and Zheng, W. (2005). The choroid plexus removes β -amyloid from brain cerebrospinal fluid. *Experimental Biology And Medicine*, 230(10), 771-776.
7. Cserr, H. (1971). Physiology of the choroid plexus. *Physiological Reviews*, 51(2), 273-311.
8. Danko, C., Preston, D., Simpson, S., and Blazer-Yost, B. (2017) Effects of a TRPV4 antagonist on hydrocephalus in the Wpk rat model. Abstract *FASEB J* 31:1042.4.
9. Darby, W., Grace, M., Baratchi, S., and McIntyre, P. (2016). Modulation of TRPV4 by diverse mechanisms. *The International Journal Of Biochemistry & Cell Biology*, 78, 217-228.
10. Ding, F., O'Donnell, J., Xu, Q., Kang, N., Goldman, N., and Nedergaard, M. (2016). Changes in the composition of brain interstitial ions control the sleep-wake cycle. *Science*, 352(6285), 550-555.
11. Earley, S., Heppner, T., Nelson, M., and Brayden, J. (2005). TRPV4 forms a novel Ca^{2+} signaling complex with ryanodine receptors and BK_{Ca} channels. *Circulation Research*, 97(12), 1270-1279.

12. Ghersi-Egea, J., Babikian, A., Blondel, S., and Strazielle, N. (2015). Changes in the cerebrospinal fluid circulatory system of the developing rat: quantitative volumetric analysis and effect on blood-CSF permeability interpretation. *Fluids And Barriers Of The CNS*, 12(1), 8.
13. Gonzalez-Mariscal, L., Contreras, R., Bolivar, J., Ponce, A., Chavez De Ramirez, B., and Cereijido, M. (1990). Role of calcium in tight junction formation between epithelial cells. *American Journal Of Physiology-Cell Physiology*, 259(6), C978-C986.
14. Günzel, D., and Yu, A. (2013). Claudins and the modulation of tight junction permeability. *Physiological Reviews*, 93(2), 525-569.
15. Halm, S., Liao, T., and Halm, D. (2006). Distinct K⁺ conductive pathways are required for Cl⁻ and K⁺ secretion across distal colonic epithelium. *American Journal Of Physiology-Cell Physiology*, 291(4), C636-C648.
16. Liedtke, W., Choe, Y., Martí-Renom, M., Bell, A., Denis, C., and Šali, A. et al. (2000). Vanilloid Receptor–Related Osmotically Activated Channel (VR-OAC), a candidate vertebrate osmoreceptor. *Cell*, 103(3), 525-535.
17. Loo, D., Brown, P., and Wright, E. (1988). Ca²⁺-activated K⁺ currents in Necturus choroid plexus. *The Journal Of Membrane Biology*, 105(3), 221-231.
18. Lu, K., Huang, T., Tsai, Y., and Yang, Y. (2017). Transient receptor potential vanilloid type 4 channels mediate Na-K-Cl-co-transporter-induced brain edema after traumatic brain injury. *Journal Of Neurochemistry*, 140(5), 718-727.
19. Ma, T., Hoa, N., Tran, D., Merryfield, M., Nguyen, D., and Tarnawski, A. (2000). Mechanism of extracellular calcium regulation of intestinal epithelial tight junction barrier: Role of cytoskeletal involvement. *Gastroenterology*, 118(4), A1268.
20. Narita, K., Sasamoto, S., Koizumi, S., Okazaki, S., Nakamura, H., Inoue, T., and Takeda, S. (2015). TRPV4 regulates the integrity of the blood-cerebrospinal fluid barrier and modulates transepithelial protein transport. *The FASEB Journal*, 29(6), 2247-2259.
21. Nilius, B., Vriens, J., Prenen, J., Droogmans, G., and Voets, T. (2004). TRPV4 calcium entry channel: a paradigm for gating diversity. *American Journal Of Physiology-Cell Physiology*, 286(2), C195-C205.
22. Praetorius, J., and Damkier, H. (2017). Transport across the choroid plexus epithelium. *American Journal Of Physiology-Cell Physiology*, 312(6), C673-C686.

23. Reiter, B., Kraft, R., Günzel, D., Zeissig, S., Schulzke, J., Fromm, M., and Harteneck, C. (2006). TRPV4-mediated regulation of epithelial permeability. *The FASEB Journal*, 20(11), 1802-1812.
24. Schilling, T., and Eder, C. (2007). TRAM-34 inhibits nonselective cation channels. *Pflügers Archiv - European Journal Of Physiology*, 454(4), 559-563.
25. Schroten, M., Hanisch, F., Quednau, N., Stump, C., Riebe, R., and Lenk, M. et al. (2012). A novel porcine in vitro model of the blood-cerebrospinal fluid barrier with strong barrier function. *Plos ONE*, 7(6), e39835.
26. Schwerk, C., Papandreou, T., Schuhmann, D., Nickol, L., Borkowski, J., and Steinmann, U. et al. (2012). Polar invasion and translocation of *Neisseria meningitidis* and *Streptococcus suis* in a novel human model of the blood-cerebrospinal fluid barrier. *Plos ONE*, 7(1), e30069.
27. Serot, J., Zmudka, J., and Jouanny, P. (2012). A possible role for CSF turnover and choroid plexus in the pathogenesis of late onset Alzheimer's disease. *Journal Of Alzheimer's Disease*, 30(1), 17-26.
28. Singh, S., O'Hara, B., Talukder, J., and Rajendran, V. (2012). Aldosterone induces active K⁺ secretion by enhancing mucosal expression of Kcnn4c and Kcna1 channels in rat distal colon. *American Journal Of Physiology-Cell Physiology*, 302(9), C1353-C1360.
29. Steinemann, A., Galm, I., Chip, S., Nitsch, C., and Maly, I. (2016). Claudin-1, -2 and -3 are selectively expressed in the epithelia of the choroid plexus of the mouse from early development and into adulthood while claudin-5 is restricted to endothelial cells. *Frontiers In Neuroanatomy*, 10.
30. Takayama, Y., Shibasaki, K., Suzuki, Y., Yamanaka, A., and Tominaga, M. (2014). Modulation of water efflux through functional interaction between TRPV4 and TMEM16A/anoctamin 1. *The FASEB Journal*, 28(5), 2238-2248.
31. Vergara, C., Latorre, R., Marrion, N., and Adelman, J. (1998). Calcium-activated potassium channels. *Current Opinion In Neurobiology*, 8(3), 321-329.
32. Weatherall, K., Goodchild, S., Jane, D., and Marrion, N. (2010). Small conductance calcium-activated potassium channels: From structure to function. *Progress In Neurobiology*, 91(3), 242-255.

33. Willette, R., Bao, W., Nerurkar, S., Yue, T., Doe, C., and Stankus, G. et al. (2008). Systemic activation of the transient receptor potential vanilloid subtype 4 channel causes endothelial failure and circulatory collapse: Part 2. *Journal Of Pharmacology And Experimental Therapeutics*, 326(2), 443-452.
34. Wright, E. (1978). Transport processes in the formation of the cerebrospinal fluid. *Reviews Of Physiology, Biochemistry And Pharmacology*, 83, 3-34.
35. Wu, Q., Delpire, E., Hebert, S., and Strange, K. (1998). Functional demonstration of Na⁺-K⁺-2Cl⁻ cotransporter activity in isolated, polarized choroid plexus cells. *American Journal Of Physiology-Cell Physiology*, 275(6), C1565-C1572.
36. Xie, L., Kang, H., Xu, Q., Chen, M., Liao, Y., and Thiyagarajan, M. et al. (2013). Sleep drives metabolite clearance from the adult brain. *Science*, 342(6156), 373-377.
37. Zeuthen, T., & Wright, E. (1981). Epithelial potassium transport: Tracer and electrophysiological studies in choroid plexus. *The Journal Of Membrane Biology*, 60(2), 105-128.

CHAPTER 4. INFLAMMATORY EFFECTS ON TRPV4 IN THE CHOROID PLEXUS

4.1 Preface

The data in this chapter will be submitted in Spring 2019 to the *American Journal of Physiology: Cell Physiology*, I am first author for the following journal article. In the drafting of the article, I was responsible for writing the manuscript, designing and conducting all experiments, analyzing all data, and designing and formatting all figures. Exceptions to my contributions include the qPCR experiments performed by my co-author, Daniel Preston, maintenance of the animal colony and collection of rat CSF performed by our laboratory technician, and the collection of human CSF performed by my co-authors at Riley's Hospital for Children in Indianapolis, IN.

4.2 Inflammatory mediator effects on TRPV4 function in the choroid plexus

Stefanie Simpson¹, Daniel Preston¹, Daniel Fulkerson², Karl Balsara², and Bonnie Blazer-Yost¹

1. Department of Biology, Indiana University-Purdue University at Indianapolis, Indiana
2. Department of Neurological Surgery, Indiana University School of Medicine, Indianapolis

4.3 Introduction

Hydrocephalus, also known as "water on the brain," is a condition characterized by an imbalance in cerebrospinal fluid (CSF) production and/or reabsorption (communicating) or by a blockage in the CSF circulation (non-communicating). This can result in the accumulation of CSF and enlargement of the ventricles in the brain, leading to an increase in hydrostatic pressure, neuronal destruction, behavioral and cognitive changes, gait changes, vision problems, and potentially death (52). The condition can occur at any age and can develop from a number of causes including head trauma, intracranial hemorrhage, infection, inflammation, brain tumor, genetic defect or neurodegenerative disease (23, 39-47). Currently, the only approved treatments in humans involve invasive brain surgery, underscoring the need to better understand the physiology of this

debilitating disease in order to find a pharmacological treatment. One of the key components of this is the regulation of fluid and electrolytes during the production of CSF.

The main production of CSF comes from the choroid plexus (CP), present in the lateral, third, and fourth ventricles (6). Composed of a high resistance barrier epithelium that surrounds a network of capillaries, the CP epithelial cells regulate the transport of ions and water between the ventricles and capillaries via electrolyte transporters, thus controlling the production and movement of CSF. Aberrant regulation of these transporters could be a causative agent leading to the emergence of hydrocephalus.

Previous data suggest a link between transepithelial ion movement in choroid plexus epithelial cells and the cation channel, Transient Receptor Potential Vanilloid-4 (TRPV4) (5, 47, 50). TRPV4 is a mechano-, osmo-, and temperature-sensitive, non-selective, calcium-permeable cation channel that can serve as a hub protein for the activation of other transporters (2-4). For example, TRPV4 activation can lead to an influx of calcium into the cells, which subsequently stimulates calcium activated ion channels, such as the intermediate conductance potassium channels (5). Once these channels are activated, there is the potential for significant ion flux across the epithelia, resulting in compensatory water movement and a change in CSF production. TRPV4 also acts as a hub protein in that it can be modulated through a number of stimuli, including pressure or flow alterations, osmotic changes, temperature fluctuations, and chemical activators, such as cytokines and inflammatory mediators (2-5). In particular, the latter activators can also be seen in neurodegenerative states related to hydrocephalus. Indeed, it has been established that the inflammatory lipid endocannabinoid anandamide (AEA) and its metabolites, including arachidonic acid (AA), are capable of activating the channel (4). In addition, cytochrome P450 epoxygenases, cyclooxygenases, and lipoxygenases can metabolize AA into anti-inflammatory factors epoxyeicosatrienoic acids (EETs), prostaglandins, and hydroperoxides respectively, which are also believed to stimulate TRPV4 activity (4, 7).

Microglia, the macrophage-like cells of the central nervous system (CNS), can be triggered to release pro-inflammatory cytokines in response to abnormal protein accumulation or neuronal injury from chemical or physical means (8, 9). It is possible that such inflammation is associated with the development of hydrocephalus in various neurological disorders (39, 41, 48-49, 51). Pro-

inflammatory cytokines found upregulated in neurodegenerative states include interleukin (IL)-1 β and tumor necrosis factor (TNF)- α . IL-10 is a well-documented anti-inflammatory cytokine also found in various hydrocephalic-associated diseases. IL-4 is also an anti-inflammatory compound while other cytokines have more complex actions. TGF- β and IL-6 have both been implicated in pro- as well as anti-inflammatory effects (9-15). These cytokines can, therefore, potentially play a role in the development and pathology of hydrocephalus.

As an *in vitro* model, the high resistance porcine choroid plexus-Rheims cell line (PCP-R) can be utilized to monitor changes in transepithelial ion flux and barrier permeability in response to factors that modulate electrolyte transporters (5). The polarity and barrier function exhibited by this cell line allows for experimentation modeling changes in the barrier function of choroid plexus *in vivo* (16). Using a TRPV4 agonist, GSK1016790A, we are able to stimulate TRPV4 activation and observe changes in ion flux and transepithelial conductance in the presence of various cytokines and inflammatory mediators.

The Wpk rat is an orthologous model of the ciliopathy Meckel-Gruber Syndrome (17, 27). This *in vivo* model contains a genetic single point mutation on chromosome 5 on the TMEM67 gene, resulting in the homozygous recessive animals that develop both severe polycystic kidney disease (PKD) and a rapidly-progressing form of hydrocephalus (17, 27). In their adulthood, heterozygous animals develop an asymmetrical mild form of hydrocephalus, while showing no signs of PKD. Because they do not develop PKD, these animals are therefore devoid of the potentially confounding variable of renal insufficiency (1). With these *in vivo* and *in vitro* models, we are able to observe potential signs of inflammation in the brain and examine its effects on the development of hydrocephalus and TRPV4 function.

While inflammation caused by hydrocephalus in the animal model is not evident, this article will show how pro-inflammatory cytokines and inflammatory mediators can play a role in the development of the disease. Specific cytokines alter the function of TRPV4 in the choroid plexus epithelia, providing more insight into the role of the cation channel in neurodegenerative states and suggesting this hub protein as a potential therapeutic target.

4.4 Materials and Methods

Cell Culture: PCP-R cells were grown on 0.4 μm pore diameter Transwell filters (Corning) until the cultures developed a high transepithelial electrical resistance (TER) (10-12 days). Only cultures with resistances above $500 \Omega\text{cm}^2$ were utilized. During experimental protocols that result in a change in resistance, cells that drop below $100 \Omega\text{cm}^2$ were also removed from analysis as their junctional complexes appear irreversibly altered. Cells were fed three times weekly with feeding media containing DMEM with 4.5 g/L glucose, 3.7 g/L NaHCO_3 , 5.71 g/L HEPES, 10% fetal bovine serum (Atlanta), 100 U/mL penicillin, 100 mg/mL streptomycin, and 5 $\mu\text{g/ml}$ insulin. Each plate contained 6 filters in 6 different wells. Transwells were bathed in 2 mL feeding media on the basolateral (bottom) side of the membrane and 1.5 mL feeding media on the apical (top) side of the membrane.

Real Time (RT)-PCR: For the RT-PCR, cells were grown in 75 cm^2 flasks until confluent. The monolayers were trypsinized, collected, and RNA from the cells extracted following the manufacturer's instructions for the New England BioLabs Monarch Total RNA Miniprep Kit (#T2010S). No template controls and cDNA were prepared by following manufacturer's protocol for the New England BioLabs LunaScript RT SuperMix Kit (#E3010S). Three primer sets for each gene were generated using Primer3 with mRNA sequences of the gene in question and tested on a temperature gradient. Only those primers used in the final images were included in Table 4.1. *Sus scrofa* mRNA sequences were obtained from Ensembl and additionally confirmed with sequences from the NCBI database. Forward and reverse primers (IDT) were combined with cDNA (approximately 500 ng) and GoTaq Green Master Mix (Promega) to perform gradients of PCR to determine the optimal annealing temperature. PCR products were then run on 1.5% agarose gels with ethidium bromide and 1kb flanking ladders. Gels were imaged using a ChemiDoc XRS imager (Bio-Rad, Hercules, CA).

Electrophysiology: Electrophysiological techniques were conducted by excising and mounting confluent (10-12 days) Transwell filters in Ussing chambers which are attached to a DVC-1000 Voltage/Current Clamp (World Precision Instruments) using voltage and current electrodes. To each side of the chamber, 10 mL of serum-free media was added. The chambers were water jacketed to allow the cells and media to be kept at a consistent physiological temperature (37°C).

Furthermore, the media was continuously oxygenated and circulated by bubbling 5% CO₂/O₂ directly into the media. Following clamping of the spontaneous transepithelial potential difference to zero for an equilibration period of at least 30 minutes, experimental compounds were added to the apical and/or basolateral membranes by means of the serum-free media and the cultures were monitored for changes in short circuit current (SCC) and TER. Transepithelial resistance is a measure of changes in epithelial barrier function and was measured every 200 seconds through a 2mV pulse. The instantaneous change in SCC from the pulse was used to calculate TERs by means of Ohm's Law. These resistance calculations were converted to conductance by taking the inverse of the resistances. These parameters provided real time information about transepithelial ion flux in response to modulators of ion channels or intracellular signaling molecules. In each experiment, the cells were pre-incubated on both basolateral and apical sides with the experimental compounds for either 10 or 20 minutes or 24 hours prior to addition of TRPV4 agonist GSK1016790A.

Statistics: Statistics were performed using Two-tailed Students t-test in Sigma Plot 13. $p < 0.05$ is considered significant.

4.5 Results

In order to determine the ability of the PCP-R cell line to respond to and/or produce various cytokines and inflammatory mediators, RT-PCR was performed to identify specific genes of interest. Toll-like receptors (TLRs) are the major membrane-bound proteins necessary for cytokine reception and production (25, 26). Within the pig genome, ten different TLRs have been described (TLR1-TLR10) (24). mRNA for all of these receptors were found to be present in the PCP-R cell line (Figure 4.1A).

Arachidonic acid (AA) is a substrate for the production of various inflammatory mediators, some of which can stimulate TRPV4 (4, 30, 31). Therefore, we investigated which of the enzymes necessary to metabolize AA were present in the cells. Reference Figure 4.1C for a simplified summary of AA metabolism. Cytochrome P450 epoxygenases (CYP) are responsible for the production of EETs from AA. EETs have been reported to be a main activator of TRPV4 (30). While there are many known isoforms of *Cyp* genes, only two of these have currently been

sequenced in the pig: *Cyp2c42* and *Cyp2e1*. Neither of these isoforms were present in the porcine CP cells. Another pathway of AA metabolism utilizes lipoxygenases to produce hydroperoxides. In pigs, there are currently four lipoxygenase (*Alox*) gene sequences available: *Alox5*, *Alox12b*, *Alox15*, and *Alox15b*. Of these, only *Alox15* and *Alox15b* were present in the PCP-R cells. Finally, prostaglandins are formed when AA is metabolized by cyclooxygenases (COX) 1 or 2. Both *Cox1* and *Cox2* mRNA were found in the cell line (Figure 4.1B).

Utilizing electrophysiology to measure changes in transepithelial ion flux and epithelial barrier permeability, several pro- and anti-inflammatory cytokines and mediators that were hypothesized to be important in hydrocephalic development were tested to assess how they would affect the basal characteristics of the PCP-R cells and subsequently their response to the TRPV4 agonist GSK1016790A. Interleukin (IL)-1 β and Tumor Necrosis Factor (TNF)- α are two of the most prominent pro-inflammatory cytokines seen in neurodegenerative diseases (9-15). Upon pre-incubation of the PCP-R cells with either cytokine for 24 hours, both cytokines had significant effects on TRPV4-mediated ion flux, measured as short-circuit current (SCC), albeit on different phases of the ion transport response. IL-1 β caused an attenuation of the agonist response particularly in the early (0-15 minute) timeframe while TNF- α caused an expedited increase in SCC toward baseline in late response to the agonist. Interestingly, these two pro-inflammatory cytokines had opposite effects on transepithelial permeability, measured as conductance. TNF- α caused no change in conductance after a 24-hour incubation compared to the control. 24-hour incubations with IL-1 β caused a significant attenuation in the TRPV4 agonist-mediated change in conductance which paralleled the effect on transepithelial ion flux measured as SCC (Figures 4.2 & 4.3).

Interestingly, pre-incubation with TGF- β , which has been reported to have both pro- and anti-inflammatory effects, had similar significant attenuation effects as IL-1 β at 24 hours. However, the same treatment with IL-6, another pro- and anti-inflammatory cytokine, yielded no significant response (Figures 4.6 & 4.7). Finally, the cells were pre-incubated with the cytokines IL-10 and IL-4. Neither of these anti-inflammatory cytokines had any long-term effect on either transepithelial ion flux or conductance (Figures 4.4 & 4.5).

NF- κ B is a transcription factor often associated with pro-inflammatory signaling pathways. Pro-inflammatory cytokines, mainly IL-1 and TNF- α , are considered activators of NF- κ B, which can have downstream effects on the activation of inflammation and further production of cytokines (18). As such, the PCP-R cells were pre-incubated with a selective inhibitor for NF- κ B, PDTC (19). By inhibiting NF- κ B 10 minutes prior to adding the TRPV4 agonist, there was a potentiation of the intermediate (5-10 min) phase of TRPV4-mediated ion flux. There was also an initial increase in permeability compared to the control that is entirely consistent with the time-course of the SCC response. However, this change did not persist; permeability returned to control levels 30 minutes after agonist addition (Figure 4.8). As NF- κ B is a transcription factor, it might take longer for its true effects to become evident. Therefore, we also inhibited the pro-inflammatory mediator 24 hours prior to adding the TRPV4 agonist (Figure 4.9). In this instance a very different result occurred. Transepithelial ion flux was significantly reduced compared to the control. Furthermore, the initial conductances in these pre-treated cells were higher than the controls prior to agonist addition. However, the cellular permeability did not increase substantially after agonist addition as seen in the control.

AA and its metabolite, 5,6-EET, are often cited as being activators of TRPV4 (4, 9, 30, 31). However, when the PCP-R cells were pre-incubated with AA for 10 minutes, the transepithelial ion movements caused by the TRPV4 agonist within the initial and intermediate timeframes were substantially inhibited, while the barrier permeability was not altered (Figure 4.10). When incubated with the anti-inflammatory AA metabolite, 5,6-EET, a different reaction occurred. In regard to ion flux (SCC), the late phase was inhibited, and this was mirrored in a trend toward a decrease in conductance although the latter did not reach statistical significance (Figure 4.11).

In order to further elucidate the role of the AA pathway in the function of TRPV4, we utilized various inhibitors for the enzymes involved in AA metabolism to determine which of the pathways were involved in TRPV4 activity. Indomethacin is a non-steroidal anti-inflammatory drug (NSAID) able to prevent the metabolism of AA into the pro-inflammatory prostaglandins by non-selectively inhibiting both cyclooxygenases (4, 7, 20-22). However, indomethacin caused no differences in TRPV4-mediated ion movement or permeability compared to the control (data not shown). Eicosatetraenoic acid (ETYA) is a suicide inhibitor of all cyclooxygenases and lipoxygenases,

which produce prostaglandins and leukotrienes, respectively. When added to the cells 20 minutes prior to the TRPV4 agonist, there were significant attenuations of both the SCC and conductance changes. Finally, we pre-incubated the cells with SKF-525A, a non-specific inhibitor of cytochrome P450, responsible for the production of EETs. This inhibitor caused a complete inhibition of both transepithelial ion flux and changes in cellular permeability caused by TRPV4 activity (Figure 4.10).

4.6 Discussion

TLRs are often found on microglia, astrocytes, and other immune cells and are well known for playing a key role in the initiation of the innate immune response to pathogen-associated molecular patterns (PAMPs). But the TLRs not only play a major role in a cell's ability to respond to inflammatory reactions, but they also enable the cells to contribute to the inflammation. When a cytokine ligand binds to the TLRs, this can cause a cascade of events leading to activation of transcription factors NF- κ B and AP-1 and subsequent cytokine production (24, 25). In particular, TLR4 is best known for producing key pro- and anti-inflammatory cytokines, such as TNF- α , IL-6, and IL-10, and is most often associated with inflammation (24, 25). It is also of interest that TLRs have been found to alter with age (25). Specifically, pro-inflammatory cytokine production increases while secretion of anti-inflammatory cytokines decreases. It is with this in mind that TLRs have been associated with age-related inflammatory neurodegenerative diseases, such as ischemic stroke, Alzheimer's disease, and multiple sclerosis (25). Therefore, the finding that the PCP-R cell line contains all 10 of the known porcine TLRs signifies that CP cells have the potential to not only respond to various inflammatory signals but can also lead to the secretion of several different cytokines into the CSF. This could also suggest that with age, the TLRs of the CP cells could cause increases in cytokine production and contribute to neurodegenerative states, including hydrocephalus.

In studies using lung and endothelial tissue, TRPV4 antagonists have been found to reduce pulmonary edema and protect against sepsis, respectively. In both studies, TRPV4 inhibition was also found to decrease inflammation and cytokine production (28, 29). This would suggest that TRPV4 acts in a pro-inflammatory manner. To confirm this in the brain, we looked at various

types of cytokines, including pro-inflammatory, anti-inflammatory, and paradoxical pro- and anti-inflammatory cytokines. Of these, the anti-inflammatory cytokines showed no detectable effect on TRPV4-mediated ion flux, and the pro-inflammatory cytokines had the most significant effects on TRPV4 activity after incubating with the cells for 24 hours. Interestingly, the responses seen with the two prominent pro-inflammatory cytokines were not the same. While IL-1 β showed a weakening of the entire response with both SCC and conductance changes reduced, TNF- α only caused a heightened return to electroneutral SCC but did not substantially alter conductance compared to the control. In addition to this, the paradoxical pro- and anti-inflammatory cytokines, TGF- β 1 and IL-6, had varying effects with TGF- β 1 causing strikingly similar results as IL-1 β but no significant changes with IL-6. It is possible that these cytokines alter whether they act via pro- or anti-inflammatory pathways depending on physiological cues. While it cannot be assumed that all pro-inflammatory pathways cause an attenuation or inhibition of the response, it is most likely, based upon our observations, that TGF- β 1 is acting in a pro-inflammatory manner while IL-6 is more anti-inflammatory in the CP cells. Together, these data imply that pro-inflammatory cytokines diminish TRPV4 function. From this, there are some possibilities of how TRPV4 is functioning in the response. It could be that TRPV4 acts to produce pro-inflammatory cytokines and is diminished in a negative feedback loop when cytokines are in excess. This theory would not disagree with the previous studies in lung and endothelial tissue as pro-inflammatory cytokine production decreased with TRPV4 inhibition (28, 29). The finding that inhibition of the pro-inflammatory transcription factor NF- κ B initially caused a potentiation of TRPV4-mediated ion flux and permeability changes cannot be easily explained. It is possible that this increase is due to the sudden increase in barrier permeability as ions are more easily able to move across the membrane. After 24 hours of inhibition, the permeability remains high, but stimulation of TRPV4 does not cause additional increase in conductance and results in significantly attenuated ion flux responses. Therefore, NF- κ B activation and possibly its downstream inflammatory effectors can be considered contributors to TRPV4-mediated ion flux and permeability changes. This also further suggests that TRPV4 is involved in the production of cytokines and regulation of inflammation.

Several publications have reported that AA and its metabolites are able to cause substantial elevation of $[Ca^{2+}]_i$ by activating TRPV4. Specifically, these studies cite EETs as the predominant

activator of the cation channel (4, 9, 30, 31). Therefore, we hypothesized that TRPV4 activity would be potentiated after pre-incubation with either of these compounds and were surprised to find this not to be the case. From our data, we can see that AA added in excess causes an inhibition of TRPV4's response. It is then possible that AA metabolism is required for TRPV4 activity, but that excess AA (i.e. inflammation) causes a down regulation of TRPV4. Under normal circumstances, endogenous AA is metabolized quickly so it likely does not have enough time to down regulate TRPV4 and the response is not seen. But when added in excess, we can see its inhibitory effect. Taken together with our cytokine data, in which the pro-inflammatory cytokines also down regulate TRPV4, this would imply that inflammation acts to decrease TRPV4 activity.

There is also controversy concerning which isoform of EET is responsible for activating TRPV4 (32). It is possible that several different isoforms of EET act differently on TRPV4 between the many tissue and cell types where the channel lies. Currently, there are no known publications on the specific EET isoform responsible for TRPV4 activation in CP cells. While 5,6-EET is most often considered to be the activating isoform in other cell types, we found this not to be the case in CP cells. Furthermore, it is unknown whether the PCP-R cell line is able to produce EETs. The production of EETs occurs when AA is metabolized by the enzymes cytochrome P450 epoxygenase, of which there multiple varieties (33). Currently, only two gene isoforms of these enzymes have been sequenced in pigs, *Cyp2c42* and *Cyp2e1*, neither of which were present in the cells. However, there are several other isoforms still untested, including those most associated with EET production, CYP2C8, CYP2C9, CYP2C19 and CYP2J2 (33). Therefore, these data cannot lead to the conclusion that there are no cytochrome P450 epoxygenases present. Furthermore, the SKF-525A CYP450 inhibitor had dramatic inhibitory effects on TRPV4-mediated ion flux and permeability changes. This implies that EET is indeed the leading cause of TRPV4's effect. It is possible that there is a threshold to EETs' effect on TRPV4. Thus, even though it is added in excess to the cells, it would be unable to further activate TRPV4 more so than the agonist is capable. More than likely, though, a different EET isoform other than 5,6-EET is affecting TRPV4 in the CP.

We determined the presence and effects of the various other AA metabolites in the CP cells. Both isoforms of cyclooxygenase were present in the PCP-R cells, meaning that the cells are able to produce prostaglandins, prostacyclin, and thromboxane A₂ (34). However, inhibition of both

COX1 and COX2 with the NSAID Indomethacin did not alter the effects of TRPV4 activation in the cells. Thus, these metabolites likely do not play a role in TRPV4-mediated pathways.

We also looked closer at the lipoxygenase (LOX) pathway of which there are seven known gene isomers: *Alox3*, *-5*, *-5ap*, *-12*, *-12b*, *-15*, and *-15b* (35). Of these, *Alox12b*, *-e3*, and *-15b* are found in the skin and other epithelial cells and *Alox5*, *-12*, and *-15* are located primarily in immune cells. Many of the isomers have been reported in different forms of cancers, but all of them can be involved in inflammation (35). However, only *Alox15* and *Alox15b* were found in our cell line of the four currently sequenced in pig. The enzymes encoded by these two isoforms have higher similarities compared to the other isoforms, hence the similar nomenclature (35). However, interestingly, only *Alox15* is considered one of the isoforms that can be partially controlled by cytokines. Anti-inflammatory cytokines, such as IL-4 and IL-13, have the potential to increase expression of this gene, which can then decrease production of pro-inflammatory cytokines, such as IL-12 (35). The isoform has also been associated with maintaining dermal integrity through anti-inflammatory suppression of inflammation in the skin (38). On the other hand, *Alox15* is also capable of increasing pro-inflammatory matrix metalloproteinase (MMP) expression and contributing to arthritic disease progression (36, 37). Once again, this leads to the question of whether TRPV4 is acting in a pro- or anti-inflammatory process. Less is known about the *Alox15b* isoform, but it has been implicated in decreasing epithelial barrier permeability (35). Thus, increases in this isoform could contribute to increases in transepithelial ion flux in the CP tissue.

To better understand how lipoxygenases affect the cell line when TRPV4 is activated, we utilized ETYA to inhibit both cyclooxygenases and lipoxygenases. We already know that inhibiting the cyclooxygenases alone does not affect the cells. However, when both are inhibited, there is a partial inhibition of the TRPV4-mediated response. We also now know that inhibiting the CYP450s and subsequent EET production results in complete inhibition of the TRPV4-mediated response. What this could translate to is that although ETYA is specific for CYP450 inhibition, it could have partial inhibitory effects. It could also be that the other AA metabolites (prostaglandins, leukotrienes, etc.) work together with EETs to act on TRPV4. Thus, inhibiting the other metabolites does attenuate the response, but because the cells are still able to produce EETs, ETYA cannot completely inhibit

the response. Future experiments will investigate how these metabolites are related in their response.

In summary, TRPV4 is negatively affected by pro-inflammatory cytokines and mediators. We also found that when arachidonic acid is added to choroid plexus cells, TRPV4-mediated transepithelial ion flux is diminished. Finally, we confirmed that in the choroid plexus, inhibition of EET production causes a complete inhibition of TRPV4-mediated transepithelial ion flux and cellular permeability changes. Therefore, in the choroid plexus, TRPV4 can be affected by increases in inflammation due to hydrocephalus and other neurodegenerative diseases.

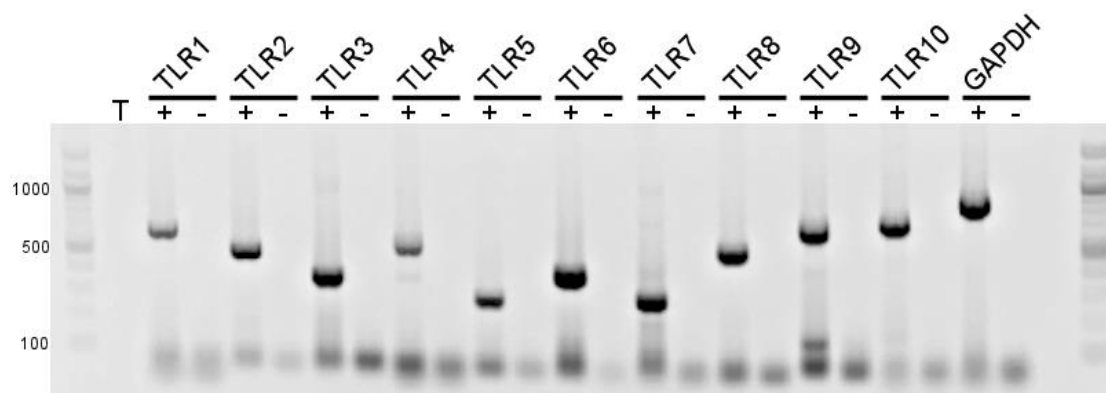
Table 4.1 Primer sequences used for RT-PCR with corresponding product sizes (bp).

Three different primer sets were generated and tested for each gene. Primers included in this table were utilized for Figure 4.1A & Figure 4.1B. *Gapdh* was used as a positive control.

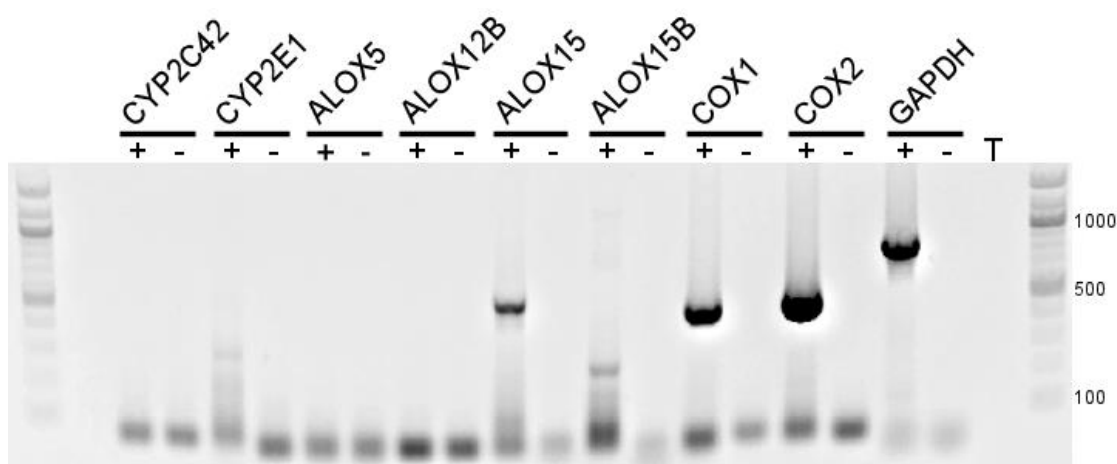
<i>Sus Scrofa</i> gene	Protein	Primer Sequences 5' - 3'		Product Size (bp)
		Forward Primer	Reverse Primer	
<i>Tlr1</i>	TLR1	TGTCCACAACAAGTTGGAGAA	TTGTGGGAAACTGAACACCTCA	650
<i>Tlr2</i>	TLR2	TCCCAAATCTGCGAATCCTGAA	ATGCAACCTCCGGACTGTTAAT	512
<i>Tlr3</i>	TLR3	CGATGACCTCCCGCAAATATA	GAGATTTCCAGTTGGAGCTGC	382
<i>Tlr4</i>	TLR4	TTCTCTCCTGCCTGAGATCTGA	ACTCCAGGTAGGTATTCTGCT	555
<i>Tlr5</i>	TLR5	TCCTGTGGTCTCTCTGATGCTA	GGGTTCATACACTTCCCCCAAT	284
<i>Tlr6</i>	TLR6	AGACAATCTTGTGCCATCCCAT	GGCCCTTGAGTGAGTTCCAATA	409
<i>Tlr7</i>	TLR7	GACACTAAAGACCCAGCAGTGA	CTGAAGGGGCTTCTCAAGGAAT	297
<i>Tlr8</i>	TLR8	CTGAGGCAGAACAGGATTTCT	TTCATCACCCAGTCTGTGACAG	542
<i>Tlr9</i>	TLR9	GCCTACGAACTCTCAACCTCAA	GGAAGTTCTCACTCAGGTCCAG	696
<i>Tlr10</i>	TLR10	TCAGGTGCTTGCCAGAAATAT	TCTTGCCAGGATCAGAGTTTCC	717
<i>Cyp2c42</i>	CYP2C42	TCCTGTCTGCTTCTCCTTTCAC	GGGAGCACAGTCCAGGATAAAA	489
<i>Cyp2e1</i>	CYP2E1	TCGAGATTTCACTGACACCCTG	GTTAAAGTGCTGCAAGATGGCA	592
<i>Alox5</i>	5-LOX	TGACAGTGGATGAAGAACTGGG	TGTTTTTGCCGTGTTTCCAGTT	259
<i>Alox12b</i>	12R-LOX	ACACCATCCAGATCAACAGCAT	CCAGAGGACCAATAGGACGATG	602
<i>Alox15</i>	12/15-LOX	CAGGAGGATGAACTCTTTGGCT	TCGAATATACCTCCGTCCGAGA	578
<i>Alox15b</i>	15-LOX2	GCGAAATGCTGAGTTCTCCATC	CAGGGTGGAATAGTTCAGCTGT	283
<i>Cox1</i>	COX1	TCACCCGCAATACTATGAGCTC	TGTGTGATAGGGAGGAGGACAT	510
<i>Cox2</i>	COX2	CCCTTTCCAAGTAGGCTTCCAA	TAGTCGTCTGGGATAGCATCT	529
<i>Gapdh</i>	GAPDH	TTTAACTCTGGCAAAGTGGAC	CATTGTCGTACCAGGAAATGAG	884

Figure 4.1: RT-PCR in PCP-R cells. A) mRNA is present for all Toll-like receptors (TLR) 1-10 in the pig. B) Results for various enzymes capable of arachidonic acid (AA) metabolism. Cytochrome P(CYP)450 epoxygenases, *Cyp2c42* and *Cyp2e1*, are both absent. mRNA for lipoxygenase (*Alox*)15 and *Alox15b* are present whereas *Alox5* and *Alox12* are absent. Cyclooxygenase (*Cox*) 1 and 2 are both present. *Gapdh* was utilized as positive controls for each gel. Band product sizes can be found in Table 1. Ladder = 1kb. C) Diagram of AA metabolism via the three different pathways, pathway inhibitors, and subsequent metabolites.

A)



B)



C)

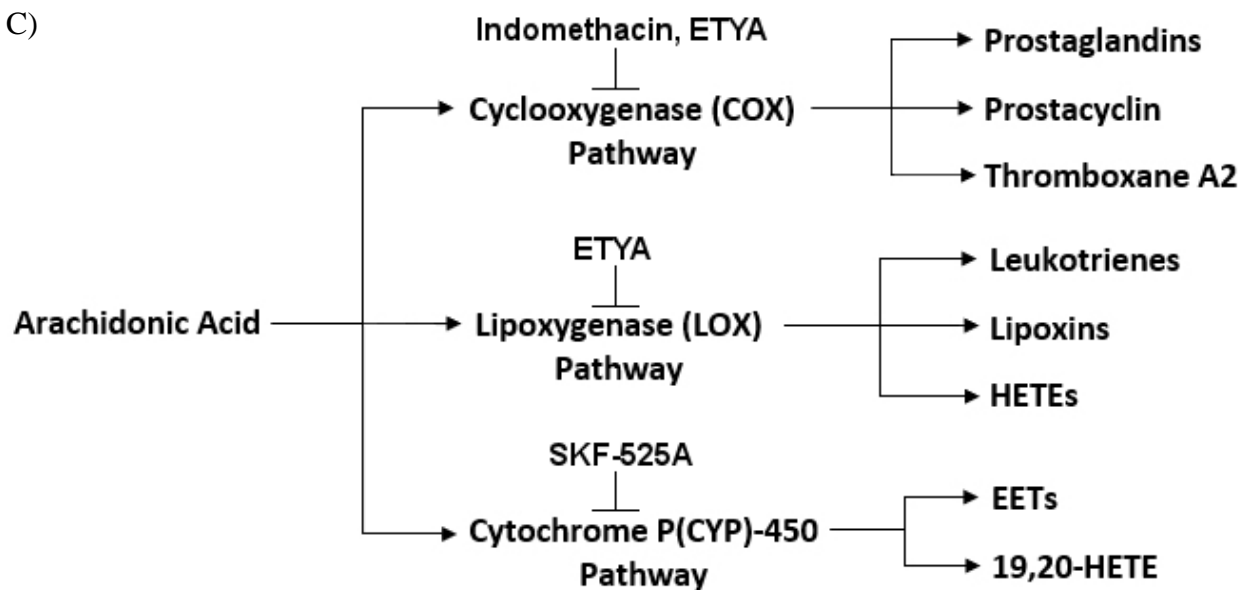


Figure 4.1 RT-PCR in PCP-R cells.

Figure 4.2: Pre-treatment of PCP-R cells with pro-inflammatory cytokine IL-1 β at 24-hours prior to TRPV4 agonist addition. Effect on transepithelial ion flux and conductance was measured. IL-1 β was added to the PCP-R media on both basolateral and apical sides of the membrane at T = -24 hours (not shown). TRPV4 agonist GSK1016790A was added to basolateral side of the membrane only at T = 0 minutes. 24-hour incubation is signified by white circles. GSK1016790A control is signified by black circles. Error bars signify mean \pm S.E.M. for number of experiments indicated. SCC = short circuit current. * = $p < 0.05$ against control.

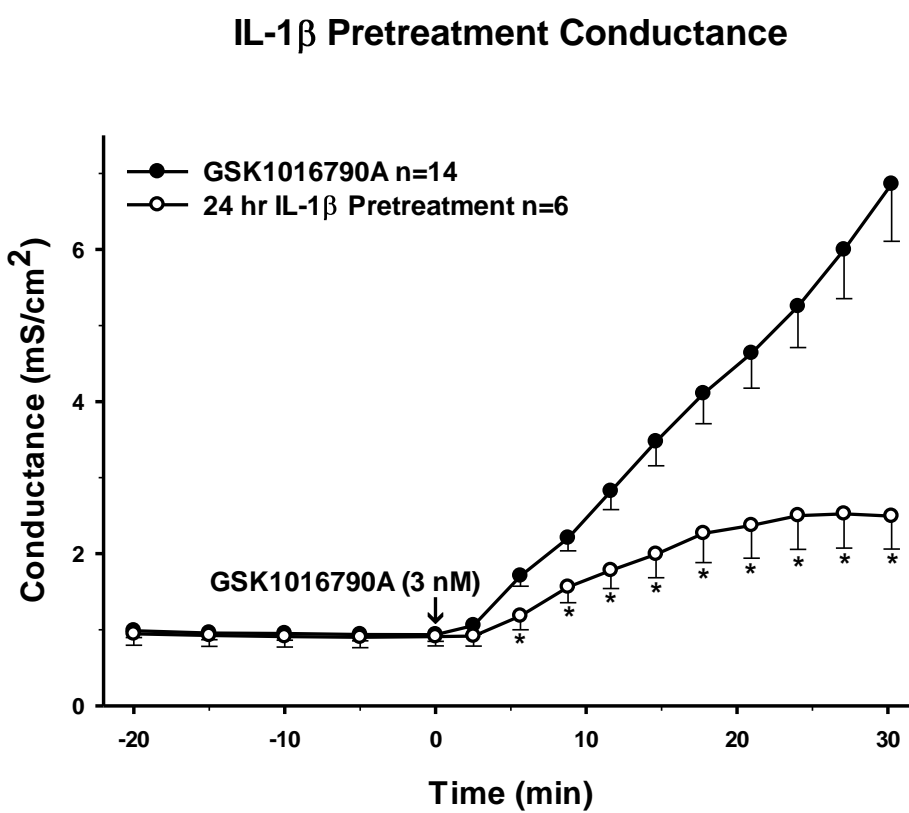
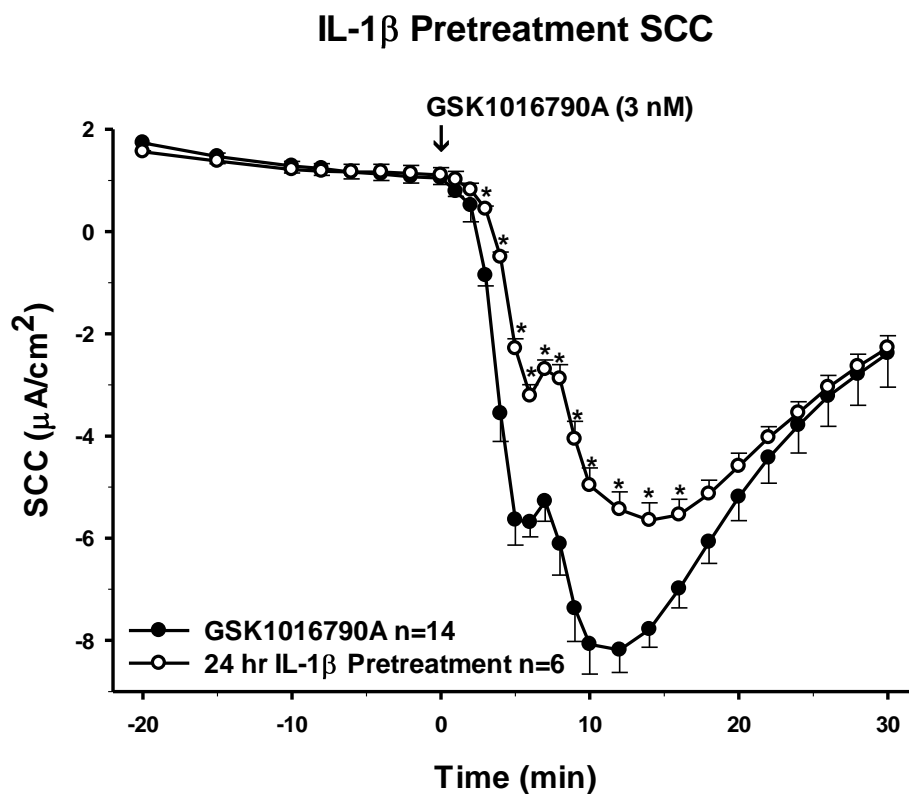


Figure 4.2 Pre-treatment of PCP-R cells with IL-1 β 24-hrs pre-TRPV4 agonist addition.

Figure 4.3: Pre-treatment of PCP-R cells with pro-inflammatory cytokine TNF- α at 24-hours prior to TRPV4 agonist addition. Effect on transepithelial ion flux and conductance was measured. TNF- α was added to the PCP-R media on both basolateral and apical sides of the membrane at T = -24 hours (not shown). TRPV4 agonist GSK1016790A was added to basolateral side of the membrane only at T = 0 minutes. 24-hour incubation is signified by white circles. GSK1016790A control is signified by black circles. Error bars signify mean \pm S.E.M. for number of experiments indicated. SCC = short circuit current. * = $p < 0.05$ against control.

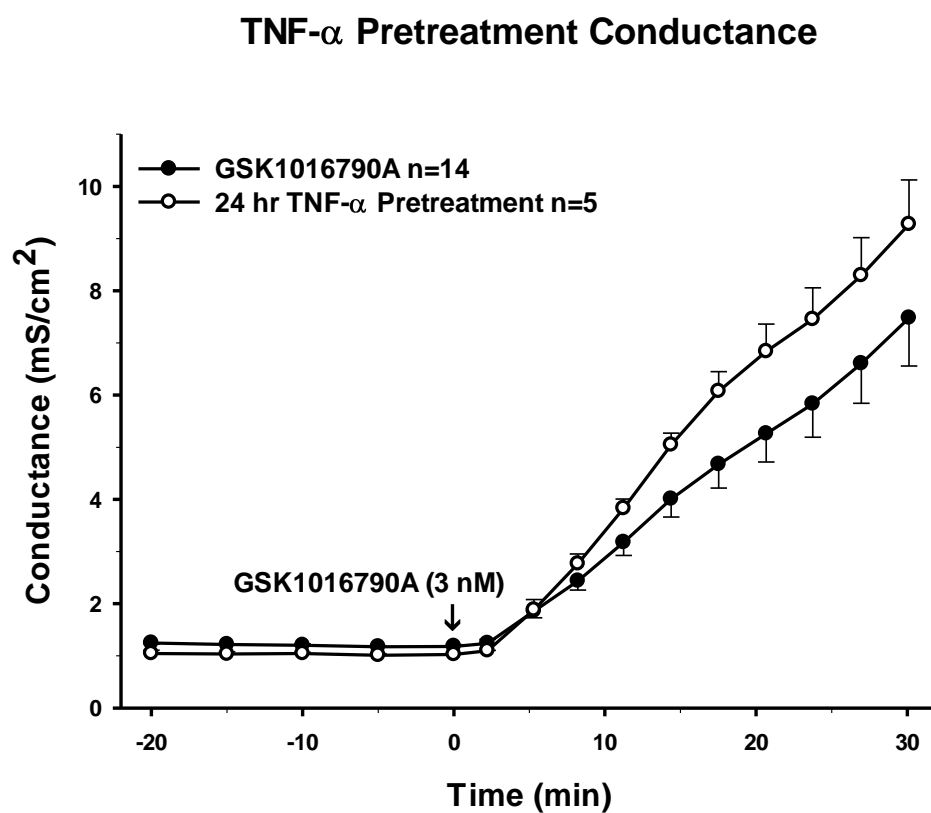
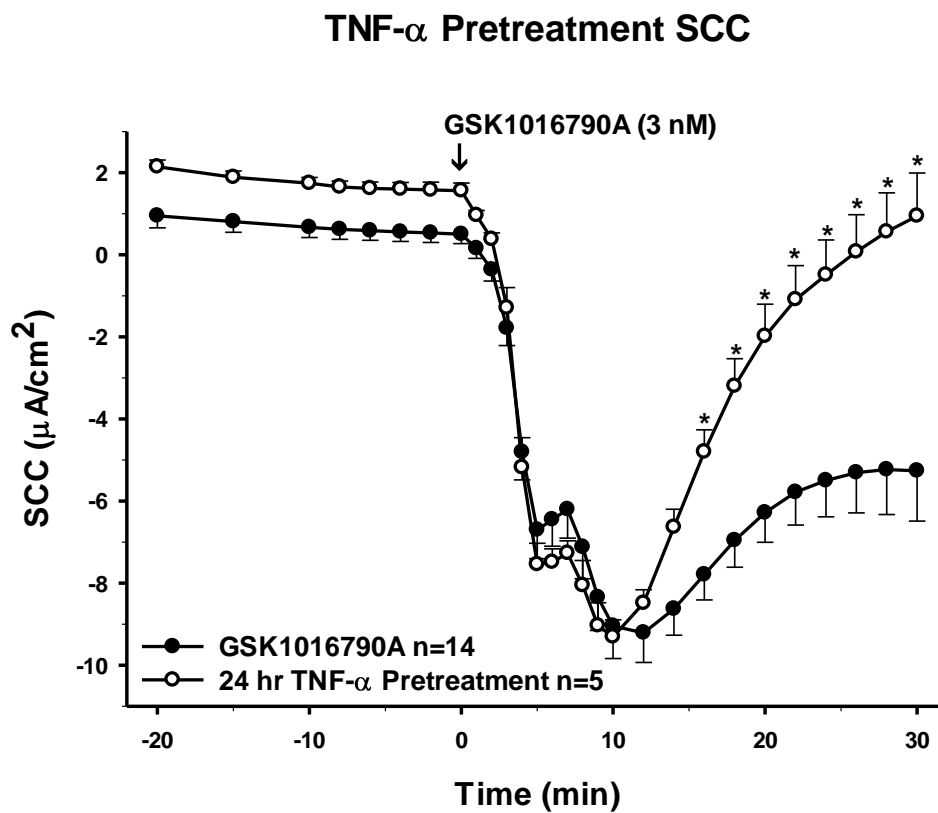


Figure 4.3 Pre-treatment of PCP-R cells with TNF- α 24-hrs pre-TRPV4 agonist addition.

Figure 4.4: Pre-treatment of PCP-R cells with anti-inflammatory cytokine IL-10 at 24-hours prior to TRPV4 agonist addition. Effect on transepithelial ion flux and conductance was measured. IL-10 was added to the PCP-R media on both basolateral and apical sides of the membrane at T = -24 hours (not shown). TRPV4 agonist GSK1016790A was added to basolateral side of the membrane only at T = 0 minutes. 24-hour incubation is signified by white circles. GSK1016790A control is signified by black circles. Error bars signify mean \pm S.E.M. for number of experiments indicated. SCC = short circuit current.

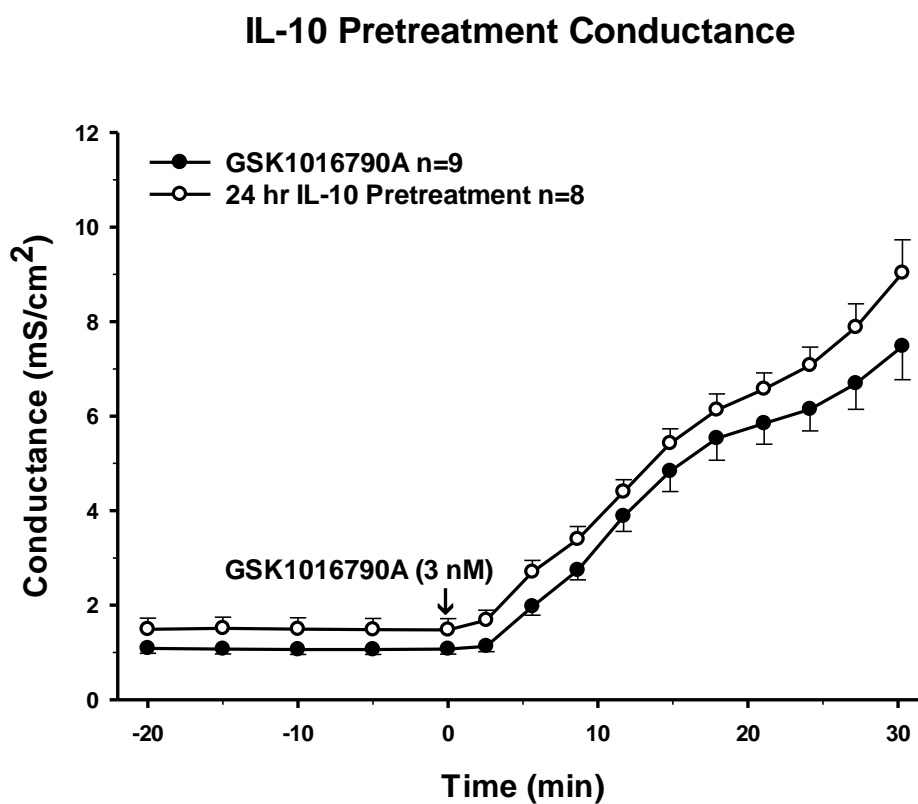
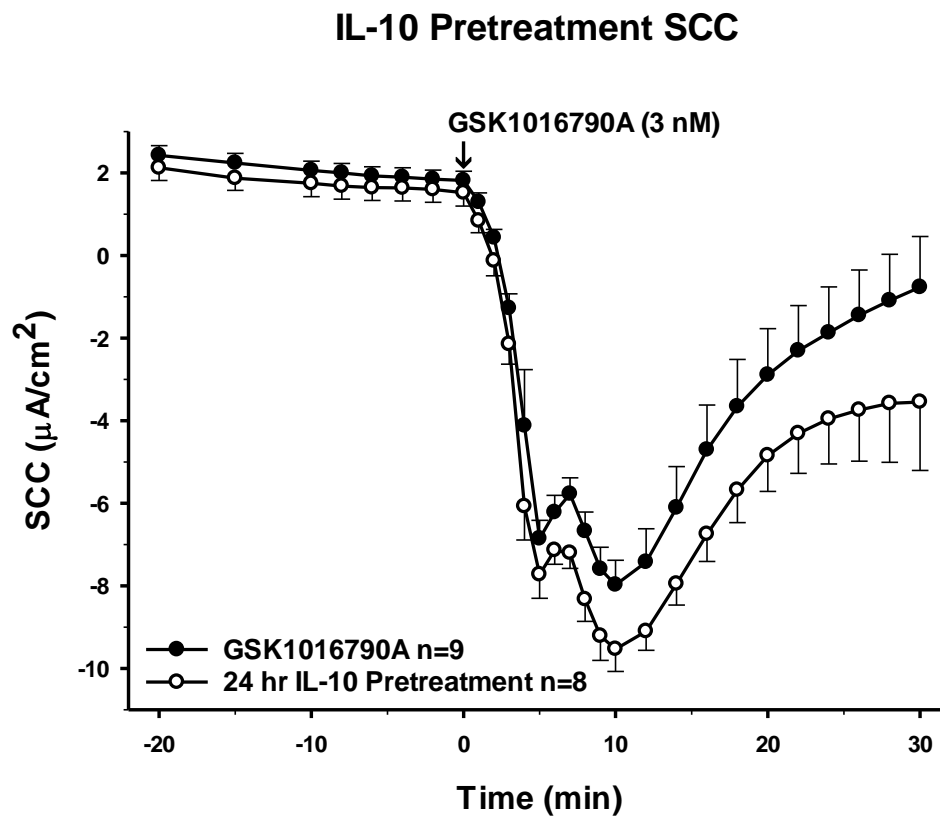


Figure 4.4 Pre-treatment of PCP-R cells with IL-10 24 hrs pre-TRPV4 agonist addition.

Figure 4.5: Pre-treatment of PCP-R cells with anti-inflammatory cytokine IL-4 at 24-hours prior to TRPV4 agonist addition. Effect on transepithelial ion flux and conductance was measured. IL-4 was added to the PCP-R media on both basolateral and apical sides of the membrane at T = -24 hours (not shown). TRPV4 agonist GSK1016790A was added to basolateral side of the membrane only at T = 0 minutes. 24-hour incubation is signified by white circles. GSK1016790A control is signified by black circles. Error bars signify mean \pm S.E.M. for number of experiments indicated. SCC = short circuit current.

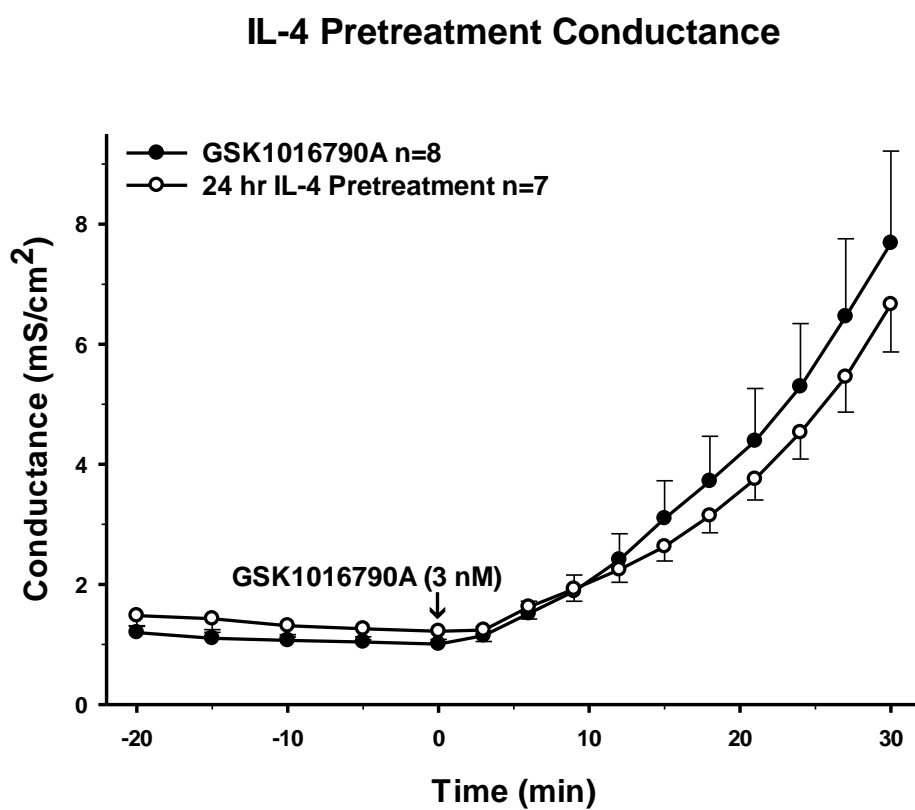
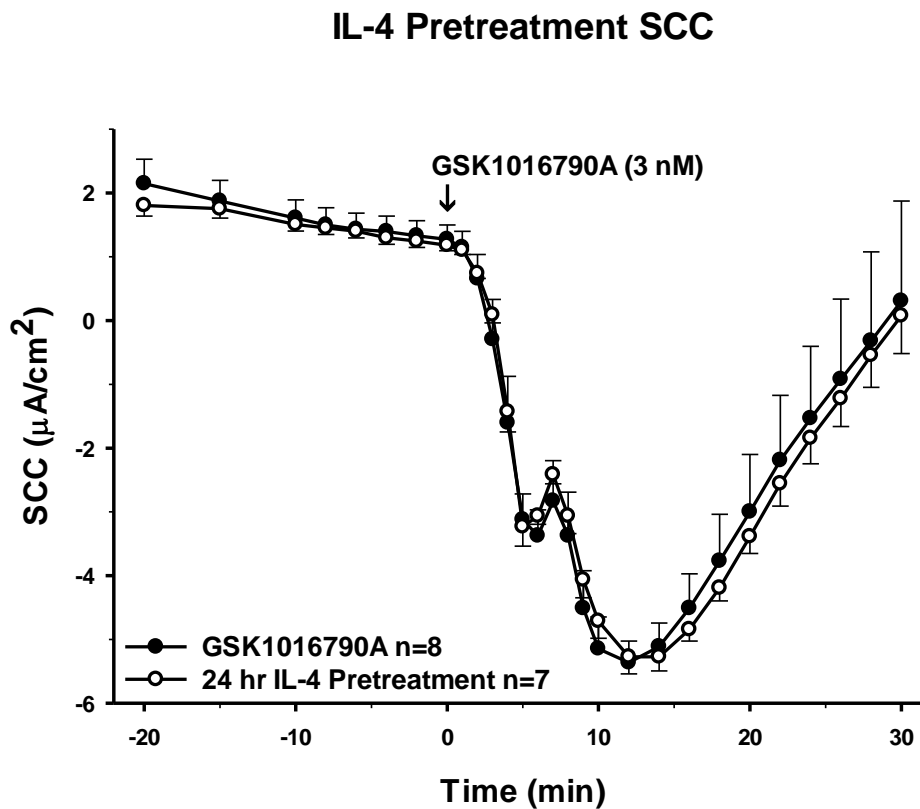


Figure 4.5 Pre-treatment of PCP-R cells with IL-4 24 hrs pre-TRPV4 agonist addition

Figure 4.6: Pre-treatment of PCP-R cells with pro- and anti-inflammatory cytokine TGF- β 1 at 24-hours prior to TRPV4 agonist addition. Effect on transepithelial ion flux and conductance was measured. TGF- β 1 was added to the PCP-R media on both basolateral and apical sides of the membrane at T = -24 hours (not shown). TRPV4 agonist GSK1016790A was added to basolateral side of the membrane only at T = 0 minutes. 24-hour incubation is signified by white circles. GSK1016790A control is signified by black circles. Error bars signify mean \pm S.E.M. for number of experiments indicated. SCC = short circuit current. * = $p < 0.05$ against control.

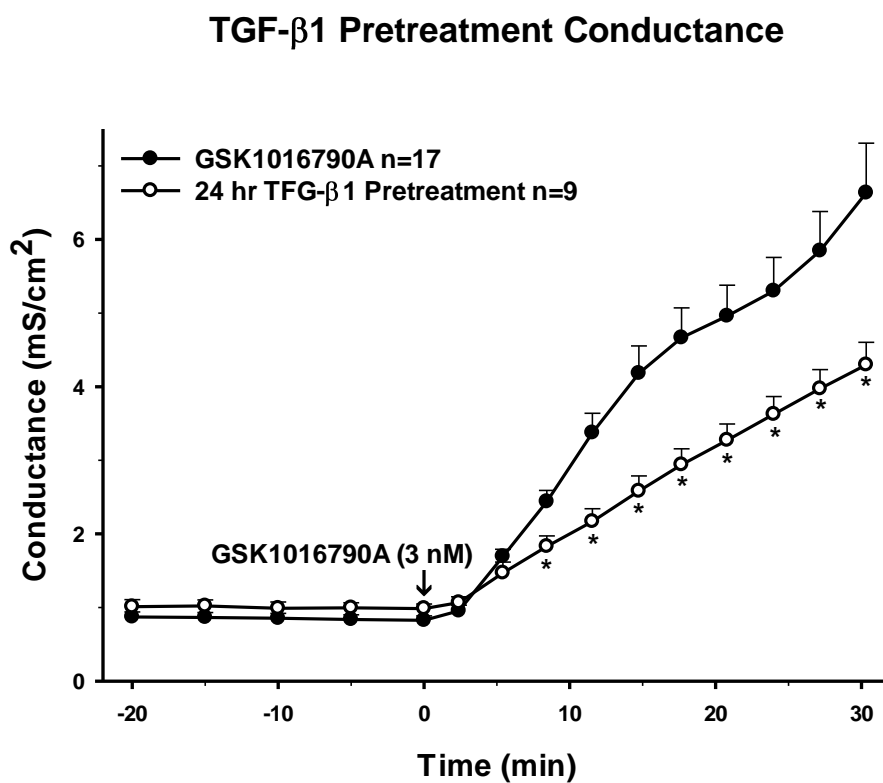
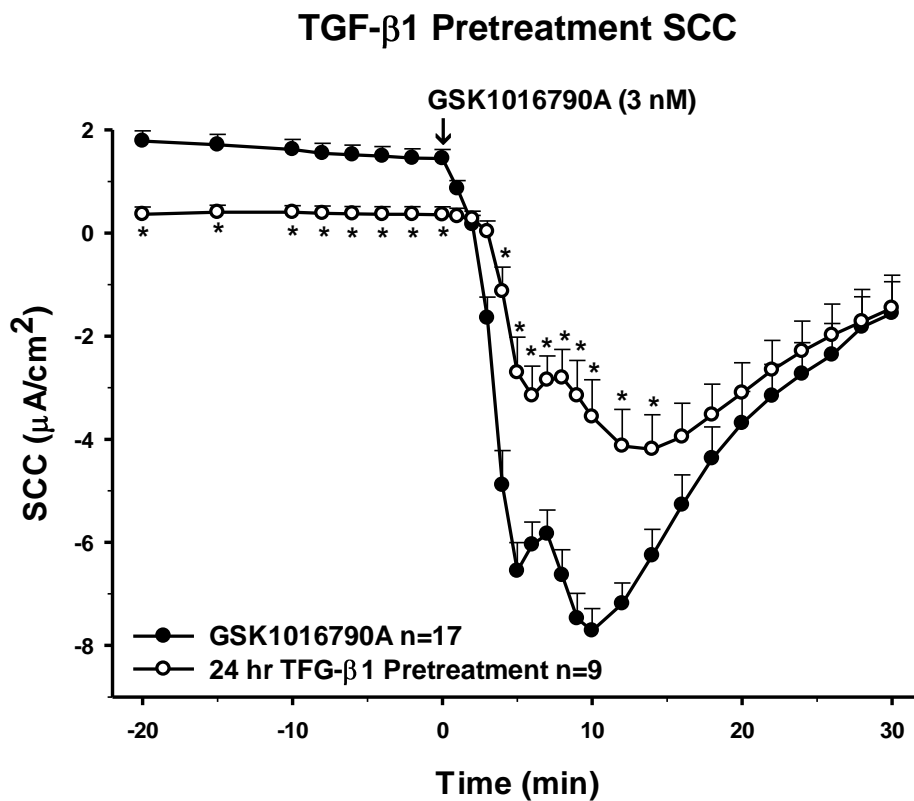


Figure 4.6 Pre-treatment of PCP-R cells with TGF- β 1 24 hrs pre-TRPV4 agonist addition

Figure 4.7: Pre-treatment of PCP-R cells with pro- and anti-inflammatory cytokine IL-6 at 24-hours prior to TRPV4 agonist addition. Effect on transepithelial ion flux and conductance was measured. IL-6 was added to the PCP-R media on both basolateral and apical sides of the membrane at T = -24 hours (not shown). TRPV4 agonist GSK1016790A was added to basolateral side of the membrane only at T = 0 minutes. 24-hour incubation is signified by white circles. GSK1016790A control is signified by black circles. Error bars signify mean \pm S.E.M. for number of experiments indicated. SCC = short circuit current.

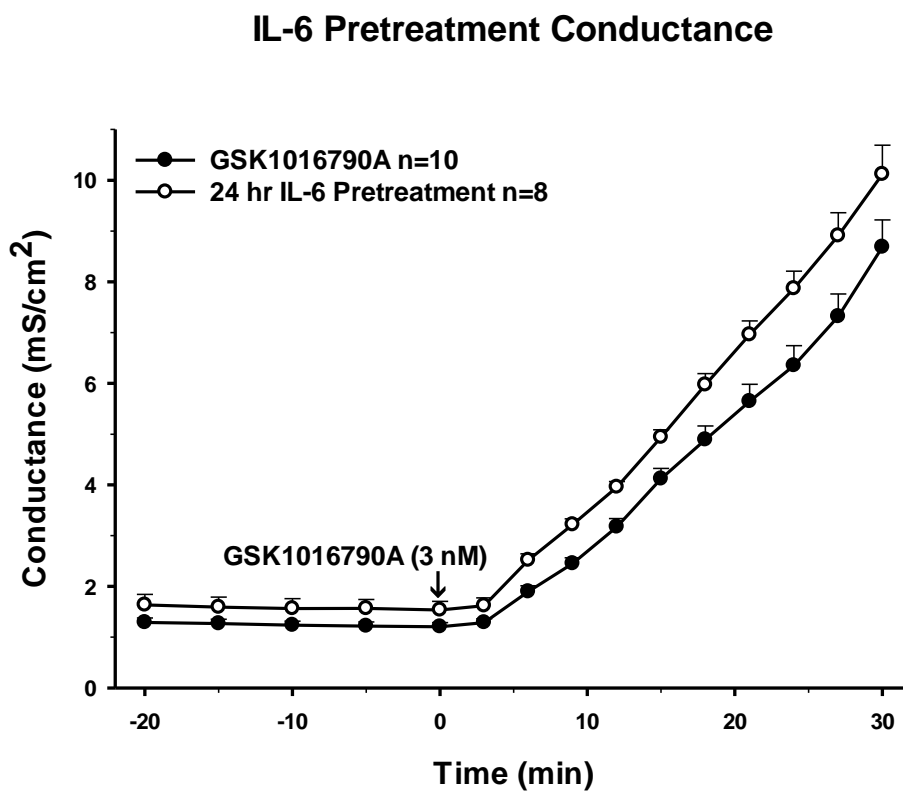
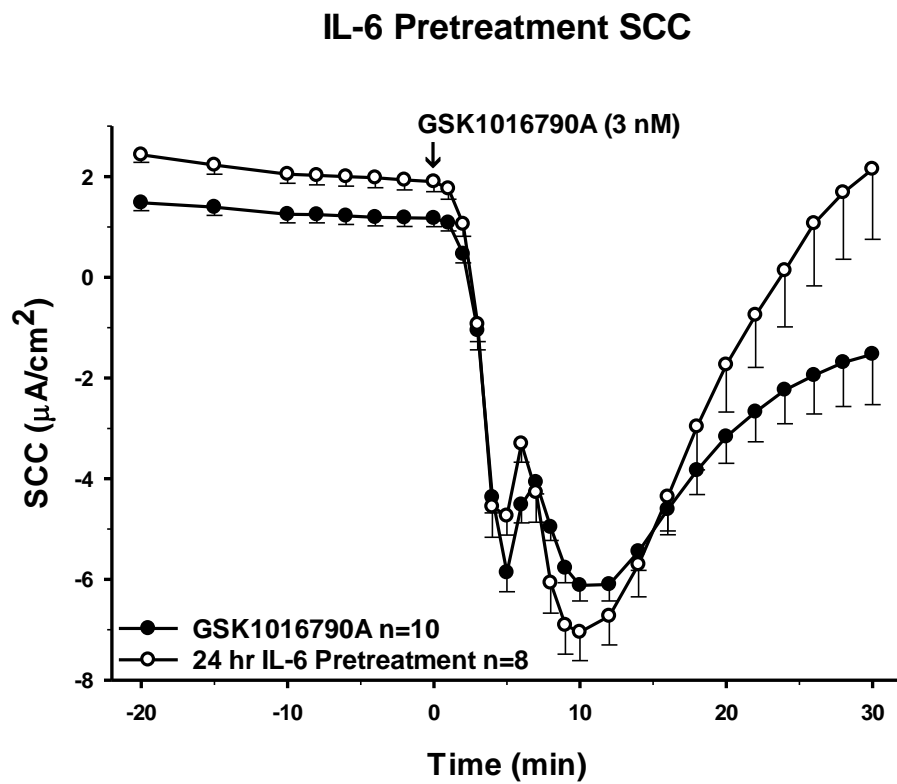


Figure 4.7 Pre-treatment of PCP-R cells with IL-6 24 hrs pre-TRPV4 agonist addition

Figure 4.8: Pre-treatment of PCP-R cells with NF- κ B inhibitor PDTC at 10 minutes prior to TRPV4 agonist addition. Effect on transepithelial ion flux and conductance was measured. PDTC was added to the PCP-R media on both basolateral and apical sides of the membrane at T = -10 minutes. TRPV4 agonist GSK1016790A was added to basolateral side of the membrane only at T = 0 minutes. 10-minute incubation is signified by white circles. GSK1016790A control is signified by black circles. Error bars signify mean \pm S.E.M. for number of experiments indicated. SCC = short circuit current. * = $p < 0.05$ against control.

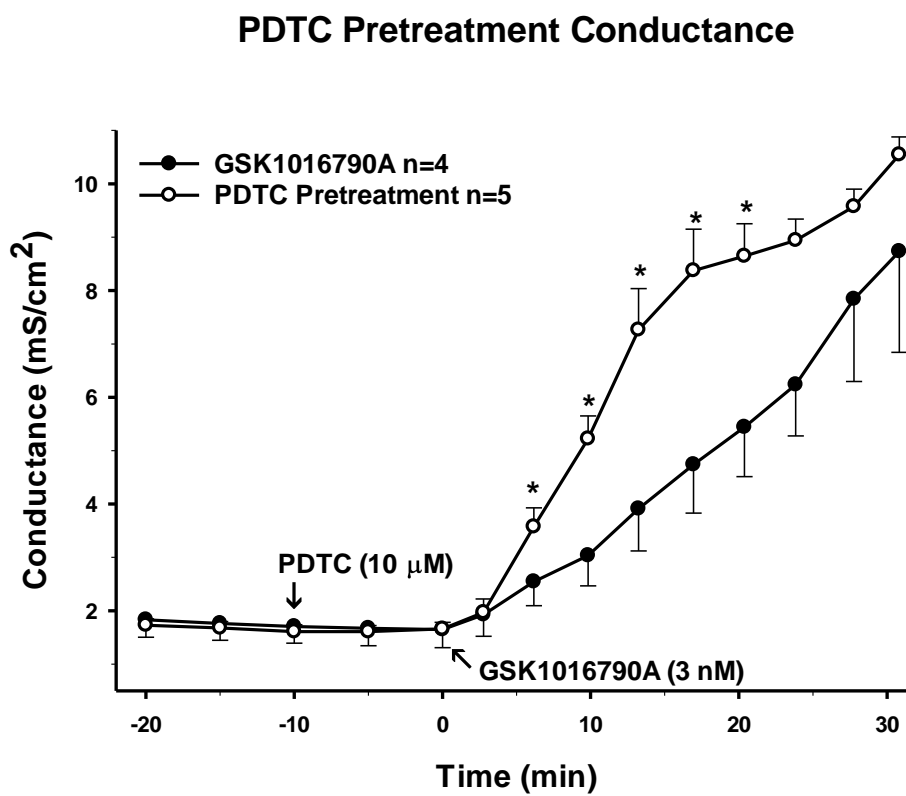
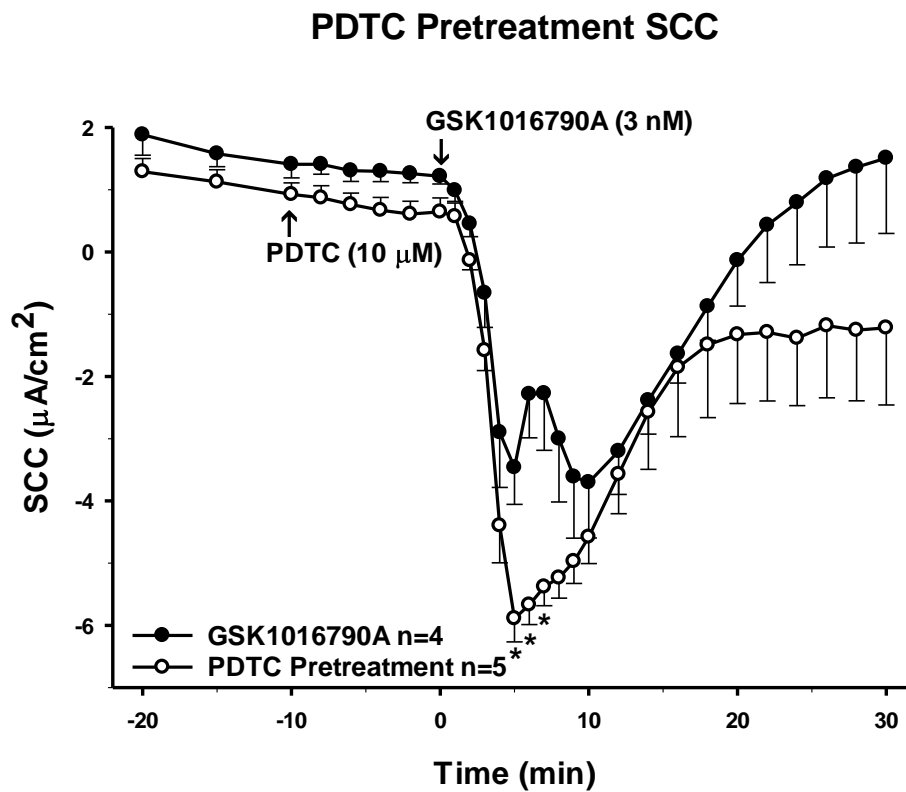


Figure 4.8 Pre-treatment of PCP-R cells with PDTC 10 min pre-TRPV4 agonist addition.

Figure 4.9: Pre-treatment of PCP-R cells with NF- κ B inhibitor PDTC at 24-hours prior to TRPV4 agonist addition. Effect on transepithelial ion flux and conductance was measured. PDTC was added to the PCP-R media on both basolateral and apical sides of the membrane at T = -24 hours (not shown). TRPV4 agonist GSK1016790A was added to basolateral side of the membrane only at T = 0 minutes. 24-hour incubation is signified by white circles. GSK1016790A control is signified by black circles. Error bars signify mean \pm S.E.M. for number of experiments indicated. SCC = short circuit current. * = $p < 0.05$ against control.

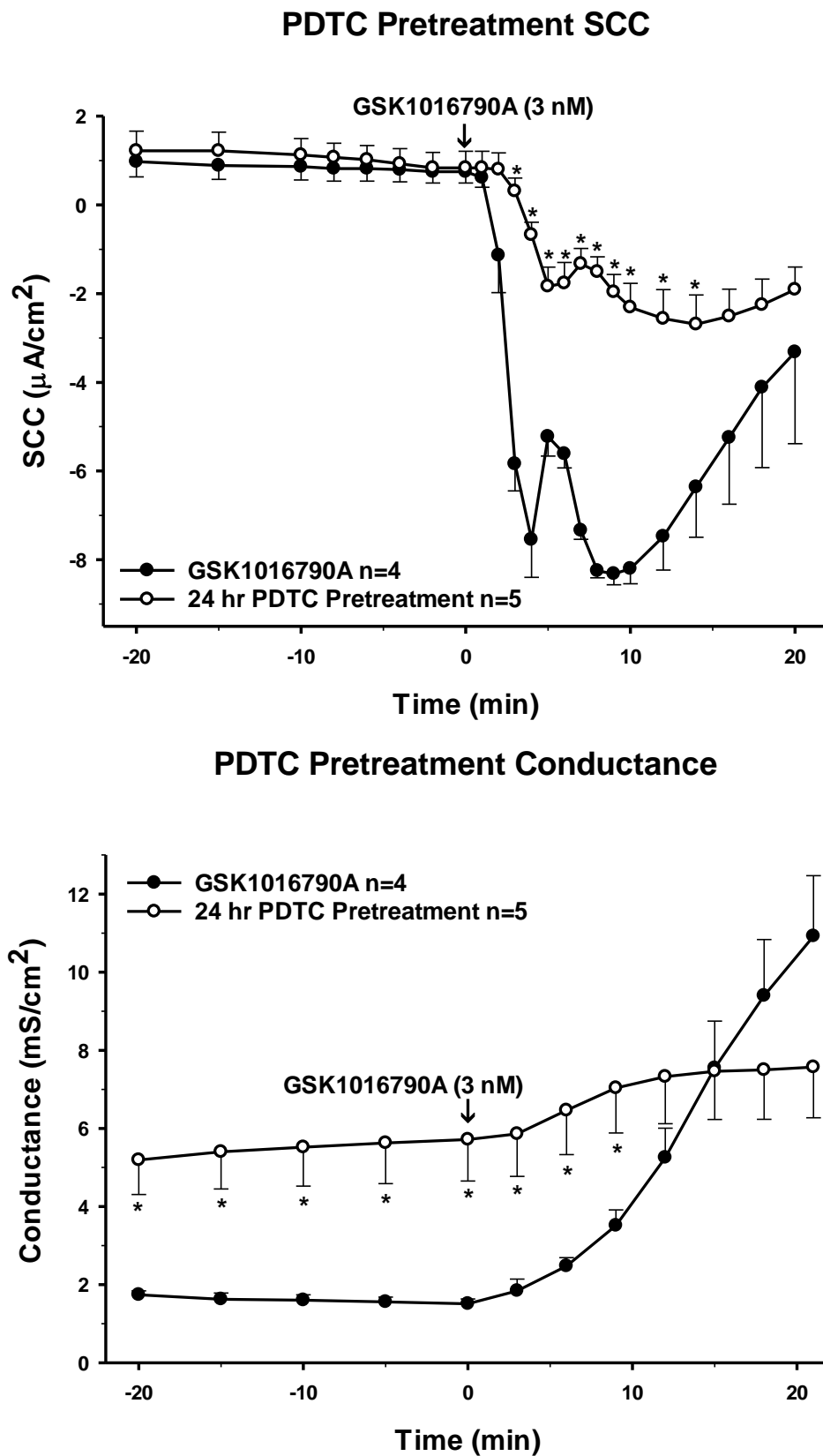
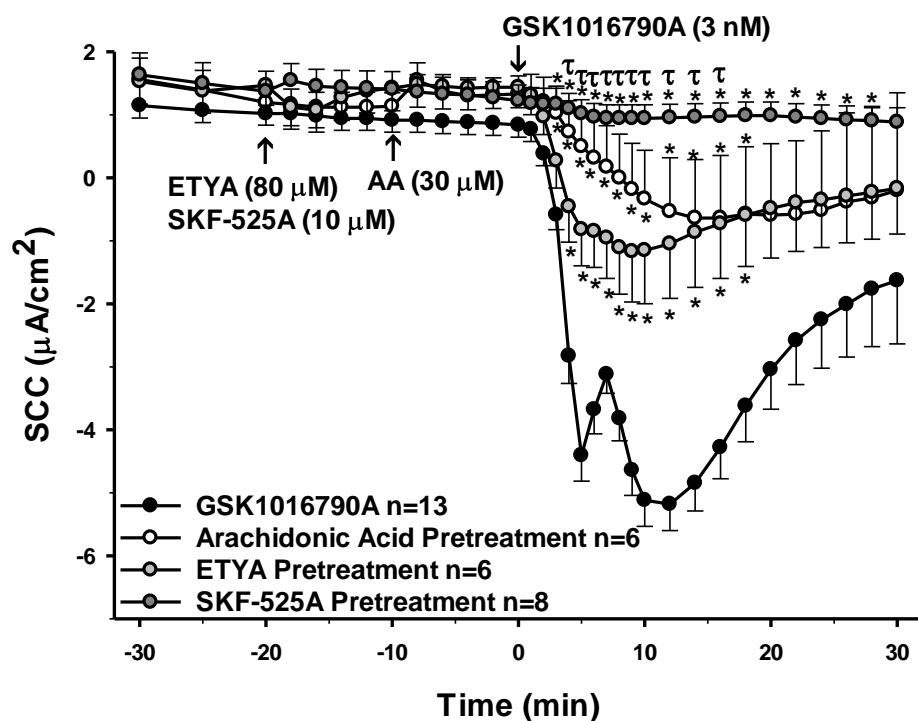


Figure 4.9 Pre-treatment of PCP-R cells with PDTC 24 hrs pre-TRPV4 agonist addition.

Figure 4.10: Pre-treatment of PCP-R cells with arachidonic acid (AA) at 10-minutes and AA metabolism inhibitors at 20-minutes prior to TRPV4 agonist addition. Effect on transepithelial ion flux and conductance was measured. AA was added to the PCP-R media on both basolateral and apical sides of the membrane at T = -10 minutes. Cyclooxygenase and lipoxygenase inhibitor ETYA was added to the PCP-R media on both basolateral and apical sides of the membrane at T = -20 minutes. Cytochrome P450 inhibitor SKF-525A was added to the PCP-R media on both basolateral and apical sides of the membrane at T = -20 minutes. TRPV4 agonist GSK1016790A was added to basolateral side of the membrane only T = 0 minutes. AA pre-treatment is signified by white circles. ETYA pre-treatment is signified by grey circles. SKF-525A pre-treatment is signified by dark grey circles. GSK1016790A control is signified by black circles. Error bars signify mean \pm S.E.M. for number of experiments indicated. SCC = short circuit current. * = $p < 0.05$ against control. τ = $p < 0.05$ against ETYA pre-treatment in SCC graph. τ = $p < 0.05$ against AA pre-treatment in Conductance graph. Ψ = $p < 0.05$ against ETYA pre-treatment in Conductance graph.

Arachidonic Acid & Metabolite Inhibitor Pretreatment SCC



Arachidonic Acid & Metabolite Inhibitor Pretreatment Conductance

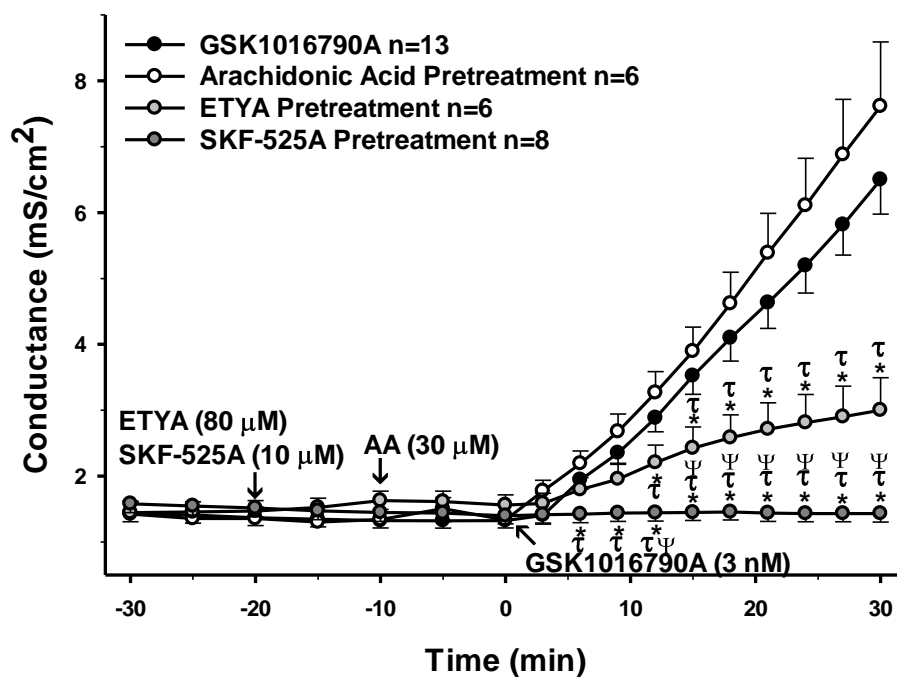


Figure 4.10 Pre-treatment of PCP-R cells with AA or metabolites pre-TRPV4 agonist.

Figure 4.11: Pre-treatment of PCP-R cells with arachidonic acid metabolite 5,6-EET at 10-minutes prior to TRPV4 agonist addition. Effect on transepithelial ion flux and conductance was measured. 5,6-EET was added to the PCP-R media on both basolateral and apical sides of the membrane at T = -10 minutes. TRPV4 agonist GSK1016790A was added to basolateral side of the membrane only at T = 0 minutes. 10-minute incubation is signified by white circles. GSK1016790A control is signified by black circles. Error bars signify mean \pm S.E.M. for number of experiments indicated. SCC = short circuit current.

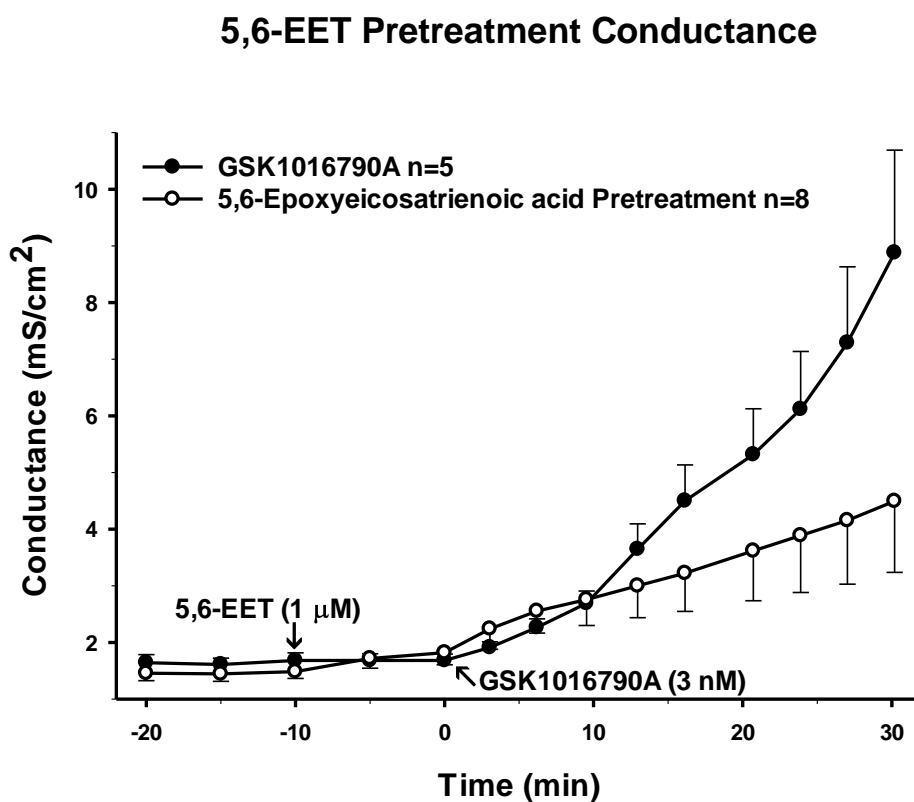
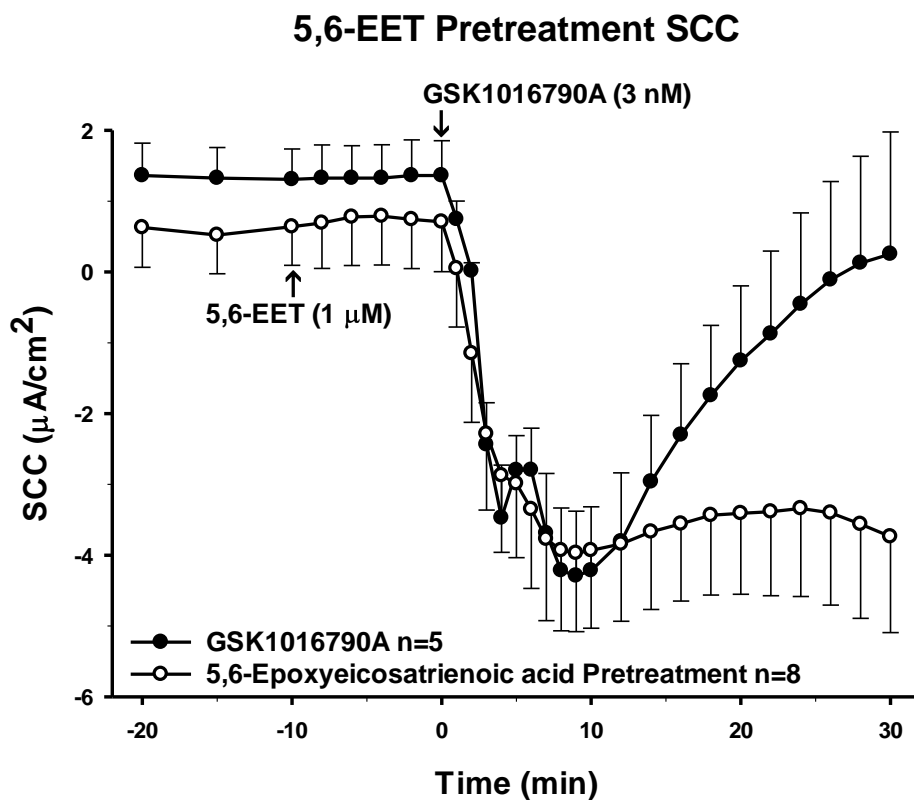


Figure 4.11 Pre-treatment of PCP-R cells 5,6-EET 10-min pre-TRPV4 agonist addition.

4.7 References

1. Shim, J., Territo, P., Simpson, S., Watson, J., Jiang, L., and Riley, A. et al. (2019). Hydrocephalus in a rat model of Meckel Gruber syndrome with a TMEM67 mutation. *Scientific Reports*, 9(1).
2. Liedtke, W., Choe, Y., Martí-Renom, M. A., Bell, A. M., Denis, C. S., Sali, A., Hudspeth, A.J., Friedman, J.M., and Heller, S. (2000). Vanilloid Receptor–Related Osmotically Activated Channel (VR-OAC), a candidate vertebrate osmoreceptor. *Cell*, 103(3), 525-535.
3. Strotmann, R., Harteneck, C., Nunnenmacher, K., Schultz, G., and Plant, T. D. (2000). OTRPC4, a nonselective cation channel that confers sensitivity to extracellular osmolarity. *Nature Cell Biology*, 2, 695-702.
4. Nilius, B., Vriens, J., Prenen, J., Droogmans, G., and Voets, T. (2004). TRPV4 calcium entry channel: A paradigm for gating diversity. *AJP: Cell Physiology*, 286(2), C195-C205.
5. Preston, D., Simpson, S., Halm, D., Hochstetler, A., Schwerk, C., Schrotten, H., and Blazer-Yost, B. (2018). Activation of TRPV4 stimulates transepithelial ion flux in a porcine choroid plexus cell line. *American Journal Of Physiology-Cell Physiology*, 315(3), C357-C366.
6. Danker, H. H., Brown, P. D., and Praetorius, J. (2013). Cerebrospinal fluid secretion by the choroid plexus. *American Physiological Society*, 93(4), 1847-1892.
7. Node, K., Huo, Y., Ruan, X., Yang, B., Spiecker, M., Ley, K., and Zeldin, D. C. (1999). Anti-inflammatory properties of cytochrome P450 epoxygenase-derived eicosanoids. *Science*, 285(5431), 1276-1279.
8. Wyss-Coray, T., and Mucke, L. (2002). Inflammation in neurodegenerative disease—a double-edged sword. *Neuron*, 35, 419-432.
9. Corrigan, F., Mander, K. A., Leonard, A. V., and Vink, R. (2016). Neurogenic inflammation after traumatic brain injury and its potentiation of classical inflammation. *Journal of Neuroinflammation*, 13(264).
10. Lee, P., Monaco, E. A., and Friedlander, R. M. (2013). Blocking TGF- β activity and associated inflammation may halt hydrocephalus. *Science Times Neurosurgery*, 73(6).

11. Sosvorova, L., Mohapl, M., Vcelak, J., Hill, M., Vitku, J., and Hampl, R. (2015). The impact of selected cytokines in the follow-up of normal pressure hydrocephalus. *Physiological Research*, 64, S283-S290.
12. Woodcock, T. and Morganti-Kossmann, M. C. (2013). The role of markers of inflammation in traumatic brain injury. *Frontiers in Neurology*, 4(18).
13. Herrero, M., Estrada, C., Maatouk, L., and Vyas, S. (2015). Inflammation in Parkinson's disease: role of glucocorticoids. *Frontiers in Neurology*, 9(32).
14. Azizi, G., Navabi, S. S., Al-Shukaili, A., Seyedzadeh, M. H., Yazdani, R., and Mirshafiey, A. (2015). The role of inflammatory mediators in the pathogenesis of Alzheimer's disease. *Sultan Qaboos University Medical Journal*, 15(3), e305-e316.
15. Scheller, J., Chalaris, A., Schmidt-Arras, D., and Rose-John, S. (2011). The pro- and anti-inflammatory properties of the cytokine interleukin-6. *Biochimica Et Biophysica Acta (BBA) - Molecular Cell Research*, 1813(5), 878-888.
16. Schrotten, M., Hanisch, F., Quednau, N., Stump, C., Riebe, R., Lenk, M., and Wolburg, H. (2012). A novel porcine in vitro model of the blood-cerebrospinal fluid barrier with strong barrier function. *PLoS ONE*, 7(6).
17. Smith, U. M., Consugar, M., Tee, L. J., McKee, B. M., Maina, E. N., Whelan, S., and Morgan, N. V. (2006). The transmembrane protein meckelin (MKS3) is mutated in Meckel-Gruber syndrome and the wpk rat. *Nature Genetics*, 38(2), 191-196.
18. Lawrence, T. (2009). The nuclear factor NF- B pathway in inflammation. *Cold Spring Harbor Perspectives In Biology*, 1(6), a001651-a001651.
19. Yan, Y., Dalmaso, G., Thi Thu Nguyen, H., Obertone, T., Sitaraman, S., and Merlin, D. (2009). Ste20-Related Proline/Alanine-Rich Kinase (SPAK) regulated transcriptionally by hyperosmolarity is involved in intestinal barrier function. *Plos ONE*, 4(4), e5049.
20. Lehmann, J. M., Lenhard, J. M., Oliver, B. B., Ringold, G. M., and Kliewer, S. A. (1997). Peroxisome proliferator-activated receptors and are activated by indomethacin and other non-steroidal anti-inflammatory drugs. *The Journal of Biological Chemistry*, 272(6), 3406-3410.

21. Langenbach, R., Tiano, H. F., Loftin, C. D., Ghanayem, B. I., Chulada, P. C., Mahler, J. F., and Lee, C. A. (1995). Prostaglandin synthase 1 gene disruption in mice reduces arachidonic acid-induced inflammation and indomethacin-induced gastric ulceration. *Cell*, 83, 483-492.
22. Yamamoto, T., and Nozaki-Taguchi, N. (1996). Analysis of the effects of cyclooxygenase (COX)-1 and COX-2 in spinal nociceptive transmission using indomethacin, a non-selective COX inhibitor, and NS-398, a COX-2 selective inhibitor. *Brain Research*, 739, 104-110.
23. Erickson, K., Baron, I., and Fantie, B. (2001). Neuropsychological functioning in early hydrocephalus: review from a developmental perspective. *Child Neuropsychology*, 7(4), 199-229.
24. Clop, A., Huisman, A., van As, P., Sharaf, A., Derdak, S., and Sanchez, A. (2016). Identification of genetic variation in the swine toll-like receptors and development of a porcine TLR genotyping array. *Genetics Selection Evolution*, 48(1).
25. Okun, E., Griffioen, K., Lathia, J., Tang, S., Mattson, M., and Arumugam, T. (2009). Toll-like receptors in neurodegeneration. *Brain Research Reviews*, 59(2), 278-292.
26. Akira, S., and Takeda, K. (2004). Toll-like receptor signalling. *Nature Reviews Immunology*, 4(7), 499-511.
27. Gattone, V., Tourkow, B., Trambaugh, C., Yu, A., Whelan, S., Phillips, C., Harris, P., and Peterson, R. (2004). Development of multiorgan pathology in the wpk rat model of polycystic kidney disease. *The Anatomical Record*, 277A(2), 384-395.
28. Balakrishna, S., Song, W., Achanta, S., Doran, S., Liu, B., and Kaelberer, M. et al. (2014). TRPV4 inhibition counteracts edema and inflammation and improves pulmonary function and oxygen saturation in chemically induced acute lung injury. *American Journal Of Physiology-Lung Cellular And Molecular Physiology*, 307(2), L158-L172.
29. Dalsgaard, T., Sonkusare, S., Teuscher, C., Poynter, M., and Nelson, M. (2016). Pharmacological inhibitors of TRPV4 channels reduce cytokine production, restore endothelial function and increase survival in septic mice. *Scientific Reports*, 6(1).
30. Watanabe, H., Vriens, J., Prenen, J., Droogmans, G., Voets, T., and Nilius, B. (2003). Anandamide and arachidonic acid use epoxyeicosatrienoic acids to activate TRPV4 channels. *Nature*, 424(6947), 434-438.

31. Cao, S., Anishkin, A., Zinkevich, N., Nishijima, Y., Korishettar, A., and Wang, Z. et al. (2018). Transient receptor potential vanilloid 4 (TRPV4) activation by arachidonic acid requires protein kinase A-mediated phosphorylation. *Journal Of Biological Chemistry*, 293(14), 5307-5322.
32. Filosa, J., Yao, X., and Rath, G. (2013). TRPV4 and the regulation of vascular tone. *Journal of Cardiovascular Pharmacology*, 61(2), 113-119.
33. Shahabi, P., Siest, G., Meyer, U., and Visvikis-Siest, S. (2014). Human cytochrome P450 epoxygenases: Variability in expression and role in inflammation-related disorders. *Pharmacology & Therapeutics*, 144(2), 134-161.
34. Palumbo, S. (2017). Pathogenesis and progression of multiple sclerosis: the role of arachidonic acid-mediated neuroinflammation. *Multiple Sclerosis: Perspectives in Treatment and Pathogenesis*, 111-124.
35. Mashima, R., and Okuyama, T. (2015). The role of lipoxygenases in pathophysiology; new insights and future perspectives. *Redox Biology*, 6, 297-310.
36. Zhao, L., Cuff, C., Moss, E., Wille, U., Cyrus, T., and Klein, E. et al. (2002). Selective interleukin-12 synthesis defect in 12/15-lipoxygenase-deficient macrophages associated with reduced atherosclerosis in a mouse model of familial hypercholesterolemia. *Journal Of Biological Chemistry*, 277(38), 35350-35356.
37. Wu, M., Lin, T., Chiu, Y., Liou, H., Yang, R., and Fu, W. (2012). Involvement of 15-lipoxygenase in the inflammatory arthritis. *Journal of Cellular Biochemistry*, 113(7), 2279-2289.
38. Kim, S., Akindehin, S., Kwon, H., Son, Y., Saha, A., Jung, Y., Seong, J., Lim, K., Sung, J., Maddipati, K., and Lee, Y. (2018). Anti-inflammatory role of 15-lipoxygenase contributes to the maintenance of skin integrity in mice. *Scientific Reports*, 8(1).
39. Vadivelu, S., Rekate, H., Esernio-Jenssen, D., Mittler, M., and Schneider, S. (2016). Hydrocephalus associated with childhood nonaccidental head trauma. *Neurosurgical Focus*, 41(5), E8.
40. Tully, H., and Dobyns, W. (2014). Infantile hydrocephalus: a review of epidemiology, classification and causes. *European Journal of Medical Genetics*, 57(8), 359-368.

41. Karimy, J., Zhang, J., Kurland, D., Theriault, B., Duran, D., and Stokum, J. et al. (2017). Inflammation-dependent cerebrospinal fluid hypersecretion by the choroid plexus epithelium in posthemorrhagic hydrocephalus. *Nature Medicine*, 23(8), 997-1003.
42. Krauss, J., Regel, J., Droste, D., Orszagh, M., Borremans, J., and Vach, W. (1997). Movement disorders in adult hydrocephalus. *Movement Disorders*, 12(1), 53-60.
43. Golomb, J., Wisoff, J., Miller, D. C., Boksay, I., Kluger, A., Weiner, H., Salton, J., and Graves, W. (2000). Alzheimer's disease comorbidity in normal pressure hydrocephalus: prevalence and shunt response. *Journal of Neurology, Neurosurgery & Psychiatry*, 68(6), 778-781.
44. Jankovic, J., Newmark, M., and Peter, P. (1986). Parkinsonism and acquired hydrocephalus. *Movement Disorders*, 1(1), 59-64.
45. Kushel, Y., Belova, Y., and Tekoey, A. (2017). Intramedullary spinal cord tumors and hydrocephalus: an analysis of the results of surgical treatment in 541 patients. *Voprosy neurokhirurgii imeni N.N. Burdenko*, 81(4), 56.
46. Lin, C., and Riva-Cambrin, J. (2015). Management of posterior fossa tumors and hydrocephalus in children: a review. *Child's Nervous System*, 31(10), 1781-1789.
47. Lu, K., Huang, T., Tsai, Y., and Yang, Y. (2017). Transient receptor potential vanilloid type 4 channels mediate Na-K-Cl-co-transporter-induced brain edema after traumatic brain injury. *Journal of Neurochemistry*, 140(5), 718-727.
48. Kant, S., Stopa, E., Johanson, C., Baird, A., and Silverberg, G. (2018). Choroid plexus genes for CSF production and brain homeostasis are altered in Alzheimer's disease. *Fluids and Barriers of the CNS*, 15(1).
49. Ott, B., Jones, R., Daiello, L., de la Monte, S., Stopa, E., Johanson, C., Denby, C. and Grammas, P. (2018). Blood-cerebrospinal fluid barrier gradients in mild cognitive impairment and Alzheimer's disease: Relationship to inflammatory cytokines and chemokines. *Frontiers in Aging Neuroscience*, 10.
50. Toft-Bertelsen, T., Križaj, D. and MacAulay, N. (2017). When size matters: transient receptor potential vanilloid 4 channel as a volume-sensor rather than an osmo-sensor. *The Journal of Physiology*, 595(11), 3287-3302.
51. Block, M. and Hong, J. (2005). Microglia and inflammation-mediated neurodegeneration: Multiple triggers with a common mechanism. *Progress in Neurobiology*, 76(2), 77-98.

52. Agarwal, N., Lariviere, W., Henry, L., Faramand, A., Koschnitzky, J. and Friedlander, R. (2019). Observations from social media regarding the symptomatology of adult hydrocephalus patients. *World Neurosurgery*, 122, e307-e314.

CHAPTER 5. ADDITIONAL DATA

5.1 TRPV4 in the Choroid Plexus

Because TRPV4 is hypothesized to be a major contributor to the development of hydrocephalus in our Wpk rat model, it was important to discover its location and relative expression levels in the CP. Therefore, using immunohistochemistry of brain tissue slices from hydrocephalic TMEM67 (-/-) and wild type (WT) animals, I was able to visualize and localize CP (Figure 5.1, yellow arrows) and TRPV4 (green) in the rat brains, with DAPI nuclear staining for orientation of individual cells. From these sections, I found that at birth (P0) expression levels of TRPV4 in hydrocephalic rats (Figure 5.1, B) were similar to that of the wild type animals (Figure 5.1, A). However, as the animals develop to P15, this expression appeared to increase in the hydrocephalic rat (Figure 5.1, D) while TRPV4 remained unchanged in the wild type animals (Figure 5.1, C). Furthermore, in wild type animals there was no detectable TRPV4 expression in the ependymal cells lining the ventricle (Figure 5.1, orange arrows). However, in the hydrocephalic rats, the ependymal cells did show detectable expression of TRPV4, suggesting further increases in TRPV4 expression. In both phenotypes, TRPV4 localized to the apical membrane of the choroid plexus, with some localized intracellularly. It is possible that the intracellular TRPV4 can be stimulated to migrate into the apical membrane. This stimulus could include activators of TRPV4, such as pressure changes or inflammatory mediators. However, whether this occurs and whether there are differences in the extent of migration of the channel between phenotypes has yet to be proven.

Further experiments determined the molecular effects of the TRPV4 antagonist, RN-1734, in the CP of treated TMEM67(-/-) rats. Again, utilizing immunofluorescence staining for TRPV4, the level of expression in RN-treated rats differed dramatically from that in untreated animals. Unlike the expression seen in untreated animals in which TRPV4 completely encompasses the apical membrane (Figure 5.2, D & F), the RN-treated CP had sporadic expression along the apical membrane with more intracellular expression (Figure 5.2, E). There also appeared to be a decrease in expression levels compared to the untreated affected animal. Assuming TRPV4 is involved in the movement of ions across the CP epithelium, this implies that antagonizing TRPV4 is causing a decrease in ion movement and therefore a decrease in CSF production. Furthermore, in most

cases, it appeared as though the remaining apical expression occurred in protruding sections of the CP. As the drug was transported through the bloodstream, it is possible that these were areas where the capillaries were unable to efficiently reach, thus the blood-borne drug was less effective.

I also returned to claudin-1 expression (as seen in Chapter 3) to compare how the tight junctions were affected by the TRPV4 antagonist. When visualizing claudin-1, the protein appeared to be more expressed in the RN-treated hydrocephalic rat (Figure 5.2, B) than in the hydrocephalic untreated animals (Figure 5.2, A) but not as prominent as in the WT untreated rat (Figure 5.2, C). Again, areas of more defined apical expression appeared sporadic, similar to that seen with TRPV4 in the antagonist-treated animal. While the tight junctional protein did not appear to be as intact as the wild type, there appeared to be slight improvement as the protein began to express apically once more. This suggests that there was less strain on the barrier and, therefore, the resistance of the monolayer likely remained intact. This finding can also be seen in the CP cell line when pretreated with RN-1734 (data not shown). These data also imply that tight junction integrity is connected to TRPV4 expression on the apical membrane. These experiments were repeated in two different animals.

Combined, these data suggest that the mechano- and osmo-sensitive cation channel plays a major role in homeostatic CSF production as well as in the formation of hydrocephalus.

5.2 Characterizing the PCP-R cell line

In order to determine the presence of various ion channels and proteins in the PCP-R cell line and to better characterize the cells, I performed RT-PCR to detect mRNA of receptors and proteins of interest (Figure 5.3). *Gapdh* was used as the positive control in all instances.

Initially, I wanted to determine whether our cell line contained the three different Na^+/K^+ ATPase subunits. The Na^+/K^+ ATPase has been reported as being particularly important for setting up ion gradients in the production of CSF (1). As previously stated in Chapter 1, this is due to the fact that in the choroid plexus, the Na^+/K^+ ATPase is known to be located on the apical membrane. However, in the rest of the body, the Na^+/K^+ ATPase is located on the basolateral membrane. It

has been reported that the β -2 subunit is responsible for this opposite targeting (2). The unique location of this transporter necessitated characterizing it in our cell line. From this experiment, I was able to determine that the cell line does show mRNA of two of the three subunits found in the Na^+/K^+ ATPase, α -1 and β -2. The subunit α -3 was not present (Figure 5.3A). As expected, the presence of the β -2 subunit suggests that the channel is able to localize to the apical membrane.

To better define the tight junction properties of our cell line, I also tested for various claudin isoforms. Claudins come in two different varieties: barrier-forming and pore-forming. For RT-PCR, claudins-1, -2, -3, -4, and -10 were examined and all but claudin-10 were present (Figure 5.3B). Of these, claudins 1, 3, and 4 are barrier-forming, and claudins 2 and 10 are pore-forming. Specifically, these barrier-forming and pore-forming claudins decrease and increase permeability to cations, respectively (3). This is important because we and others have shown that activation of TRPV4 causes a change in permeability (4). Exactly how these claudins may change during hydrocephalus and in response to TRPV4 agonists is unknown but may be the topic of future studies.

In the WNK pathway, the kinase SPAK plays an integral role for the regulation of various ion channels, importantly including the NKCCs, NCC, and KCCs, as previously stated in Chapter 1(5, 6). Due to the multitude of related pathways through which SPAK is involved in ion transportation, this kinase is an important target of study in the hydrocephalus field. Therefore, I tested whether the gene which encodes the protein was present in the PCP-R cells. I found that the gene for the kinase SPAK, *Stk39*, was, indeed, present in the cell line (Figures 5.3C).

These characterization studies of the PCP-R cells help to better understand and confirm the impact this cell line can have as a CP model. By comparing these findings to those in vivo, we are also able to determine the viability as a comparable in vitro model.

5.3 SPAK and Associated Channels in the Choroid Plexus

SPAK has been reported as playing a role in the hypersecretion of CSF in intraventricular hemorrhage (IVH). The TLR4-dependent kinase phosphorylates and activates NKCC1, a Na-K-

Cl cotransporter also implicated in CSF production on the apical membrane of the CP epithelium (5). In hyperosmotic conditions, SPAK transcription is increased due to an increase in NF- κ B binding and subsequent SPAK activation (6). Therefore, I determined this protein to be of interest and stained P15 Wpk rat brains for SPAK expression. From this, I found that SPAK was increased in the hydrocephalic animals. I also found that treatment of the hydrocephalic rats with the TRPV4 antagonist, RN-1734, decreased SPAK expression to a level comparable to that seen in the wild type (Figure 5.4).

Due to the increase in SPAK seen in the hydrocephalic animals and the fact that SPAK is known to phosphorylate and activate NKCC1, I stained for phosphorylated NKCC1 (pNKCC1) in the PCP-R cells, untreated and treated for 10 minutes with the TRPV4 agonist, GSK1016790A (Figure 5.5). I found that pNKCC1 was present in the lateral junctions of the cells and that pNKCC1 intensity increased when treated with TRPV4 agonist. This increase could be due to a TRPV4-dependent increase in SPAK, leading to increases in the phosphorylation of NKCC1.

Based on these data linking TRPV4 and SPAK activity, I inhibited SPAK and the redundant kinase, OSR1, in the PCP-R cells prior to adding TRPV4 agonist using an inhibitor called Rafoxanide (Figure 5.6). Interestingly, inhibition of SPAK/OSR1 causes significant changes to both transepithelial ion flux and barrier permeability prior to activation of TRPV4. This can be attributed to SPAK and OSR1's role in other ion channels, such as the NKCCs, KCCs, and NCC (7). After addition of the TRPV4 agonist, there was a substantial inhibition of TRPV4-mediated ion flux as well as a significant increase in conductance with SPAK/OSR1 inhibition alone followed by a leveling after TRPV4 agonist addition.

Together, these data suggest a very strong correlation between the WNK pathway, SPAK, and TRPV4. The connection is likely due to the interaction between both SPAK and TRPV4 with other important ion channels believed to regulate CSF production. However, more experiments will need to be conducted in order to further elucidate this connection.

5.4 Microglia in Wpk rat brain

Determining whether inflammation is taking place in our hydrocephalic model is an integral piece to discovering the underlying cause of the disease. Sites of injury and neuronal death can cause of the activation of the central nervous system's macrophage-like immune cells, microglia. Activated microglia release pro-inflammatory cytokines and activate other cells of the immune system (8). It is possible that the activation of microglia and subsequent inflammatory pathways is a contributing factor to the pathology of hydrocephalus. To test this theory, I stained adult and juvenile Wpk brains for activated microglia and found that in the older, severely affected heterozygous hydrocephalic brain (P356) activated microglia are increased around the subventricular and hippocampal regions (Figure 5.7). These areas are of interest as they are areas of neurogenesis (9).

Following this initial discovery, I repeated the experiment in even older (P460) WT and TMEM67(+/-) brains (Figure 5.8). However, the heterozygous brain tested was not as severely affected as the P356 brain previously observed and was therefore labeled as having "mild" hydrocephalus. The mild hydrocephalic adult did not exhibit the same microglial activation as seen in the severely hydrocephalic animal. This could signify that the microglia activation is dependent on the severity of the condition. Interestingly, the WT control brain did show an area of microglial activation in the region of the hippocampus. However, these microglia did not appear to be activated due to hydrocephalus. Rather, this instance could be due to other outside means, such as hemorrhage or trauma in the area.

In order to test whether disease severity was the causative effect of microglia activation, I repeated the experiment again in P330 brains with the WT having small ventricles and the TMEM67(+/-) having large ventricles (Figure 5.9). In this experiment, no difference in microglia activation was seen between the WT and hydrocephalic TMEM67(+/-). It should be of note that these "large" ventricles were indeed larger than the "mild" hydrocephalus seen in the P460 animal. However, these "large" ventricles in the P330 animal were still smaller than the "severe" hydrocephalus seen in the P356 animal. Therefore, it is possible that the severity of the disease could still be a contributing factor to inflammation.

In addition to the adult animals, I also stained for microglia in the juvenile (P15) WT, TMEM67(+/-), and TMEM67(-/-) animals (Figure 5.10). Considering that the homozygous animals have the most severe hydrocephalus, this experiment would best answer the question of whether the severity of hydrocephalus determined the amount of microglia activation. However, no difference was observed between the three genotypes. To confirm these results, WT and homozygous brains at P17 were stained for activated microglia with the idea that the hydrocephalus would be worse at P17 compared to P15 (Figure 5.11). While the hydrocephalus was indeed worse in the affected animal, there was still no difference seen between the WT and homozygous animal. Therefore, the conclusion must be made that severe hydrocephalus does not cause activation of microglia.

5.5 Discussion

These additional experiments complement the data found in previous chapters in that the reasoning and results behind the previous data becomes clearer. TRPV4 appeared to be increased in the hydrocephalic animals. This suggests that TRPV4 is a contributing factor towards the disease. Therefore, we use a TRPV4 antagonist drug to combat the hydrocephalus, and, as previously mentioned in Chapter 1, we have seen promising results of attenuation in the head dimensions of treated animals. In addition to this, we see decreases in TRPV4 expression in the CP epithelial upon antagonism and partial restoration of the blood-CSF barrier as evidenced by increases in claudin-1 expression in these treated animals. This implies that the drug treatment is effective.

As demonstrated in Chapters 2 and 3, we have also strived to characterize efficient *in vivo* and *in vitro* hydrocephalus and CP models through the Wpk rat and the PCP-R cell line, respectively. By further characterizing the PCP-R cells through RT-PCR and confirming the presence of polarizing and barrier-forming channels, we have shown that this model is, indeed, an effective model for studying this interesting tissue type.

Several different pathways likely interact with TRPV4 or are in some way modulated by its activity. Deciphering these various pathways and how they are all connected is an important aspect to understanding how TRPV4 plays a role in the secretion and/or absorption of CSF. Therefore, the discovery that TRPV4 and the WNK pathway can have significant effects on each other provides

a crucial key to the mechanism of the ion channel's function. These data suggest that, in addition to the calcium-sensitive potassium channels mentioned in Chapter 3, TRPV4 can potentially act on various other ion channels through the kinase, SPAK, providing a means of transepithelial ion flux, as evidenced by the increase in activated phosphorylated NKCC1 in the PCP-R cells when pretreated with the TRPV4 agonist. Furthermore, it appeared that not only is TRPV4 necessary for SPAK expression, specifically on the apical membrane of the CP where it is potentially co-expressing with and activating NKCC1, but SPAK/OSR1 is also necessary for TRPV4-mediated ion flux and permeability changes. Together, this implies that TRPV4 and SPAK are dependent on each other.

Finally, as a continuation from Chapter 4, I showed that TRPV4 can be modulated by increases in pro-inflammatory cytokines and mediators. Therefore, considering that TRPV4 has been shown to be increased in the hydrocephalic Wpk rats, I hypothesized that this increase was due to inflammation in the brain due to hydrocephalus. As a means to measure inflammation, microglia activation was observed in several ages and brain regions of hydrocephalic Wpk rats, and I was surprised to find that of 23 animals tested, only one showed signs of inflammation likely due to hydrocephalus. While this cannot rule out that inflammation from different origins is present, such as from neutrophils or monocytes, in any of these animals, it does suggest that inflammation is not present due to microglial activation.

Based on these data, we can make further assumptions and come another step closer towards the mechanism of TRPV4 as well as the pathology and development of hydrocephalus.

Table 5.1 Primer sequences used for RT-PCR with corresponding product sizes (bp).

Three different primer sets were generated and tested for each gene. Primers included in this table were utilized for Figure 5.3. *Gapdh* was used as a positive control.

<i>Sus Scrofa</i> gene	Protein	Primer Sequences 5' - 3'		Product Size (bp)
		Forward Primer	Reverse Primer	
<i>Atp1a1</i>	NaK ATPase α 1	TCCCTCAACTCCACCAACAA	TTCAAGATGTCATCCAGCTGCT	610
<i>Atp1a3</i>	NaK ATPase α 3	AGAAGGTGAGAAGATGCAGGTG	CTCCAGGTTTTTACAAGGCAG	568
<i>Atp1b2</i>	NaK ATPase β 2	CTTCCTCACCCTGTCTCTGAC	TTGCTCCTGCGTAGAAGTTGAT	395
<i>Cldn1</i>	CLDN1	CTACGCTGGTGACAACATTGTG	CACGTAGTCTTTCCACTGGAA	532
<i>Cldn2</i>	CLDN2	CTCTCGGCCTCCAACCTTGTAG	AGTAGAGAGCCTCTCCGATCTC	489
<i>Cldn3</i>	CLDN3	CTTCATCGGCAGCAGCATTATC	CCAGCAGAGAGTCGTACACTTT	113
<i>Cldn4</i>	CLDN4	CTTCATCGGCAGCAACATCG	CTGAGTAGGGCTTGTCTGGTAC	482
<i>Cldn10</i>	CLDN10	CAGGCATGTCGAGGACTTATGA	CCTCCTCCGTGATACTTTGTCC	410
<i>Stk39</i>	SPAK	TAGCAACAGGGGGTGATGTTAC	GGAAGTTCTCACTCAGGTCCAG	432
<i>Gapdh</i>	GAPDH	TTTAACTCTGGCAAAGTGGAC	CTCTTTGGGCTATGTCTGGTGT	884

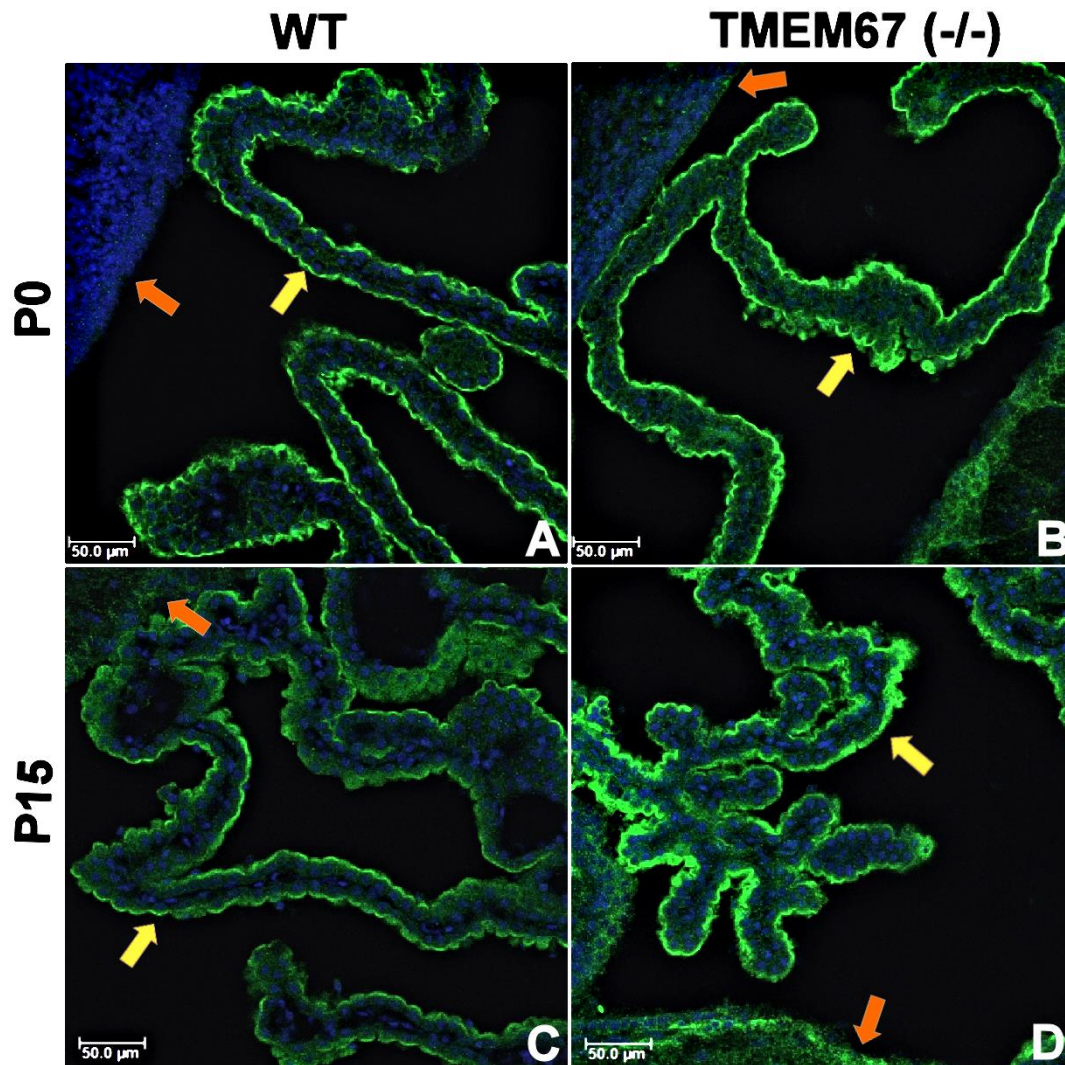


Figure 5.1 Immunofluorescence of TRPV4 in the Wpk rat CP.

Brain tissue was sectioned at 20 μm and incubated with primary antibody for TRPV4 (1:200 dilution, Alomone anti-TRPV4). Images correspond with wild type (WT, A & C) and hydrocephalic (TMEM67 (-/-), B & D) animals at birth (P0, A-B) and at the time of sacrifice (P15, C-D). DAPI staining allows for visualization of nuclei (500ng/mL, Sigma). Images were taken on a Leica TCS SP8 (upright high-speed multiphoton and confocal imaging system). $n=3$. Scale bars = 50 μm .

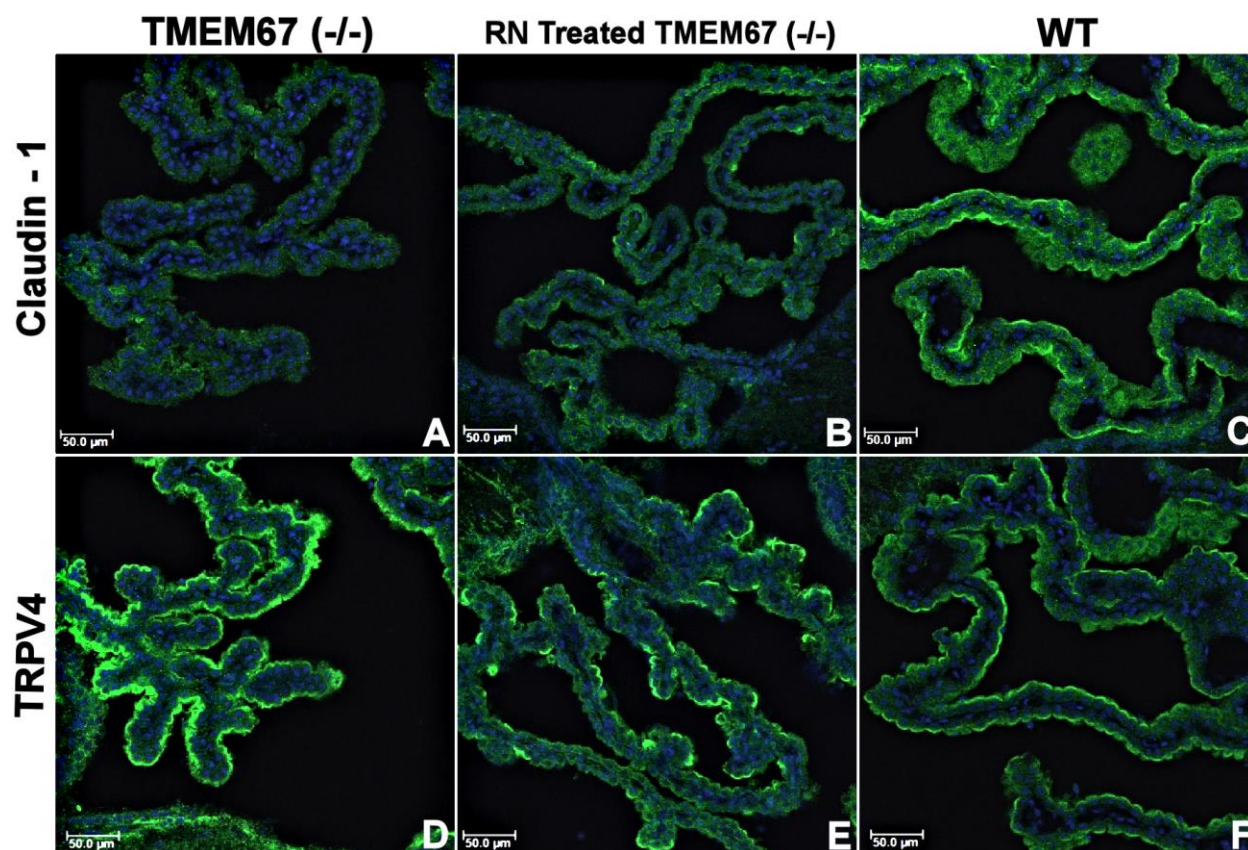
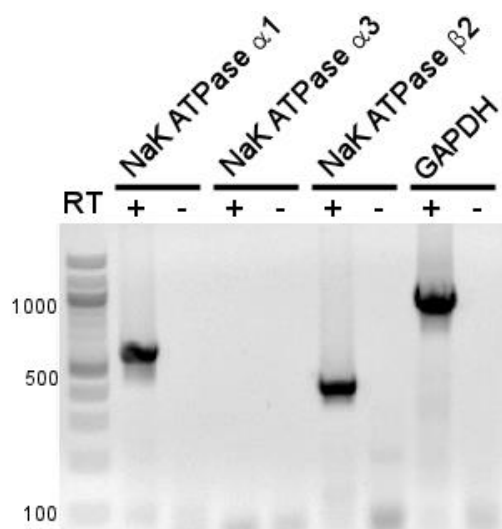


Figure 5.2 Immunofluorescence of Claudin-1 and TRPV4 in RN-1734-treated P15 Wpk CP.

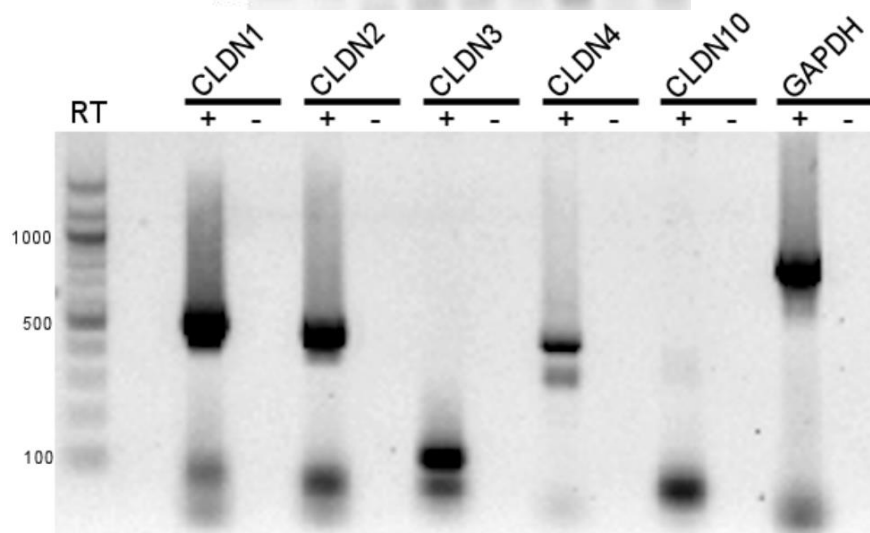
Immunofluorescence of Claudin-1 (A-C) and TRPV4 (D-F) in P15 Wpk choroid plexus treated with TRPV4 antagonist RN-1734. Brain tissue was sectioned at 20 μm and incubated with primary antibody for TRPV4 (1:200 dilution, Alomone anti-TRPV4) and for the tight junction protein, claudin-1 (1:100 dilution, Abcam anti-Claudin 1). DAPI staining allows for visualization of nuclei (500ng/mL, Sigma). Images were taken on a Leica TCS SP8 (upright high-speed multiphoton and confocal imaging system). Images from TMEM67 (-/-) and WT were taken from Figures 2.8 and 5.4. $n=2$. Scale bars = 50 μm .

Figure 5.3: RT-PCR in PCP-R epithelial cells. A) mRNA is present for the Na⁺/K⁺ ATPase subunits α 1 and β 2, but not α 2. B) Results for the tight junctional proteins claudin-1-4, and 10. Claudins-1-4 were present. Claudin-10 was not present. C) The gene which transcribes the kinase SPAK, *Stk39*, is present in the PCP-R cell line. *Gapdh* was utilized as positive controls for each gel. Band product sizes can be found in Table 5.1. Ladder = 1kb.

A)



B)



C)

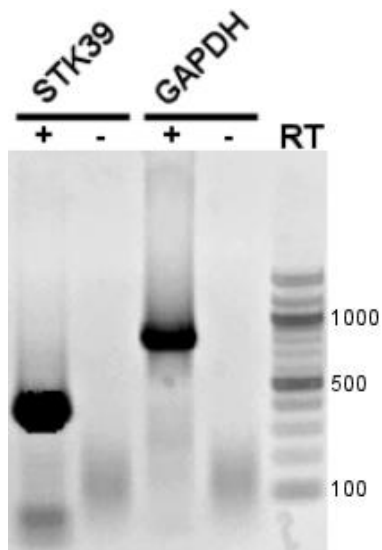


Figure 5.3 RT-PCR in PCP-R epithelial cells.

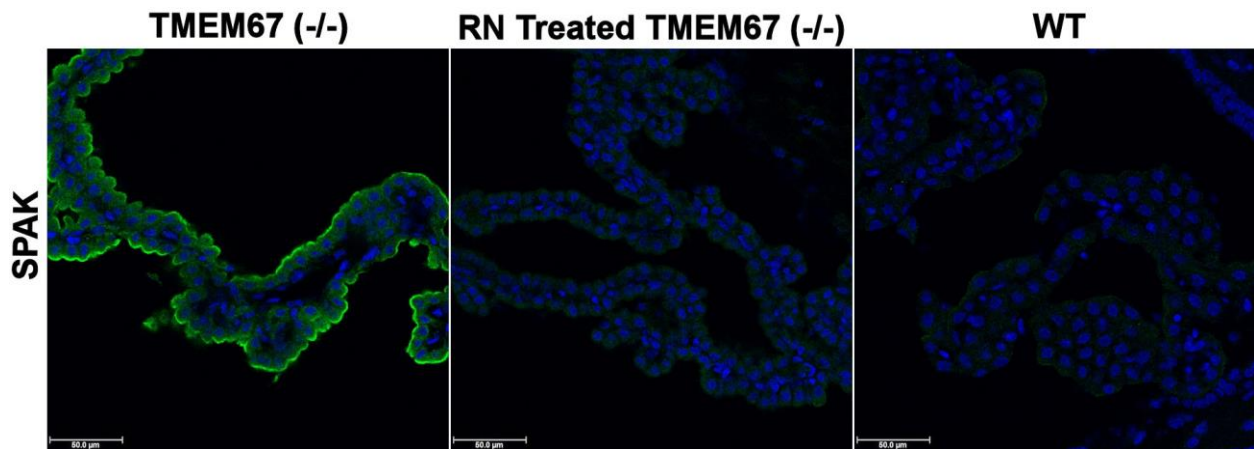


Figure 5.4 Immunofluorescence of SPAK in P15 Wpk CP treated with RN-1734.

Immunofluorescence of SPAK in P15 Wpk WT, TMEM67(-/-), and TMEM67 (-/-) CP treated with RN-1734. Brain tissue was sectioned at 20 μm and incubated with primary antibody for SPAK (1:50 dilution, Cell Signaling Technology Anti-SPAK). DAPI staining allows for visualization of nuclei (500ng/mL, Sigma). Images were taken on a Leica TCS SP8 (upright high-speed multiphoton and confocal imaging system). n=3. Scale bars = 50 μm.

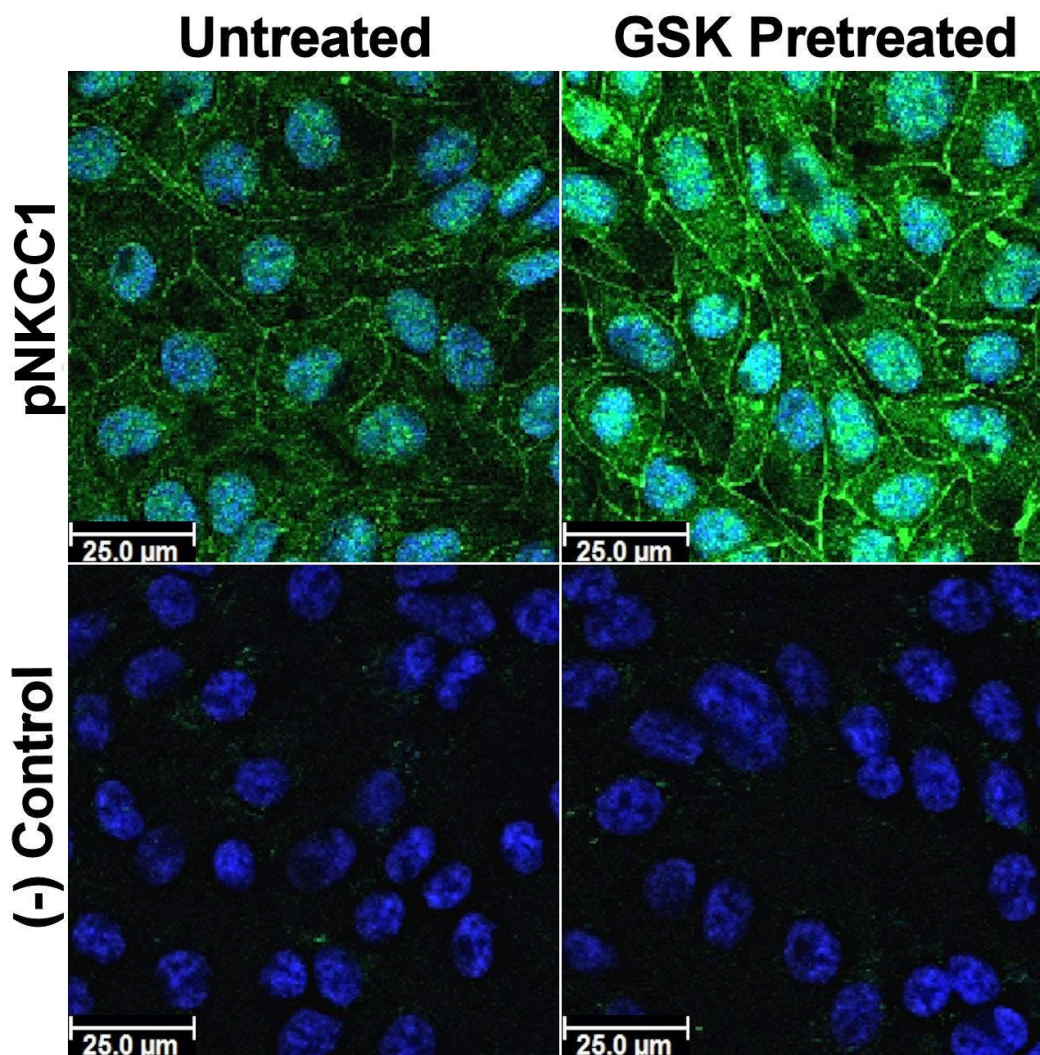


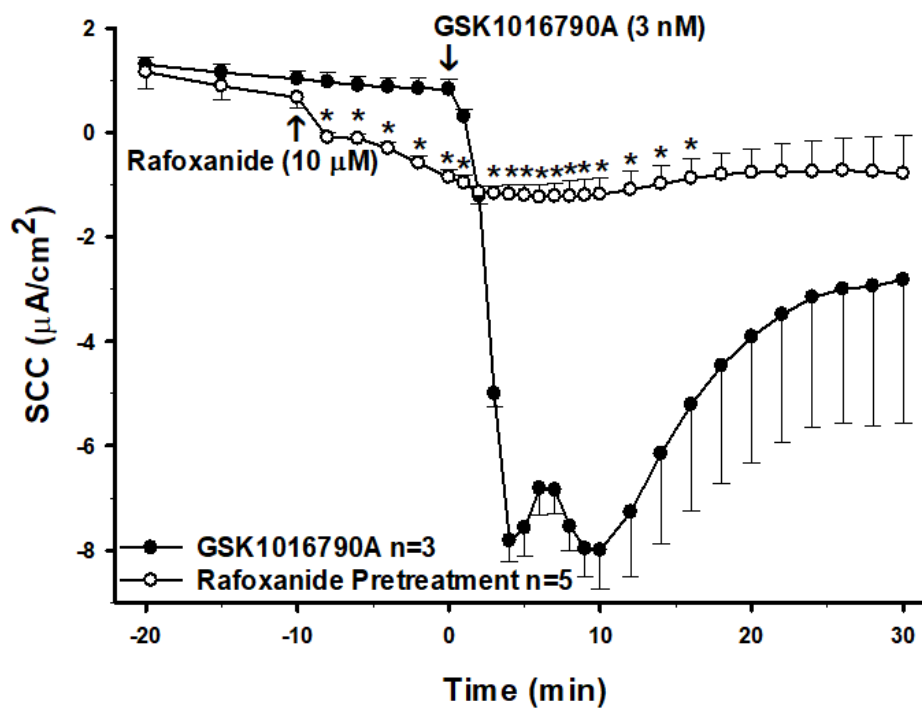
Figure 5.5 Immunofluorescence of pNKCC1 in TRPV4 agonist (GSK)-treated PCP-R cells.

Cells were stained with DAPI (blue) to visualize nuclei and anti-pNKCC1 antibody (1:200 dilution, Millipore anti-pNKCC1). Treated cells were pre-incubated with TRPV4 agonist, GSK1016790A (3nM), for 10 minutes before fixation and staining. Negative control cells were stained with DAPI and secondary antibody only. n= 3. Scale bars = 25μm.

Figure 5.6: Pre-treatment of PCP-R cells with SPAK/OSR1 inhibitor Rafoxanide at 10 minutes prior to TRPV4 agonist addition. Effect on transepithelial ion flux (A) and conductance (B) was measured. Rafoxanide was added to the PCP-R media on both basolateral and apical sides of the membrane at T = -10 minutes. TRPV4 agonist GSK1016790A was added to basolateral side of the membrane only at T = 0 minutes. 10-minute incubation is signified by white circles. GSK1016790A control is signified by black circles. Error bars signify mean \pm S.E.M. for number of experiments indicated. SCC = short circuit current. * = $p < 0.05$ against control.

A)

Rafoxanide Pretreatment SCC



B)

Rafoxanide Pretreatment Conductance

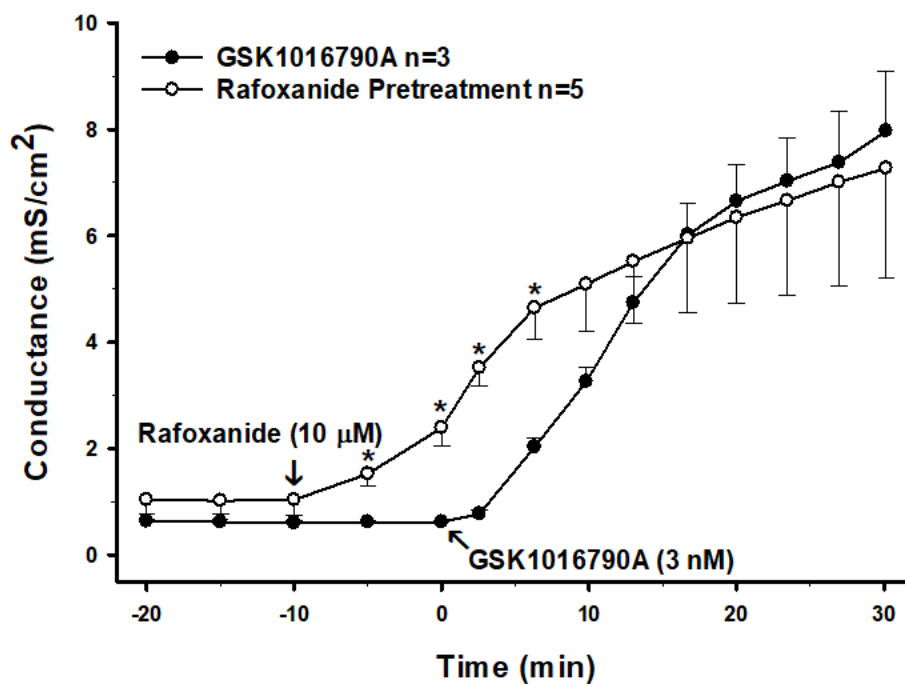


Figure 5.6 PCP-R epithelial cells pretreated with SPAK/OSR1 inhibitor Rafoxanide.

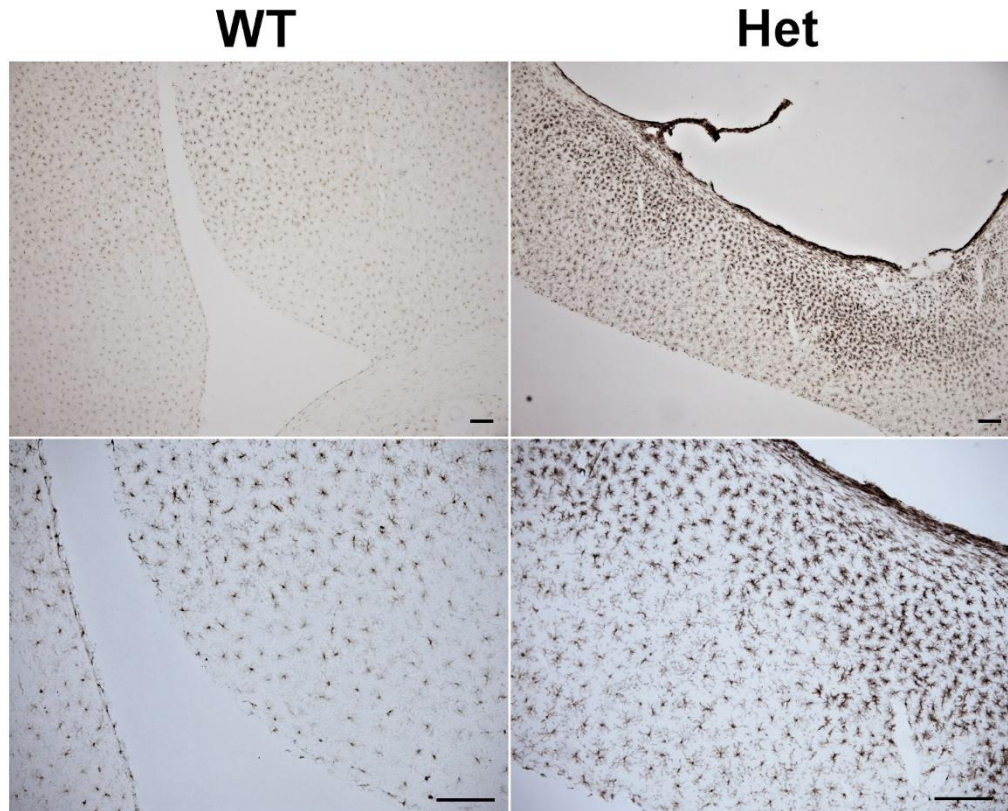
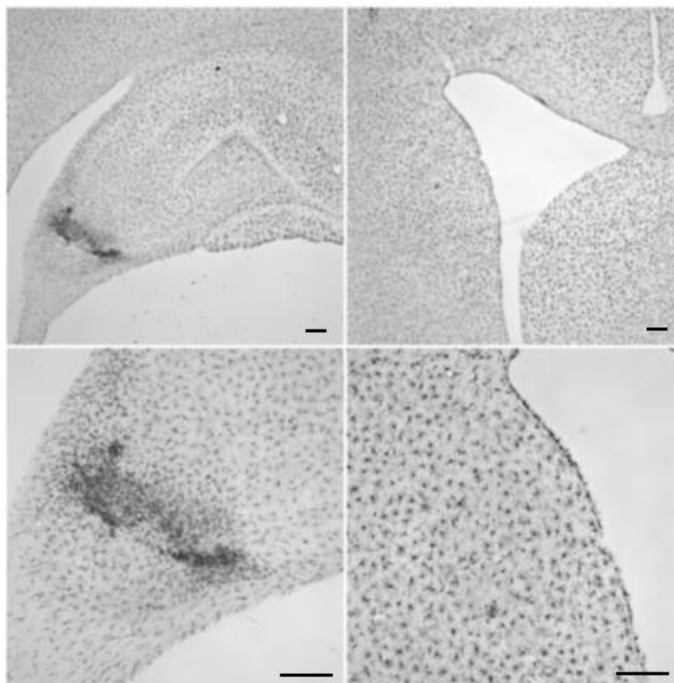
P356 Untreated

Figure 5.7 Microglia in P356 Wpk WT and TMEM67 (+/-) rats.

Brains were sectioned at 40 μm and incubated with primary antibody for Iba1 (1:5000 dilution, Wako anti-Iba1). DAB was used as a chromogen to visualize activated microglia (brown). 4x and 10x magnifications were used. Scale bars = 250 μm .

Figure 5.8: Microglia in P460 Untreated Wpk WT (A) and TMEM67(+/-)-Mild (B) rats. Brains were sectioned at 40 μm and incubated with primary antibody for Iba1 (1:5000 dilution, Wako anti-Iba1). DAB was used as a chromogen to visualize activated microglia (brown). 4x and 10x magnifications were used. Two different brain regions were visualized: hippocampal (left) and subventricular (right). Scale bars = 250 μm .

A)

P460 WT

B)

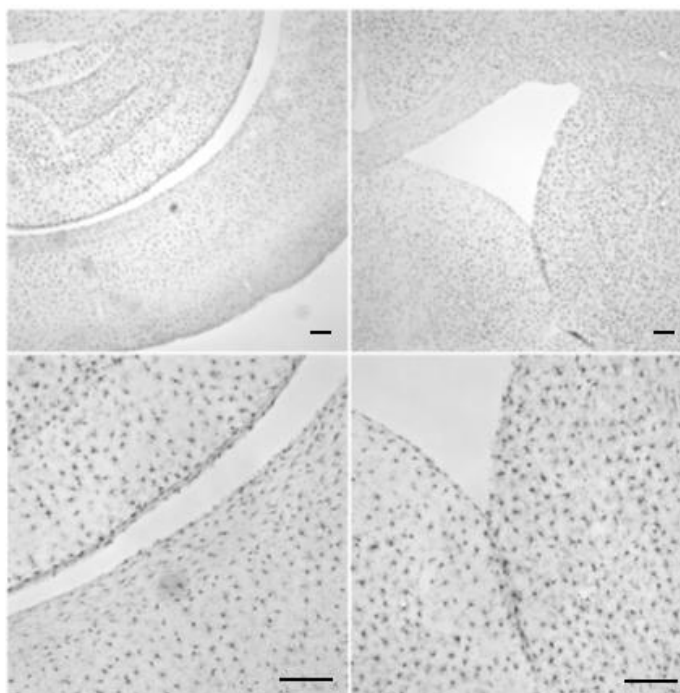
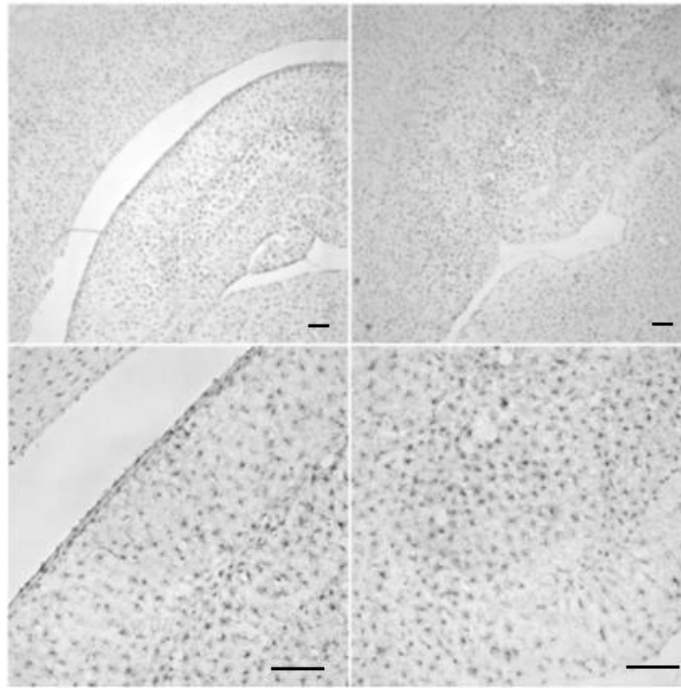
P460 TMEM67 (+/-) - Mild

Figure 5.8 Microglia in P460 Wpk WT and TMEM67 (+/-) rats.

Figure 5.9: Microglia in P330 Wpk WT (A) and TMEM67 (+/-)-Severe (B) rats. Brains were sectioned at 40 μm and incubated with primary antibody for Iba1 (1:5000 dilution, Wako anti-Iba1). DAB was used as a chromogen to visualize activated microglia (brown). 4x and 10x magnifications were used. Two different brain regions were visualized: hippocampal (left) and subventricular (right). Scale bars = 250 μm .

A)

P330 WT

B)

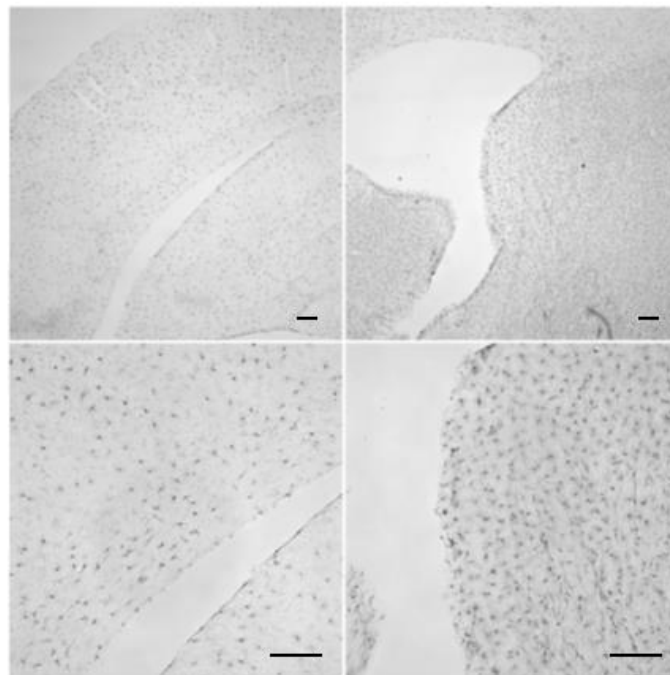
P330 TMEM67 (+/-) - Severe

Figure 5.9 Microglia in P330 Wpk WT and TMEM67 (+/-) rats.

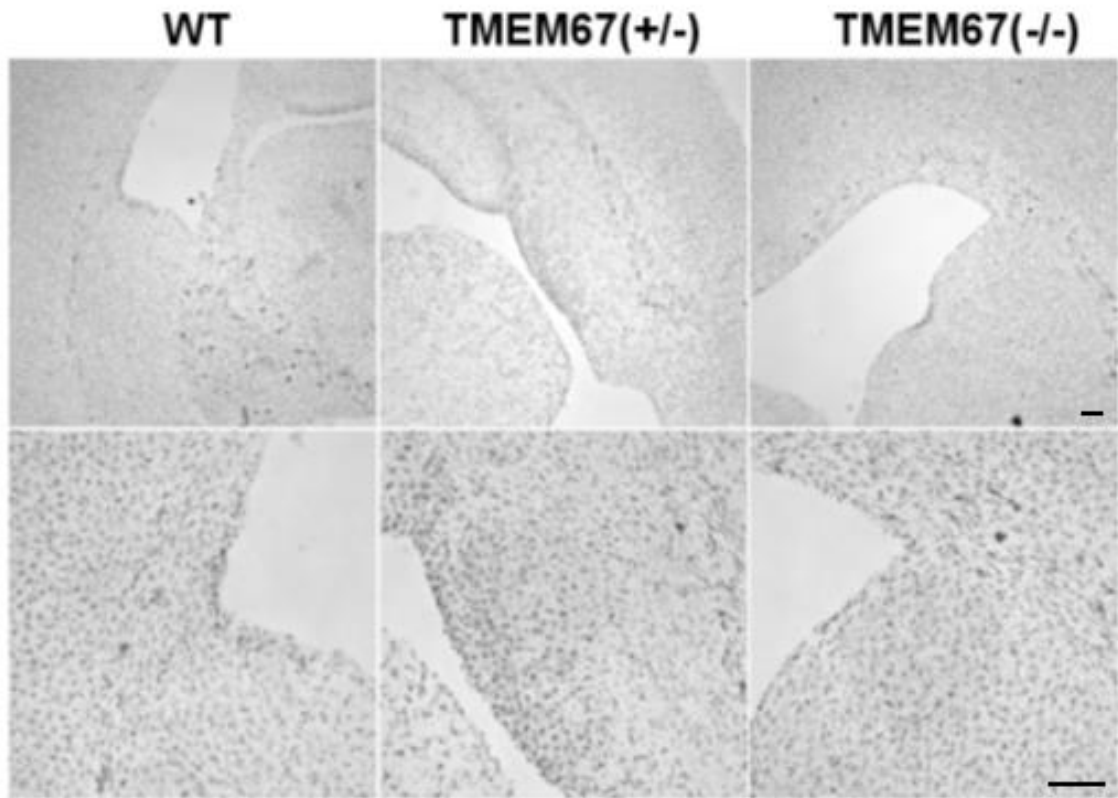
P15 Untreated

Figure 5.10 Microglia in P15 Wpk WT, TMEM67 (+/-) and TMEM67 (-/-) rats.

Brains were sectioned at 40 μm and incubated with primary antibody for Iba1 (1:5000 dilution, Wako anti-Iba1). DAB was used as a chromogen to visualize activated microglia (brown). 4x and 10x magnifications were used. Scale bars = 250 μm .

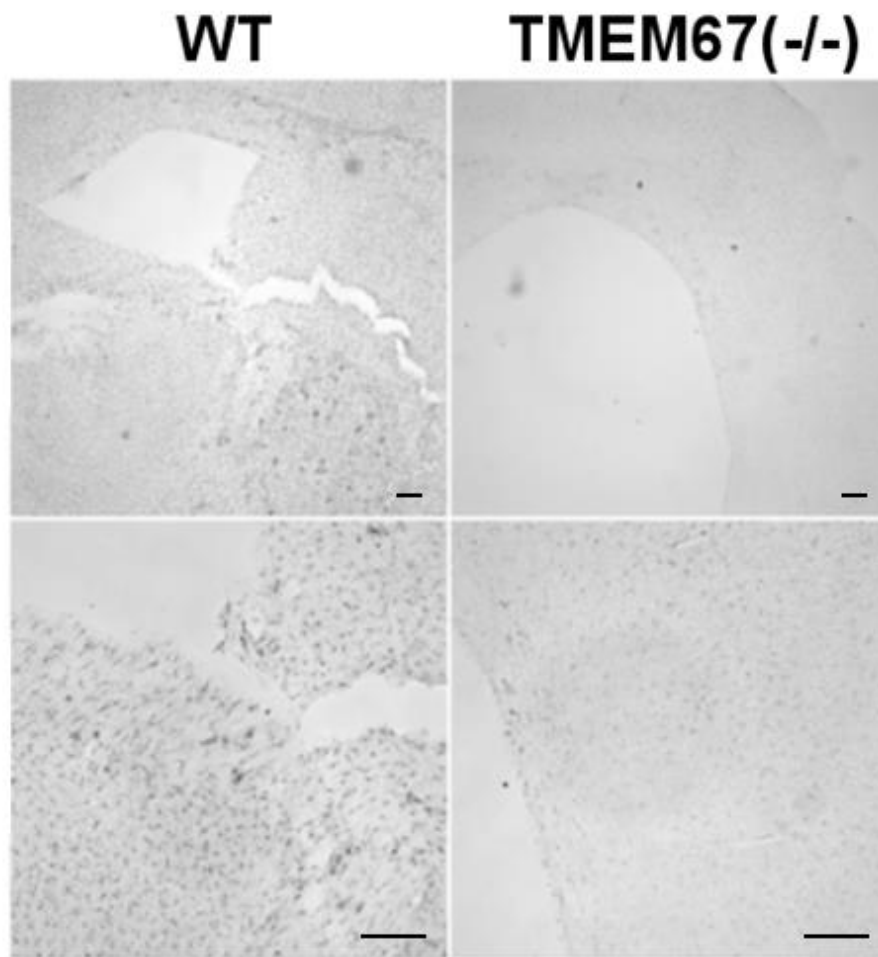
P17 Untreated

Figure 5.11 Microglia in P17 Wpk WT and TMEM67 (-/-). rats.

Brains were sectioned at 40 μm and incubated with primary antibody for Iba1 (1:5000 dilution, Wako anti-Iba1). DAB was used as a chromogen to visualize activated microglia (brown). 4x and 10x magnifications were used. Scale bars = 250 μm.

5.6 References

1. Brown, P., Davies, S., Speake, T. and Millar, I. (2004). Molecular mechanisms of cerebrospinal fluid production. *Neuroscience*, 129(4), 955-968.
2. Lobato-Álvarez, J., Roldán, M., López-Murillo, T., González-Ramírez, R., Bonilla-Delgado, J. and Shoshani, L. (2016). The apical localization of Na⁺, K⁺-ATPase in cultured human retinal pigment epithelial cells depends on expression of the β2 subunit. *Frontiers in Physiology*, 7.
3. Günzel, D., and Yu, A. (2013). Claudins and the modulation of tight junction permeability. *Physiological Reviews*, 93(2), 525-569.
4. Reiter, B., Kraft, R., Günzel, D., Zeissig, S., Schulzke, J., Fromm, M. and Harteneck, C. (2006). TRPV4-mediated regulation of epithelial permeability. *The FASEB Journal*, 20(11), 1802-1812.
5. Karimy, J., Zhang, J., Kurland, D., Theriault, B., Duran, D., and Stokum, J. et al. (2017). Inflammation-dependent cerebrospinal fluid hypersecretion by the choroid plexus epithelium in posthemorrhagic hydrocephalus. *Nature Medicine*, 23(8), 997-1003.
6. Yan, Y., Dalmasso, G., Thi Thu Nguyen, H., Obertone, T., Sitaraman, S., and Merlin, D. (2009). Ste20-Related Proline/Alanine-Rich Kinase (SPAK) regulated transcriptionally by hyperosmolarity is involved in intestinal barrier function. *Plos ONE*, 4(4), e5049.
7. Richardson, C., and Alessi, D. (2008). The regulation of salt transport and blood pressure by the WNK-SPAK/OSR1 signaling pathway. *Journal of Cell Science*, 121(20), 3293-3304.
8. Streit, W., Mrak, R. and Griffin, W. (2004). Microglia and neuroinflammation: a pathological perspective. *Journal of Neuroinflammation*, 1(1), 14.
9. Alvarez-Buylla, A., and García-Verdugo, J. (2002). Neurogenesis in Adult Subventricular Zone. *The Journal of Neuroscience*, 22(3), 629-634.

CHAPTER 6. SUMMARY

Treatment options for hydrocephalus patients are dim. Currently, the only approved methods of treatment are ineffective and require invasive, life-threatening brain surgery. In order to discover a suitable alternative pharmacotherapy for hydrocephalus, we need to understand the mechanisms of the disorder to determine the best way to combat it.

By characterizing and establishing two genetic *in vivo* hydrocephalic rodent models, the fast-progressing homozygous and slow-progressing heterozygous Wpk rat, we and other research groups can utilize this animal to study the development of the model analogous to both pediatric and geriatric hydrocephalus (1). Several previous *in vivo* models of hydrocephalus utilize kaolin to induce hydrocephalus by injecting the chemical into the cisterna magna or the ventricular space. However, this method causes a breakdown of the epithelial lining of the ventricles and CP and therefore, does not effectively mimic real instances of hydrocephalus (2). As the Wpk rat has a genetically-based hydrocephalus, we can study the disease in a model that is similar to instances of hydrocephalus in humans.

While the *in vivo* model is excellent for studying the macroscale characteristics of hydrocephalus and the CP, we have also established an effective *in vitro* model for studying the molecular mechanisms for CSF production by means of the PCP-R cell line. This cell line allowed us to determine drug effects on transepithelial ion flux and barrier permeability, both necessary aspects to CSF production and CP integrity as part of the blood-CSF barrier. The high resistance property of this continuous cell line as well as its ability to grow as a polarized monolayer better imitates the CP barrier seen *in vivo* than primary culture. Thus, we can conclude that the PCP-R cell line is an effective means of studying the molecular mechanisms of the CP epithelia.

Furthermore, from the characterization studies presented in this thesis, we are not only able to distinguish ion channels, genes, and proteins specifically in the CP epithelium as we are able to determine potential targets for drug treatment in the CP as well. Specifically, we identified the ion channel, TRPV4, as a promising target for regulation of CSF production. Utilizing our hydrocephalic rat model, I showed that TRPV4 is upregulated in the affected animals. As such, we turned to the *in vitro* model to determine TRPV4's molecular function. As evidenced, we

determined various effectors involved with TRPV4 and further elucidated the mechanisms behind the ion channel's function in the CP. From Chapter 3, it was discovered that the transepithelial ion flux mediated by TRPV4 is resultant of activation of the calcium-sensitive potassium channel, IK, likely due to the influx of calcium into the cell via TRPV4. Activation of the IK channel allows potassium ions to be secreted into the luminal space, thus increasing extracellular potassium. In addition to this, from Chapter 5, I was able to determine that TRPV4 can potentially interact with the kinase SPAK to activate downstream ion channels. Previous works have concluded that NKCC1 is the predominant channel responsible for ion movement related to CSF production (3, 4). Indeed, activated pNKCC1 appeared upregulated in response to TRPV4 agonism in the PCP-R cells. Thus, this leads to the conclusion that TRPV4 can activate several ion channels capable of contributing to the regulation of CSF production, highlighting the cation channel's potential as a drug target.

Finally, I wanted to determine how and why TRPV4 would be upregulated during hydrocephalus and hypothesized that inflammation in the brain was the causative agent. While characterizing the PCP-R cells, all known TLRs were present, meaning the CP epithelia can respond to and produce various cytokines. Upon testing the effects of various pro- and anti-inflammatory cytokines and inflammatory mediators on TRPV4-mediated transepithelial ion flux and barrier permeability in the cells, I found that pro-inflammatory mediators attenuated the effects of TRPV4 stimulation. Upon further study, I also clarified the interaction between TRPV4 and the inflammatory mediator AA and its metabolites. While AA is claimed to activate TRPV4 (5), my studies suggested that TRPV4 is inhibited by increases in AA. Rather, I have found that AA metabolites are indeed the activators of TRPV4-mediated changes in the cell, including ion flux across the epithelium. Specifically, metabolism of AA into EETs by the CYP-450 epoxygenases appeared to be the most important mediator, as its inhibition prevented all TRPV4-mediated changes, while the other metabolites minorly affect TRPV4 function. Together, this implies that TRPV4 is affected by inflammation in that inflammation downregulates TRPV4. This could mean that inflammation is utilized to control TRPV4 activity and therefore is not the causative agent of TRPV4 activation.

To then determine whether inflammation was present in our animal model, I sought to observe inflammation using immunohistochemistry for activated microglia. From these data, the conclusion was made that there were no distinguishable signs of inflammation in the affected animals due to microglia activation. Therefore, inflammation is likely not causing an increase in TRPV4 expression in either of our rat models of hydrocephalus.

In conclusion, with 6.4 million individuals across the globe and of all walks of life affected by hydrocephalus, there is a need for an effective, non-invasive treatment (6). With these data through the use of tissue and cellular models more analogous to the disease in humans, I hope to bring the scientific community one step closer to finding a suitable treatment.

6.1 References

1. Shim, J., Territo, P., Simpson, S., Watson, J., Jiang, L., Riley, A., McCarthy, B., and Blazer-Yost, B. (2019). Hydrocephalus in a rat model of Meckel Gruber syndrome with a TMEM67 mutation. *Scientific Reports*, 9(1).
2. Hochwald, G., Sahar, A., Sadik, A., and Ransohoff, J. (1969). Cerebrospinal fluid production and histological observations in animals with experimental obstructive hydrocephalus. *Experimental Neurology*, 25(2), 190-199.
3. Lu, K., Huang, T., Tsai, Y. and Yang, Y. (2017). Transient receptor potential vanilloid type 4 channels mediate Na-K-Cl-co-transporter-induced brain edema after traumatic brain injury. *Journal of Neurochemistry*, 140(5), 718-727.
4. Karimy, J., Zhang, J., Kurland, D., Theriault, B., Duran, D., and Stokum, J. et al. (2017). Inflammation-dependent cerebrospinal fluid hypersecretion by the choroid plexus epithelium in posthemorrhagic hydrocephalus. *Nature Medicine*, 23(8), 997-1003.
5. Nilius, B., Vriens, J., Prenen, J., Droogmans, G., and Voets, T. (2004). TRPV4 calcium entry channel: A paradigm for gating diversity. *AJP: Cell Physiology*, 286(2), C195-C205.
6. Isaacs, A., Riva-Cambrin, J., Yavin, D., Hockley, A., Pringsheim, T., and Jette, N. et al. (2018). Age-specific global epidemiology of hydrocephalus: Systematic review, metaanalysis and global birth surveillance. *PLOS ONE*, 13(10), e0204926.